Kinetic Studies of Sulfide Mineral Oxidation and Xanthate Adsorption

Neeraj K. Mendiratta

Dissertation submitted to the Faculty of the
Virginia Polytechnic Institute and State University
in partial fulfillment of the requirement for the degree of

Doctor of Philosophy

in

Materials Engineering and Science

COMMITTEE

Dr. Roe-Hoan Yoon, Chair
Dr. G. T. Adel
Dr. G. H. Luttrell
Dr. S. G. Corcoran
Dr. J. D. Rimstidt

May 2000

Blacksburg, Virginia

Keywords:
Activation, Activation Energy, Chalcocite, Chalcopyrite, Covellite, DETA, Pyrite, Pyrrhotite, SO_2, Sphalerite, Sulfides, Tafel, Xanthate.

Kinetic Studies of Sulfide Mineral Oxidation and Xanthate Adsorption

Neeraj K. Mendiratta

Chair: Dr. R.-H. Yoon

Materials Engineering and Science

ABSTRACT

Sulfide minerals are a major source of metals; however, certain sulfide minerals, such as pyrite and pyrrhotite, are less desirable. Froth flotation is a commonly used separation technique, which requires the use of several reagents to float and depress different sulfide minerals. Xanthate, a thiol collector, has gained immense usage in sulfide minerals flotation. However, some sulfides are naturally hydrophobic and may float without a collector.

Iron sulfides, such as pyrite and pyrrhotite, are few of the most abundant minerals, yet economically insignificant. Their existence with other sulfide minerals leads to an inefficient separation process as well as environmental problems, such as acid mine drainage during mining and processing and SO_2 emissions during smelting process. A part of the present study is focused on understanding their behavior, which leads to undesired flotation and difficulties in separation. The major reasons for the undesired flotation are attributed to the collectorless hydrophobicity and the activation with heavy metal ions.

To better understand the collectorless hydrophobicity of pyrite, Electrochemical Impedance Spectroscopy (EIS) of freshly fractured pyrite electrodes was used to study the oxidation and reduction of the mineral. The EIS results showed that the rate of reaction increases with oxidation and reduction. At moderate oxidizing potentials, the rate of reaction is too slow to replenish hydrophilic iron species leaving hydrophobic sulfur species on the surface. However, at higher potentials, iron species are replaced fast enough to depress its flotation. Effects of pH and polishing were also explored using EIS.

Besides collectorless hydrophobicity, the activation of pyrrhotite with nickel ions and interaction with xanthate ions makes the separation more difficult. DETA and SO_2 are commonly used as pyrrhotite depressants; however, the mechanism is not very well understood. Contact angle measurements, cyclic voltammetry and Tafel studies have been used to elucidate the depressing action of DETA and SO_2. It was observed that DETA and SO_2 complement each other in maintaining lower pulp potentials and removing polysulfides. DETA also helps in

deactivating pyrrhotite. Therefore, the combined use of DETA and SO_2 leads to the inhibition of both the collectorless flotation and the adsorption of xanthate.

The adsorption of xanthate on sulfide minerals is a mixed-potential mechanism, i.e., the anodic oxidation of xanthate requires a cathodic counterpart. Normally, the cathodic reaction is provided by the reduction of oxygen. However, oxygen can be replaced by other oxidants. Ferric ions are normally present in the flotation pulp. Their source could be either iron from the grinding circuit or the ore itself. The galvanic studies were carried out to test the possibility of using ferric ions as oxidants and positive results were obtained.

Tafel studies were carried out to measure the activation energies for the adsorption of ethylxanthate on several sulfide minerals. Pyrite, pyrrhotite (pure and nickel activated), chalcocite and covellite were studied in 10^{-4} M ethylxanthate solution at pH 6.8 at temperatures in the range of 22 – 30 ^{0}C. The Tafel studies showed that xanthate adsorbs as dixanthogen (X_2) on pyrite and pyrrhotite, nickel dixanthate (NiX_2) on nickel-activated pyrrhotite and cuprous xanthate (CuX) on both chalcocite and covellite. However, the mechanism for xanthate adsorption on each mineral is different. The free energy of reaction estimated from the activation energies are in good agreement with thermodynamically calculated ones.

ACKNOWLEDGMENTS

First and foremost I would like to thank my advisor, Dr. Roe-Hoan Yoon, for his guidance, suggestions, criticism and the financial support he has provided throughout the course of my research and studies.

I would like to express my gratitude towards Dr. Paul Richardson for introducing me to the field of electrochemistry. Thanks are also due to the other faculty and committee members for their continuous moral support and feedback.

I would also like to express my sincere appreciation to my parents and sisters for their years of patience, affection and encouragement. Last, but not the least, special thanks go to my friends over here to for giving me memories that I will cherish for the rest of my life.

TABLE OF CONTENTS

LIST OF FIGURES

LIST OF TABLES

CHAPTER 1

INTRODUCTION

1.1. GENERAL

Sulfide ores (Table 1.1) are abundant in nature and constitute a major source of metals. Froth flotation, discovered in mid 18th century has become the single most important process in the recovery of metal sulfides (Fuerstenau, M.C., 1999). The process of froth flotation can be defined as a separation process which utilizes the surface-chemical properties of the minerals to be separated. The process has been extended beyond metal sulfides to non-sulfides and non-metallic minerals, coal, oil recovery, soil cleaning, wastewater treatment and recycling (Leja, 1982; Fuerstenau, D.W., 1999).

Though the process has been studied extensively and there exists a vast amount of literature, the process still poses questions yet to be answered. Most of the literature and reviews available emphasize the thermodynamics of the oxidation of the sulfide minerals and their flotation with or without collector. The collectors commonly used for sulfide flotation are thiols. The most commonly used thiol collectors are xanthates, which are alkali metal (e.g. Na+, K+) salts of monoalkyl esters of dithiocarbonic acid (e.g. Potassium Ethyl Xanthate: RCOSSK) (Harris, 1988). The birth of xanthate in the flotation industry took place in 1925, which led to the development of other collectors (Fuerstenau, M.C., 1999). Understanding of froth flotation is confined by limited study of various aspects of the process, namely, hydrodynamics (quiescent vs. turbulent conditions), surface chemistry, and kinetics (Biegler et al., 1975 and 1977; Biegler, 1976; Rand, 1977; Haung and Miller 1978; Schubert and Bischofberger, 1979; Pillai and Bockris, 1984; Yoon and his colleagues, 1989, 1992, 1993 and 1997; Pazhianur, 1999).

Although the process dates back to mid 19th century, the detailed study of mechanisms of collector adsorption on sulfide minerals commenced in early 20th century. Maurice Fuerstenau in his honorary lecture quoted Sir Ian Wark, according to whom, “flotation was the happy hunting ground of the theorist, and there were almost as many ‘theories of flotation’ as there were writers on the subject.” (Sutherland and Wark, 1955; Fuerstenau, M.C., 1999). The early views of xanthate adsorption on sulfide minerals include the chemical theory by Taggart and his co-workers (Taggart et al., 1930 and 1934; Taggart & Arbiter, 1943 and 1944; Taggart 1944-45; Kellogg & V-Rosas, 1945); the theory of ion exchange between sulfide ions of the minerals and

xanthate by Gaudin, Wark and their collegaues (Gaudin, 1929, 1930, 1932 and 1957; Gaudin et al., 1930; Wark and Cox, 1934a, b & c; Gaudin & Schuhmann, 1936; Sutherland and Wark, 1955) which also led to the neutral molecule theory by Cook and his colleagues (Barksy 1934; Cook and Nixon, 1950; Wadsworth et al., 1951; Last and Cook, 1952; Cook and Wadsworth, 1957; Cook and Last, 1959). The supporting evidence for each theory came from other researchers such as Steininger (1968).

In the late 1950s, Plaskin and Bessonov (1957) established the necessity of oxygen for the flotation of sulfide minerals with thiol collectors. Plaskin (1959) proposed the role of oxygen to cause conversion of n-type of galena to p-type galena, which facilitates xanthate (an anionic surfactant) adsorption. Due to the semiconducting nature of sulfide minerals, many researchers took on the task of studying the role of semiconductivity on xanthate adsorption and oxygen reduction on sulfide minerals (Plaskin and Shafeev, 1963; Eadington and Prosser, 1969; Guarnaschelli, 1970; Dixon et al., 1975; Richardson and Maust, Jr., 1976; Richardson and Eldelstein, 1978; Grandke and Cardona, 1980; Richardson and O' Dell, 1984; Fletcher and Horne, 1991). Another role of oxygen was to oxidize the mineral's surface, thereby facilitating the exchange between sulfur ions of metal sulfide minerals and collector (Gaudin, 1957; Gaudin and Finkelstein, 1965). However, with the advent of studies of thermodynamics and electrical double layer in the flotation, the role of oxygen was elucidated by electrochemical mechanisms, which was termed as the mixed potential theory. This theory not only filled the gap between previously existing theories, but also provided a new avenue for research in the study of adsorption of thiol collectors on sulfide minerals.

In early 1950s, Salamy and Nixon (1953 and 1954) studied the adsorption of xanthate on mercury (thereby eliminating the chemical, ion exchange and neutral molecule theories from the study) and observed the hydrophobic nature of mercury surface. Similar to the work done by Evans and his co-workers (1932, 1947 and 1963) for corrosion studies, Salamy and Nixon proposed the mixed potential theory. This work was followed by Tolun and Kitchener (1964), who studied galena in the presence of xanthate and oxygen. In 1968, Majima and his colleagues and Fuerstenau et al. independently showed that dixanthogen was the surface species responsible for the flotation of pyrite. However, a similar discovery made by Gaudin in 1933 went unnoticed until now. The work by Majima and his colleagues (Majima and Takeda, 1968; Peters and Majima, 1968) and Fuerstenau et al. (1968) gave a boost to the mixed potential theory. Now it is

well established that the adsorption of xanthate on sulfide mineral occurs by mixed-potential, corrosion-type mechanism.

1.2. LITERATURE REVIEW

1.2.1. Mixed Potential Theory

(a) Development

In late 1950s, Plaskin and his co-workers (1957, 1959 and 1963) established the necessity of oxygen in the adsorption of xanthate on sulfide minerals. According to Plaskin and Shafeev (1963), the oxygen converts n-type galena to p-type by consuming free electrons from surface layers of crystalline lattice, thereby leading to adsorption of negatively charged xanthate ions. Gaudin, Finkelstein and co-workers (1957, 1965 and 1972) explained the requirement of oxygen as a species required for the chemical reaction and ion exchange between sulfide minerals and xanthate. However, the studies of xanthate adsorption on mercury by Salamy and Nixon (1953 and 1954) opened the new doors for the better understanding of the mechanism.

Salamy and Nixon (1953 and 1954) studied the adsorption of xanthate on mercury. Their experiments showed clearly that reaction was under mixed control and the process reached equilibrium when the cathodic reduction of oxygen matched the anodic dissolution of mercury. Also, they showed that unlike the neutral molecule theory postulated by Cook and his co-workers (1950, 1952, 1957 and 1959), it was either the xanthate ion or the combined effect of xanthate ion and xanthic acid, not xanthic acid alone, that caused the changes in the mixed potential and activation polarization.

This work was followed by the electrochemical study of galena conducted by Tolun and Kitchener (1964). They observed that the polarograms (potential vs. current curves) for galena in the presence of both xanthate and oxygen were in between that for the anodic oxidation of xanthate alone and the cathodic reduction of oxygen alone, thereby supporting the mixed-potential theory. They described the role of oxygen to be two-fold: first, it reacts with galena to form a thin layer of thiosulfate, which is converted to lead xanthate when reacted with potassium ethyl xanthate. Secondly, it raises the electrochemical potential of galena and hence, catalyzes the oxidation of xanthate to dixanthogen. The latter role also supports the semi-conductor theory of Plaskin and his co-workers (1957, 1959 and 1963), as increase in electrochemical potential inadvertently changes the surface of n-type galena to p-type.

In 1968, Fuerstenau et al. studied the flotation of pyrite in the presence of xanthate and iron ions. Their studies led to the conclusion that the dixanthogen was the active species responsible for the flotation of pyrite (FeS_2). Meanwhile, Majima and his colleagues carried out electrochemical studies of pyrite in the presence and the absence of xanthate. (Majima and Takeda, 1968; Peters and Majima, 1968). Their work showed that dixanthogen is indubitably the active species formed due to the oxidation of xanthate on pyrite. Since the formation of dixanthogen could not be explained by any of the previous theories, the mixed potential theory became the new focus of the research in the field of sulfide flotation. This led to an extensive electrochemical study of sulfide minerals and their flotation in presence of various sulfyhydryl collectors by various research groups.

(b) Electrochemical Studies

The definitive work in this area came from Allison et al. (1972) and Goold and Finkelstein (1972). Although for past four decades numerous studies had been done on the interaction of sulfide minerals and xanthate collectors, the nature of the product formed on the surface of sulfide minerals was still debatable. For example, Wottgen and Luft (1968) believed that the mixed films of the metal xanthate and dixathogen were formed on all the sulfide minerals, whereas Rao (1969) showed that the species responsible for the hydrophobicity of galena, pyrite and sphalerite were all different. Allison et al. (1972) correlated the reaction products extracted from the xanthate solutions to the rest potential of various sulfide minerals in the solution (Table 1.2). They showed that if the rest potential of the mineral in xanthate solution was above the reversible potential for the formation of dixanthogen, then the dixathogen was primary species. Such minerals were found to be pyrite, aresonpyrite, chalcopyrite, molybdenite and pyrrhotite. In the case of bornite and galena, where the rest potentials were below the reversible potential for xanthate/dixanthogen couple, metal xanthate were detected. For chalcocite and sphalerite, the products could not be positively identified with ethyl xanthate, whereas higher homologues of xanthate exhibited metal xanthate formation. An exception to this generality was covellite which exhibited lower rest potential, yet dixanthogen was detected on its surface. This anomaly was explained in terms of a reaction between xanthate and cupric ions which were released in the solution (Allison et al., 1972).

Goold and Finkelstein (1972) conducted similar experiments with other thiol reagents, viz., sodium diethyl dithiocarbamate (DTC), dithiophosphate (DTP) and mercaptobenzothiazole

(MBT). It was observed that dithiolates (disulfides) formed when the rest potential of the sulfide mineral was above reversible potential for thiol and its dithiolate. For minerals, which exhibited rest potentials below thiol/dithiolate couple, metal thiolate were observed. These results were analogous to the ones obtained by Allison et al. (1972). Although, different research studies have shown influence of disulfides on sulfide minerals' flotation, in industrial practice, dithiolates are never added directly in the flotation pulp. Therefore, Finkelstein and Poling (1977) studied role of dithiolates in the flotation of sulfide minerals, specifically galena. In their experiments, they added dithiolates directly into the flotation system and did not find significant differences compared to addition of thiol reagents.

Winter and Woods (1973) carried out flotation tests for galena in the presence of xanthate and monothiocarbonate (MTC) and correlated flotation efficiency with the redox potential for xanthate/dixanthogen and MTC/carbonate disulfide couples. They observed that the flotation efficiency increased with the ease of oxidation of xanthate and MTC. They concluded that decrease in pH would improve the flotation efficiency because of the two-fold effect. First, low pH may prevent decomposition of adsorbed species and/or replacement by hydroxyl ions. Secondly, a decrease in pH results in decrease in reversible potential of oxygen reduction (by 59 mV per unit pH), thereby increasing the ease of collector oxidation (Winter and Woods, 1973).

Another definitive work on mixed potential theory was produced by Ahmed (1978a & b). He observed that in the absence of oxygen, xanthate is specifically adsorbed thereby rendering surface hydrophilic. Similar observations were also made by Woods (1971) and Poling (1976). This interaction could also be due to the formation of hydrogen-bonded structure with water of hydration on sulfide surfaces (Ahmed 1978a). In the presence of oxygen, the surface is rendered anodic causing reorientation of xanthate ions and rendering surface hydrophobic. He concluded that the catalytic activity for oxygen reduction was dependent on the electronic, crystallographic and surface characteristics of the sulfide. In the following study, he carried out experiments with two galena electrodes kept separately in a galvanic cell (Ahmed 1978b). Oxygen was controlled in one half-cell, while KEX was added in another half-cell maintaining it oxygen free. When both galena electrodes were short-circuited, high galvanic current were observed only when oxygen or hydrogen peroxide (H_2O_2) was passed through one half-cell, while keeping xanthated half-cell oxygen (or H_2O_2) free. From this experimental work, he concluded that the oxidation of xanthate and the reduction of oxygen occur on separate sites and the direct reaction between

xanthate and oxygen does not cause the xanthate adsorption (Ahmed 1978b). Secondly, although dixanthogen is responsible in many sulfide flotation systems, its direct addition is not productive. However, it may render surface hydrophobic when two chemisorbed xanthate ions on the galena surface cross link and form dixanthogen (Ahmed 1978b).

(c) Mixed Potential And Indicator Electrodes

In order to facilitate electrochemical studies and correlate flotation recoveries, it is essential to measure the potential in the flotation systems. A pair of electrodes consisting of an inert indicator electrode and a reference electrode is commonly used for measurements of potential in flotation systems. The most commonly used reference electrode is the standard calomel reference electrode (SCE). The potential measured using SCE can be converted to standard hydrogen scale (SHE) by adding 245 mV to values measured against SCE (Bates, 1964). The choice of indicator electrode depends upon application, but usually platinum is used for such purpose. Other researchers have used different inert indicator electrodes. Before choosing an inert indicator electrode, it is necessary to understand difference between the reversible (rest) and the mixed potential.

When a system is controlled by a single reversible redox couple such as:

$$R_1 + R_2 + \ldots + ne \rightarrow O_1 + O_2 + \ldots \qquad [1.1]$$

the measured potential is the reversible potential of the couple given by the Nernst Equation:

$$E_r = E^0 - (2.303RT/nF)\log(\Sigma O/\Sigma R) \qquad [1.2]$$

In the presence of more than one redox couple in equilibrium (say two), the Equation [1.2] will still hold true because each redox couple will have the same reversible potential. However, the redox couples may not be in equilibrium and have different reversible potentials:

$$Red_1 + n_1e \rightarrow Oxd_1 \qquad E_{r,1} = E_1^{\,0} - (2.303RT/n_1F)\log(Oxd_1/Red_1) \qquad [1.3a]$$

$$Red_2 + n_2e \rightarrow Oxd_2 \qquad E_{r,2} = E_2^{\,0} - (2.303RT/n_2F)\log(Oxd_2/Red_2) \qquad [1.3b]$$

$$E_{r,1} \neq E_{r,2} \qquad [1.3]$$

In such a case, the redox conditions of solutions are represented by two potentials. The inert indicator electrode will measure a potential at which the rate of cathodic process of one redox couple will be equal to the rate of anodic process of the other redox couple. Such a potential will lie in between the reversible potential of the two couples given by Equations [1.3a] – [1.3b], and is referred as to "mixed potential" (Rand and Woods, 1984).

The mixed potential concept can be illustrated with the help of the Evans diagram (Figure 1.1). The Evans diagrams were originally developed for corrosion of metal in acidic solutions and have been used to elucidate xanthate (collector) adsorption on sulfide minerals (Evans and Hoar, 1932; Evans, 1947, 1963; Petrocelli, 1950; Salamy and Nixon, 1953, 1954). As can be seen from Figure 1.1, the top curve represents the cathodic reaction given by Equation [1.3a], whereas, the bottom curve represents an anodic reaction given by Equation [1.3b] in the reverse direction. The electrons generated by anodic reaction (Equation [1.3b]) will be consumed by cathodic reaction (Equation [1.3a]). Therefore, both redox couples will reach a certain rate (given by current) and attain a common potential, know as the "mixed potential", $E_{mix.}$

It has been shown by Rand and Woods (1984) that the value of E_{mix} depends on the nature of the indicator electrode used for potential measurements. For a single redox system, reversible potential, E_r, can be measured by any appropriate indicator electrode. For the mixed-potential systems, potential is determined not only by thermodynamics (the reversible potentials of the individual redox couples), but also by the kinetics of the redox couples (slopes of the lines depicted in Evans diagram, Figure 1.1) at the electrode-solution interface. Different indicator electrodes exhibit different kinetics and rates for redox couples leading to different E_{mix} values for the same system (Rand and Woods, 1984).

Rand and Woods (1984) suggested that the most appropriate indicator electrode for a flotation system would be the one which has been constructed from the minerals being floated. But it has two drawbacks: first, the surface of such electrode might get passivated with the oxidation surface products and it might not respond rapidly to changes in flotation pulp (Rand and Woods, 1984). Secondly, a real flotation system consists of more than one mineral. Therefore, use of a mineral indicator electrode may not give meaningful measurements related to other sulfide minerals. This may require use of several different mineral indictor electrodes (Report for RedDog – Probe, 1994). Various indicator electrodes have been studied and tested: carbon, galena, gold, iridium, platinum, platinum-black, and other mineral electrodes (Natarajan and Iwasaki, 1970, 1973; Rand and Woods, 1984; Zhou and Chander, 1990; Cheng and Iwaskai, 1992).

(d) Summary

It is now very well accepted that the xanthate adsorption on sulfide minerals occurs through a corrosion type mixed potential mechanism. According to the mixed potential theory,

an anodic reaction can occur only if there is a cathodic reaction proceeding at finite rate at that potential (Woods, 1984). For the flotation systems, the cathodic reaction is usually given by the reduction of oxygen:

$$O_2 + 4H^+ + 4e \rightarrow 2H_2O \qquad E_r = 1.23 - 0.059pH \qquad [1.4]$$

The cathodic reduction of oxygen proceeds through different steps depending upon the applied potential and pH (Damjanovic, 1969). The most common ascribed path is through formation of hydrogen peroxide (H_2O_2) (Ahmed 1978b, Haung and Miller, 1978) as follows:

$$O_2 + 2H^+ + 2e \rightarrow H_2O_2 \qquad E_r = 0.68 - 0.059pH \qquad [1.5]$$

$$H_2O_2 + 2H^+ + 2e \rightarrow 2H_2O \qquad E_r = 1.77 - 0.059pH \qquad [1.6]$$

Biegler et al., (1975) also proposed a reaction scheme for cathodic reduction of oxygen; it will be discussed in the next section.

The corresponding anodic reaction involves interaction of xanthate on the sulfide minerals in various ways:

(a) Chemisorption of the xanthate ion (X^-):

$$X^- \rightarrow X_{ads} + e \qquad [1.7]$$

(b) Reaction of xanthate with the sulfide mineral (MS) to form metal xanthate (MX_n):

$$MS + nX^- \rightarrow MX_n + S^0 + ne \qquad [1.8]$$

where, n = oxidation state of metal in the sulfide mineral

At high potentials, sulfoxy species such as sulfate (SO_4^{2-}) may form instead of elemental sulfur as given by overall reaction:

$$MS + nX^- + 4H_2O \rightarrow MX_n + SO_4^{2-} + 8H^+ + (6+n)e \qquad [1.9]$$

(c) Oxidation of xanthate to dixanthogen (X_2) at the mineral surface:

$$2X^- \rightarrow X_2 + 2e \qquad [1.10]$$

It is important to note here that all of the xanthate oxidation products render mineral surface hydrophobic. Figure 1.2 shows the schematic representation of anodic reactions (Equations [1.7] – [1.10]) coupled with cathodic reduction of oxygen (Equation [1.4]) (Woods, 1984).

Figure 1.3 shows the Evans diagram for these redox couples. The mixed potential of the sulfide mineral in the flotation pulp will determine the oxidation product on its surface. If the mixed potential of the mineral in the presence of oxygen, xanthate and other reagents is above the mixed potential for X^-/X_2 redox couple ($E_{mix}^{X_2}$), then dixanthogen would be the surface product. In case of a lower mixed potential, either metal xanthate or chemisorbed xanthate

would render the surface hydrophobic. Table 1.2 shows the correlation between the potential and the xanthate oxidation product (Allison et al., 1972 and Goold and Finkelstein, 1972).

1.2.2. Electrochemical Studies

Despite the definitive works done by Ahmed, Allison, Goold, Finkelstein, Richardson, Woods and other researchers, the surface products are still debatable. The differences can be attributed to both the experimental techniques as well as the thermodynamic aspects of predictions. In most of the studies, the products were extracted from the solution, dried and studied using various spectroscopy techniques. The extraction may be biased against strongly bound products and the whole process may alter the products (Allison et al. 1972). On the other hand, the thermodynamic predictions based on the rest potentials refer to bulk species, whereas flotation involves sub-monolayer quantities of surface species (Woods, 1976). The thermodynamic properties of sub-monolayer of surface species may differ significantly from the equivalent bulk species, thereby deviating from thermodynamic predictions (Sutherland and Wark, 1955; Woods, 1984). Secondly, it has been shown that disulfides may be detected on the surface when added excessively, even when the rest potentials do not suggest presence of disulfides (Finkelstein and Poling, 1977). They also observed the formation of metal xanthate and chemisorbed xanthate even when the rest potentials suggested formation of dithiolates.

Galena can be cited as example, for which different researchers have claimed different surface products. For example, Wottegen and Luft (1968), Tolun and co-workers (1963, 1969) and Woods (1971) believed the oxidation product on galena to be dixanthogen, whereas Leja et al., (1963), Finkelstein and Poling (1977), Leppinen and Rastas (1986) and Persson (1994) concluded it to be lead xanthate. Prasad and Rao (1970) calculated the surface product to be a mixed film of lead xanthate and dixanthogen in the ratio of 3:1.

Another dimension to this controversy arises due to the chemisorption of thiol collectors on the sulfide minerals. Woods and his colleagues studied metals and sulfide minerals (more specifically galena) under xanthate solutions and detected chemisorbed xanthate with cyclic voltammetry, contact angle measurements and XPS (Woods, 1971 and 1988; Gardner and Woods, 1973, 1974 and 1977; Buckley and Woods, 1991, 1993, 1994, 1995 and 1997; Woods et al., 1990, 1992, 1993, 1994, 1995 and 1997). It was observed that the xanthate chemisorbs well below the potentials for formation of metal xanthate and dixanthogen and chemisorbed species are hydrophobic enough to float galena. The correlation with flotation work of Guy and Trahar

(1984) and potential dependence of flotation observed by Rastas et al. (1990 – with Leppinen) showed that the flotation commenced with very low coverage of chemisorbed xanthate (Woods, 1996). Similar observations were made by other researchers on galena (Richardson and O'Dell, 1984 and 1985), chalcocite (Kowal and Pomianowski, 1973; O'Dell et al., 1984 and 1986; Richardson et al., 1984; Basilio et al., 1985), copper (Szeglowski et al, 1977; Taloenen et al., 1991). Chander and Fuerstenau (1974 and 1975) also observed the chemisorption with diethyl dithiophospahte (DTP) on chalcocite. Therefore, Gardner and Woods (1977) concluded that the chemisorbed xanthate is sufficiently hydrophobic to float galena and dixanthogen is not essential for galena flotation. However, the presence of dixanthogen enhances the hydrophobicity of galena in addition to the chemisorbed layer (Gardner and Woods, 1977).

1.2.3. Oxygen Reduction Studies

Despite the fact that the reduction of oxygen constitutes one half of the process of collector adsorption on the sulfide minerals, it has received only limited attention. Tolun and Kitchener (1964) developed polarograms for aerated solutions on platinum, lead and galena. Similarly, Peters and Majima (1968) developed polarization curve for oxygen reduction on pyrite. However, there was not sufficient data to obtain kinetic parameters for oxygen reduction. Toperi and Tolun (1969) further studied oxygen reduction and developed polarograms on platinum and galena in oxygenated, aerated and nitrogenated (containing very small amount of oxygen) solutions. The potential for zero current was highest for oxygenated and least for nitrogenated solutions. Also, they observed that the zero-current-potential decreased by 59 mV per pH unit. This result is consistent with the Nernst equation for oxygen reduction (Equation [1.4]). However, their work was more concentrated on oxidation and reduction of pyrite rather than on oxygen reduction.

The most interesting work on oxygen reduction was carried out by Biegler, Rand and Woods (1975). They prepared rotating pyrite electrodes and conducted cyclic voltammetry in 1 M perchloric acid. The cathodic currents were also recorded for other pH values. Their results indicated that at low pHs (< 7), the rate-determining step is the first electron transfer to form O_2^- as follows:

$$O_2 + e \rightarrow O_2^- \qquad [1.11]$$

For alkaline solutions, they proposed the cathodic reduction of oxygen *via* following reaction scheme:

$$O_2(\text{bulk}) \xrightarrow{a} O_2(\text{surface}) \xrightarrow{b} H_2O_2(\text{surface}) \xrightarrow{c} H_2O \qquad [1.12]$$
$$\downarrow d$$
$$H_2O_2(\text{bulk})$$

where H_2O_2 formation proceeds through formation of O_2^- and second electron addition. The Tafel slopes and current vs. rotational speed suggested that for alkaline solutions, the rates of subsequent steps (Equation [1.12]) are also important in rate-determining step.

In a following study, Biegler (1976) studied different pyrite specimens. The specimens were characterized into according to their semiconducting properties, viz. n-type, n-type metallic and p-type. Although the voltammograms, Tafel slopes and electrocatalytic activity of oxygen differed for each sample, no correlation was observed with the semiconducting properties of pyrite. The differences were attributed mainly to the impurities. Rand (1977) extended similar studies to the other sulfide minerals: arsenopyrite, bornite, chalcocite, chalcopyrite, covellite, galena, pentlandite, pyrite and pyrrhotite. Figure 1.4 shows the activity of sulfide minerals for the oxygen reduction in acidic and alkaline solutions (Biegler et al., 1977; Rand, 1977). As it can be seen from the figure, pyrite is the most active (better catalyst for oxygen reduction) among the sulfide minerals and approach the activity of gold. The sulfide minerals were ranked on the basis of catalytic activity, which correlated very well with the requirement of oxygen in flotation with xanthate determined by Plaskin and Bessonov (1957). The exception to this generality was galena. Galena exhibited least activity, i.e., it was the poorest catalyst, yet required the least amount of oxygen. Rand (1977) proposed that this anomaly might be due to the difference in nature of the hydrophobic surface compared to that of other sulfide minerals.

Pillai and Bockris (1984) studied reduction of oxygen on pyrite at pH 9.1 using steady state polarization (Tafel) technique and developed Tafel plots (E vs. log *i*) for partial pressure (pO_2) of 1 and 0.33. The Tafel plots for oxygen reduction were mixed and matched with the same for xanthate oxidation in the presence and absence of oxygen. Based on their results, they considered 17 reaction schemes for oxygen reduction and proposed the following one:

$$O_2 + H_2O \leftrightarrow [O_2H^+]_{ads} + OH^- \qquad [1.13a]$$

$$[O_2H^+]_{ads} + e \rightarrow [O_2H]_{ads} \qquad [1.13b]$$

$$[O_2H]_{ads} + e \leftrightarrow [O_2H^-]_{ads} \qquad [1.13c]$$

$$[O_2H^-]_{ads} \leftrightarrow \tfrac{1}{2}O_2 + OH^- \qquad [1.13d]$$

$$O_2 + 2H_2O + 4e \leftrightarrow 4OH^- \qquad [1.13]$$

In this reaction scheme, the reaction 1.13b was ascribed as the rate-determining step with the condition that both species in the reaction are present at "limitingly low coverage" (Pillai and Bockris, 1984). For more reaction schemes, please refer to Appendix in their publication (1984).

Doo and Sohn (1989) studied oxygen reduction in acidic solutions using d.c. polarization and a.c. impedance spectroscopy. Their results were consistent with Biegler et al. (1975). They concluded that above 0 V (SHE), formation of superoxide (O_2^-) was the rate-determining step, whereas below 0 V, formation of hydrogen peroxide (H_2O_2) was the rate-determining step. Ahlberg and Broo (1996a, b & c, 1997) studied oxygen reduction on galena, gold, platinum and pyrite in the presence and absence of xanthate using cyclic voltammetry technique on rotating ring disc electrodes (RRDE). Their results were consistent with that of Biegler et al., (1975). The rate-determining step was ascribed as first electron transfer and formation of O_2^- (Equation [1.11]). The oxygen reduction mechanism suggested by Alhberg and Broo (1996a &b) is almost similar to one resolved by Biegler et al., (1975) as given by Equation [1.12].

Alhberg and Broo (1996b) detected H_2O_2 while studying oxygen reduction on pyrite, gold and platinum in the presence of xanthate. It was speculated that H_2O_2 may react with xanthate leading to formation of perxanthate and play important role in flotation of pyrite (Ahlberg and Broo, 1996a). Jones and Woodcock (1978, 1979) have described perxanthate to attribute hydrophobicity in the flotation systems and supported mixed potential theory through formation of perxanthate. However, the UV spectrophotometry revealed that the rate of reaction between H_2O_2 and xanthate was too slow to be of any significance in the flotation of pyrite (Ahlberg and Broo, 1996b).

1.2.4. Natural/Collectorless Flotation

Natural hydrophobicity of sulfide minerals is the second most debatable issue in the field of sulfide flotation. Various schools of thoughts differ not only on the issue of whether sulfide are naturally hydrophobic or not, but also on the reasons behind the either case. Although as early as in 1930s, Ravitz and his colleague (1933 and 1940) suggested that galena is naturally hydrophobic, the issue is still questioned. Based on the type of intrinsic bonding (ionic, metallic or covalent) and presence of residual bonds, which controls the structure and polarity of the surfaces, Gaudin (1957) classified crystal types (atomic, molecular, ionic, metallic, etc.) to their native floatability. According to this classification, a vast majority of sulfide minerals are hydrophilic. Gaudin (1957) suggested that the native floatability of minerals is due to either

contamination of surface by hydrocarbon bearing groups or the intentional modification of the surface. However, Chander (1988, 1999) quotes Gaudin (1932) that the surfaces formed due to rupture of van der Waals bonds are naturally hydrophobic.

In order to characterize natural hydrophobicity and identify the causes, several researchers conducted flotation tests under various conditions. Lepetic (1974) found that dry-ground chalcopyrite floated well without collector. Finkelstein et al. (1975) conducted a comprehensive study on floatability of several sulfide minerals and observed chalcopyrite, pyrite and stibnite floated well without collector under different conditions, whereas galena exhibited low floatability (10-15%). Orpiment, realgar and molybdenite floated under all the conditions investigated, which might be explained on the basis of lattice structure and bonding (Gaudin et al., 1957; Rogers, 1962). Stibnite was also observed to be naturally floatable, however, the reasons behind it are not well understood (Arbiter et al., 1975; 1960; Hough and White, 1980; Kitchener, 1984; Ralston, 1991). Experiments by Finkelstein et al. (1975) produced some anomalous results related with sulfur. They observed that sulfide minerals could be rendered floatable by the presence of sulfur at their surfaces; however, they could not establish a correlation between amount of sulfur on surface (even for several hypothetical layers) and degree of floatability. It was suggested that it could be due to the co-presence of other hydrophilic oxidation products, such as sulfates and hydroxides. However, flotation was also observed with sulfur-free and oxidized samples. On the basis of cluster formation mechanism suggested by Eadington and Prosser (1969), they also proposed that this anomaly could be due to the redistribution and recrystallization of sulfur at surface in patches rendering hydrophobic only a small fraction of the total surface. Consequently, they concluded that sulfide minerals are not either strongly hydrophobic or hydrophilic. The natural floatability of sulfide minerals depends upon not only the type of hydrophobic entity on the surface, but also on the intrinsic nature of the mineral.

Another explanation for natural floatability for sulfide minerals was that unlike oxides, sulfur of sulfide minerals does not form hydrogen bond with water and therefore, is weakly hydrated and does not interact with water (Ravitz and Porter, 1933; Finkelstein, 1975; Fuerstenau and Sabacky, 1981). The experimental results by Fuerstenau and Sabacky (1981) showed that the surfaces of chalcocite, chalcopyrite, galena and pyrite were more hydrophobic than hydrophilic. The surface of sphalerite was in between air and water and the natural

hydrophobicity increased with activation with cupric (Cu^{2+}) ions compatible with natural hydrophobicities of copper sulfide minerals (Finkelstein et al., 1975; Fuerstenau and Sabacky, 1981; Yoon, 1981). They proposed that, however, in the presence of oxygen, oxidation of surface would result in hydrophilic sulfoxy species.

(a) Role Of Oxygen

The role of oxygen in natural hydrophobicity is also highly debatable. Plaskin (1959) suggested that adsorbed oxygen decreases surface hydration rendering it hydrophobic. As described earlier, Plaskin and Shafeev suggested that molecular oxygen converts n-type galena to p-type enriching the surface with sulfur. Heyes and Trahar (1977) observed that mild oxidation is required for collectorless flotation of chalcopyrite. Gardner and Woods (1979) and Trahar (1983) also proposed that oxidizing conditions were required for flotation of chalcopyrite. According to them, the oxidation of chalcopyrite led to formation of hydrophobic elemental sulfur, S^0, responsible for flotation. This hypothesis was originally proposed by Wark (1938). Miller (1988) also suggested that even in oxygen-free solutions, sufficient oxygen remains to oxidize sulfide leading to formation of hydrophobic elemental sulfur. In contrast, Fuerstenau and Sabacky (1981) concluded that presence of oxygen would cause formation of hydrophilic oxidation products and strip sulfide minerals of their natural floatability. Chander and Fuerstenau (1972) also observed that the hydrophobicity of molybdenite decreased when the samples were oxidized. They suggested that it might be due to the formation of insoluble oxidized as confirmed by cleansing with water and KOH.

Yoon (1981) observed collectorless flotation of chalcopyrite in presence of Na_2S, a strong reducing agent used for cleaning surfaces for oxidation products. He suggested that sulfide ions would displace the hydrophilic sulfoxy products from the surface, thereby restoring fresh unoxidized surface, which may be naturally hydrophobic. Also, chalcopyrite surface was analyzed using ECSA and elemental sulfur was not detected (Pritzker et al., 1980). This may be due to either insensitivity of ESCA to elemental sulfur or low quantity of sulfur. This was in agreement with Heyes and Trahar (1977) who could not detect elemental sulfur on chalcopyrite too. However, Buckley and Woods (1984) detected elemental sulfur on oxidized chalcopyrite using ESCA. Walker et al. (1984) studied chalcocite using microflotation electrochemical cell at alkaline pH. They observed that chalcocite floated only between –0.1 through –0.5 V (SHE). They suggested that it could be due to formation of Cu_2S or other CuS species along with

elemental or excess sulfur. At reducing potentials (e.g., -0.6 V), the surface is rendered hydrophilic due to formation of $Cu(OH)_2$ on Cu enriched surface, whereas at oxidizing potentials, surface is hydrophilic due to soluble sulfoxy or hydroxide species.

Buckley et al. (1984, 1985 and 1987) and Woods (1987) proposed formation of hydrophobic metal-deficient sulfur layer upon mild oxidation. Pang and Chander (1993) also observed formation of iron oxide on chalcopyrite and agreed that a metal deficient layer (specifically, iron deficient layer on chalcopyrite) can be floated without collector. Chander and Briceno (1989) distinguished three different forms of sulfur on oxidized gold surface: atomic sulfur, S^0, polysulfides, S_{x+1}^{2-}, and elemental sulfur represented by S_8. They observed that polysulfides and elemental sulfur in S_8 form rendered the gold surface hydrophobic.

Luttrell and Yoon (1984a and b) carried out flotation and surface studies of chalcopyrite in sodium sulfide (Na_2S). Although Yoon (1981) had suggested that Na_2S displaces hydrophilic sulfoxy species and creates fresh unoxidized surface, which may be naturally hydrophobic, latest findings differed slightly. According to Luttrell and Yoon (1984a and b), although Na_2S striped the surface of hydrophilic species, slightly oxidizing conditions were still required for collectorless flotation of chalcopyrite. These findings unequivocally supported previous findings that oxidizing conditions were required for collectorless flotation, but it was not the sole critrion (Heyes and Trahar, 1977; Gardner and Woods, 1979; Buckley and Woods, 1984; Trahar, 1983; Guy and Trahar, 1984; Miller, 1988). Based on flotation and surface studies, they concluded that Na_2S played a two-fold role. First, it displaced the hydrophilic sulfoxy species, such as SO_4^{2-} and $S_2O_3^{2-}$, and created relatively fresh surface. Secondly, it sulfidized the mineral surface, which under slight oxidation led to formation of hydrophobic sulfur species. However, caution was prescribed for amount of Na_2S to be added as excess sulfide ions may depress the potential and hence, the flotation. It was observed that when oxygen was introduced, the oxidation of these reductant species would speed up increasing the potential rapidly and improving flotation recovery. Similar observations were made by Trahar (1983) and Crayon (1983). The increase in recovery was also observed with decreasing pH as explained in following paragraphs.

The most important conclusion from the work of Luttrell and Yoon (1984a and b) was the role of polysulfides in the collectorless flotation of chalcopyrite. It was proposed that although elemental sulfur was important, it was not the sole species responsible for the collectorless flotation. This conclusion was drawn on the basis that elemental sulfur was not

detected unambiguously on the chalcopyrite surface (Buckley and Woods, 1984; Yoon, 1981; Luttrell and Yoon, 1984b). Also, no correlation could be established between sulfur and flotation recoveries (Finkelstein et al., 1975; Luttrell and Yoon, 1984b). Luttrell and Yoon (1984a and b) suggested that polysulfides (S_n^{2-}; $2 \leq n \leq 8$), rather than elemental sulfur, may be responsible for collectorless flotation at alkaline pH values. The formation of polysulfides, similar to elemental sulfur, is also favored at oxidizing potentials. Hamilton and Woods (1983 and 1984) and Chander and Briceno (1989) have also observed formation of polysulfides on gold in alkaline pH. Mycroft et al (1990) also detected polysulfides on electrochemically oxidized pyrite using XPS and Raman spectroscopy. They suggested that the polysulfides are metastable and intermediate species in the formation of sulfur. According to Chen and his colleagues (1972 and 1973), the stability of polysulfides is critically dependent upon pH. Since elemental sulfur is likely to be more hydrophobic than polysulfides, it flotation recovery increase with decrease in pH as observed. Finally, Luttrell and Yoon (1984a) concluded that excess sulfide ions may be oxidized to elemental sulfur or polysulfides, depending upon pH, and may deposit on the mineral surface rendering it more hydrophobic.

Kocabag et al. (1990a and b) investigated oleophilicity (oil-loving)/hydrophobicity of galena and pyrite by using two-fluid flotation (iso-octane and water) under controlled redox and pH conditions. They measured contact angles at mineral-oil (or gas)-water interfaces in order to study the wettability of the minerals. Although they interchangeably used oleophilicity with hydrophobicity, their results showed that oleophilic did not turn out to be exactly hydrophobic. Unoxidized galena and pyrite were oleophilic in mineral-oil-water system, but hydrophilic in mineral-gas-water system. The effect of oxidation was pH dependent: at acidic pHs, oleophilicity increased due to formation of sulfur, whereas at alkaline and neutral pH values, it decreased due to the formation of metal hydroxides and/or sulphoxy compounds. Liu and Somasundaran (1994) studied role of n-dodecane and alcoholic frothers on separation of pyrite from coal. They also observed that pyrite was oeleophilic at oil-water interface, but hydrophilic at air-water inetrface.

(b) Ranking

Ralston (1991) used data from Fuerstenau and Sabacky (1981), Heyes and Trahar (1979) and Guy and Trahar (1984) to rank sulfide minerals according to their natural hydrophobicities. The general order was found, in descending-order, as follows:

Chalcopyrite > Galena > Pyrrhotite > Pentlandite > Covellite > Bornite > Chalcocite > Sphalerite > Pyrite > Arsenopyrite.

Ralston (1991) correlated the natural floatability of sulfide minerals with their rest potentials. He observed that, except for chalcopyrite, the collectorless floatability of sulfide minerals decreased with increasing rest potentials. This could be attributed to the difficulty in oxidation of sulfide minerals as suggested by Ralston (1991): the more cathodic or reducing the rest potential and the less easily oxidized the sulphide mineral, the more readily it floats without a collector.

1.3. REPORT LAYOUT

The overall objective of this investigation was to study the oxidation of sulfide minerals and the adsorption of xanthate. Therefore, different sulfide minerals were studied using various electrochemical techniques in order to achieve the particular objective. Each chapter (2 – 5) consist of an introduction, objective, experimental techniques, results, discussion and conclusion section.

In Chapter 2, pyrite has been studied using Electrochemical Impedance Spectroscopy (EIS). Pyrite is one of the most abundant sulfide minerals, yet it is economically insignificant. Beside poor economic values, it is a major source of pollution (SO_2 emission, acid mine drainage). Therefore the rejection of pyrite is desired. However, the separation of pyrite from other minerals and coal has proven to be difficult because of its self-induced hydrophobicity arising from superficial oxidation. Chapter 2 investigates superficial and incipient oxidation of pyrite using EIS.

It has been mentioned numerous times that oxygen is required for adsorption of xanthate on sulfide minerals. However, a study at Red Dog concentrators (Alaska) revealed that despite low oxygen levels, minerals were being floated. The chemical analysis of concentrators showed that iron was present at high levels. Chapter 3 investigates the possibility that iron ions in their oxidized form (ferric, Fe^{3+}) may enact the role of oxygen and render the minerals floatable.

Numerous studies of xanthate-sulfide interactions have focused on the oxidation products and generating the thermodynamic data, but only limited studies have been geared towards measuring kinetic parameters of the redox processes. In Chapter 4, Tafel studies have been aimed towards measuring the rate of reaction and estimating activation energy for adsorption of xanthate on the sulfide minerals, such as, pyrite, pyrrhotite (pure and nickel-activated),

chalcocite and covellite. Tafel plots are commonly used in corrosion studies for rate measurements.

Similar to pyrite, pyrrhotite is an abundant sulfide mineral with almost no economic value and high pollution menaces. Therefore its separation is desired from copper-nickel ores, which is difficult to achieve without the aid of depressants. Recently DETA and SO_2 have been patented as pyrrhotite depressants. Various mechanisms for their depressing actions have been speculated by patentee. Chapter 5 investigates the mechanisms, specifically electrochemical, of pyrrhotite depression by DETA, SO_2 and their combination. Finally, conclusions from the present study have been summarized in Chapter 6.

1.4. REFERENCES

Agar, G.E., Kipkie, W.B. and Wells, P.F., 1982. Canadian Patent No. 1104274.

Ahlberg, E. and Broo, A.E, 1996a. *IJMP*, **46**, 73-89.

Ahlberg, E. and Broo, A.E, 1997. *J. ECS*, **144(4)**, 1281-1286. 1997.

Ahlberg, E. and Broo, A.E., 1988. Proc. Intl. Symp. Electrochem. in Mineral and Metal Process. II (Eds. P.E. Richardson and R. Woods). ECS: Pennington (NJ) 36-48.

Ahlberg, E. and Broo, A.E., 1996b. *IJMP*, **47**, 33-47.

Ahlberg, E. and Broo, A.E., 1996c. *IJMP*, **47**, 49-60.

Ahmed, S.M., 1978a. *IJMP*, **5**, 163-174.

Ahmed, S.M., 1978b. *IJMP*, **5**, 175-182.

Allison, S.A., Goold, L.A., Nicol, M.J. and Granville, A., 1972. *Metall Trans.*, **3**, 2613-2618.

Aplan, F.F. and Chander, S., 1988. Reagents in Mineral Technology (Eds. P. Somasundaran and B.M. Moudgil). Marcel Dekker: New York. Ch 10, 335-369.

Arbiter, N., Fuji, V., Hansen B. and Raja A., 1975. Advances in Interfacial Phenomena of Particulate/Solution/Gas Systems (Eds. P. Somasundaran and R.B. Grieves). AIChE: New York. **71(150)**, 176-182.

Barksy, G., 1934. *Trans AIME*, **112**, 236.

Basilio, Pritzker and Yoon, 1985. SME Annual Meeting, New York (NY). SME: Littleton (CO). Preprint No. 85-86.

Buckley, A.N. and Woods, R., 1990. *IJMP*, **28**, 301-311.

Buckley, A.N. and Woods, R., 1991. *Surf. Interf. Anal.*, **17**, 655-659.

Buckley, A.N. and Woods, R., 1993. *J. Electroanal. Chem. Interf. Electrochem*, **357**, 387-405.

Buckley, A.N. and Woods, R., 1994. *Coll. Surf.*, **89**, 71-76.

Buckley, A.N. and Woods, R., 1995. *Coll. Surf.*, **104**, 295-305..

Buckley, A.N. and Woods, R., 1997. *IJMP*, **51**, 15-26.

Buckley, Hamilton and Woods, 1985. Flotation of Sulfide Minerals (Ed. K.S.E. Forssberg). 41-60.

Cander, S., 1988. Reagents in Mineral Technology (Eds. P. Somasundaran and B.M. Moudgil). Marcel Dekker: New York. Ch 14, 429-469.

Chander, S. and Briceno, A., 1988. SME Annual Meeting, Phoenix (AZ). SME: Littleton (CO).

Chander, S. and Briceno, A., 1989. Precious and Rare Metal Tech. (Eds. A.E. Torma and I.H. Gundiler). Elsevier: New York. 137-148.

Chander, S. and Fuerstenau, D.W., 1972. *Trans AIME*, **252**, 62-69.

Chander, S. and Fuerstenau, D.W., 1974. *Trans AIME*, **256**, 193-196.

Chander, S. and Fuerstenau, D.W., 1975. *Trans AIME/SME*, **258**, 284-285.

Chander, S., 1999.Advances in Flotation Technology (Eds. B.K. Parekh and J.D. Miller). SME: Littleton (CO). 129-145.

Chander, S., Pang, J. and Briceno, A., 1988. Proc. Intl. Symp. Electrochem. in Mineral and Metal Process. II (Eds. P.E. Richardson and R. Woods). ECS: Pennington (NJ). 247-263.

Cheng, X. and Iwasaki, I., 1992. *Minl. Pro. Extract. Metall.*, **11**, 187-210.

Cook, M.A. and Last, A.W., 1959. Utah Engg. Exp. Station. Bulletin 449.

Cook, M.A. and Nixon, J.C., 1950. *J. Phy. Coll. Chem.*, **54**, 445-459.

Cook, M.A. and Wadsworth, M.E., 1957. Proc. 2nd Intl Cong. on Surf Act. (Ed. J.H. Schulman). **3**, 228-242.

Crayon, 1983

Damjanovic, A., 1969. Modern Aspects of Electrochemistry, 5 (Eds. J.O'M Bockris and B.E. Conway). 369-485.

Eadington, P. and Prosser, A.P., 1969. *Trans IMM, Sect. C: Min. Pro. Ext. Metall.* **78**, 74-82.

Evans, U.R. and Hoar, T.P., 1932. *Proc. Royal. Soc. London*, **137**, 343-365.

Evans, U.R., 1947. Proc. 11th Intl Cong Pure Appl Chem. Lond. **5**, 743.

Finkelstein, N.P. and Poling, G.W., 1977. *Minl Sci. Engg.* **9(4)**, 177-197.

Finkelstein, N.P., Allsion, S.A., Lovell, V.M. and Stewart, B.V., 1975. Advances in Interf Pheno. of Particulate/Solution/Gas Systems (Eds. P. Somasundaran and R.B. Grieves). AIChE: New York. **71(150)**, 165-175.

Fletcher, S. and Horne, M.D., 1991. *IJMP*, **33**, 145-163.

Fuerstenau, D.W., 1999. Advances in Flotation Technology (Eds. B.K. Parekh and J.D. Miller). SME: Littleton (CO). 3-21.

Fuerstenau, M.C. and Sabacky, B.J., 1981. *IJMP*, **8**, 79-84.

Fuerstenau, M.C., 1999. Advances in Flotation Technology (Eds. B.K. Parekh and J.D. Miller). SME: Littleton (CO). xi-xxxiii.

Fuerstenau, M.C., Kuhn, M.C. and Elgillani, D.A., 1968. *Trans SME/AIME*, **241**, 148-156.

Gardner, J.R. and Woods, R, 1974. *Aust J. Chem.*, **27**, 2139.

Gardner, J.R. and Woods, R, 1974. *Aust J. Chem.*, **30**, 981-991.

Gardner, J.R. and Woods, R., 1973. *Aust J. Chem.*, **26**, 1635-1644.

Gardner, J.R. and Woods, R., 1979a. *IJMP*, **6**. 1-16. 1979

Gardner, J.R. and Woods, R., 1979b. *J. Electroanal. Chem. Interf. Electrochem*, **100**. 447-459. 1979

Gaudin, A.M. and Finkelstein, N.P., 1965. *Nature*, **July 24**, 389-391.

Gaudin, A.M. and Schuhmann, R., 1936. *J. Phys. Chem.*, **40**, 257.

Gaudin, A.M., 1929. *Mining and Met*., **10**, 19.

Gaudin, A.M., 1930. *Trans AIME*, **87**, 417.

Gaudin, A.M., 1932. Flotation, 1st Ed., McGraw-Hill: New York.

Gaudin, A.M., 1957. Flotation, 2nd Ed., McGraw-Hill: New York.

Gaudin, A.M., Fuerstenau, D.W. and Turkanis, M.M., 1957. *Trans AIME*, **208**, 65.

Gaudin, A.M., Haynes, C.B. and Haas, E.C., 1930. Tech. Paper No. 7, Univ. of Utah nd USBM.

Gaudin, A.M., Miaw, H.L. and Spedden, H.R., 1957. Proc. 2nd Intl Cong. on Surf Act. (Ed. J.H. Schulman). **3**, 202-219.

Gebhardt, J.E. and Richardson, P.E., 1987. *Minl Metall. Process.* **Aug.** 140-145.

Goold, L.A. and Finkelstein, N.P., 1972. Report No. 1439, NIM, South Africa.

Grandke, T. and Cardona, M., 1980. *Surf Sci.*, **92**, 385-392.

Granville, A., Finkelstein N.P. and Allsion, S.A., 1972. *Trans IMM*, C1-C30.

Guarnaschelli, C., 1970. *Trans SME/AIME*, **247**, 324-329.

Guy, P.J. and Trahar, W.J., 1984. *IJMP*, **12**, 15-38.

Hamilton, I.C. and Woods, R., 1983. *J. App. Electrochem.* **13**, 783-794.

Hamilton, I.C. and Woods, R., 1984. Proc. Intl. Symp. Electrochem. in Mineral and Metal Process. I (Eds. P.E. Richardson, S. Srinivasan and R. Woods). ECS, Pennington (NJ). 259-285.

Harris, P.J. 1988. Reagents in Mineral Technology (Eds. P. Somasundaran and B.M. Moudgil). Marcel Dekker: New York. Ch 11, 371-384.

Haung, H.H. and Miller, J.D., 1978. *IJMP*, **5**, 241-266.

Heyes, G.W., and Trahar, W.J., 1977. *IJMP*, **4**, 317-344.

Heyes, G.W., and Trahar, W.J., 1979. *IJMP*, **6**, 229-252.

Jones, M.H. and Woodcock, J.T., 1978. *IJMP*, **5**, 285-296.

Jones, M.H. and Woodcock, J.T., 1979, *Talanta*, **26**, 815-820.

Kellogg, H.H. and V-Rosas, H., 1945. *Min. Tech.*, **Nov**.

Kitchener, J.A., 1984. Principles of Minerals Flotation: The Wark Symposium (Eds. M.H. Jones and J.T. Woodcock), AusIMM. No. 40

Last, G.A. and Cook, M.A., 1952. *J. Phys. Chem.*, **56**, 637.

Leja, J., 1982. Surface Chemsitry of Froth Flotation. Plenum: New York (NY).

Leja, J., Little, L.H. and Poling, G.W., 1963. *Trans IMM*, **72**, 407-423.

Lepetic, V.M., 1974. *CIM Bulletin*, **67**, 71.

Leppinen, J.O. and Rastas, J.K., 1986. *Coll. Surf.*, **20**, 259.

Liu, D. and Somasundaran, P., 1994. *IJMP*, **41**, 227-238.

Luttrell, G.H. and Yoon, R.-H., 1984a. *IJMP*, **13**, 271-283.

Luttrell, G.H. and Yoon, R.-H., 1984b. *Coll. Surf.* **12**, 239-254.

Majima, H. and Takeda, M., 1968. *Trans. SME*, **241**, 431-436.

Majima, H., 1969. *Can. Metall. Quart.*, **8(3)**, 269-273.

Mao, L. and Yoon, R.-H., 1997. *IJMP*, **51**, 171-181.

Martin C.J., Rao, S.R., Finch, J.A. and Leroux, M., 1989, *IJMP*, **26**, 95-110.

Mycroft, J.R., Bancroft, G.M., McIntyre, N.S., Lorimer, J.W. and Hill, I.R., 1990. *J. Electroanal. Chem. Interf. Electrochem*, **292**, 139-152.

Natarajan, K.A. and Iwasaki, I., 1970. *Trans SME/AIME*, **247**, 317.

Natarajan, K.A. and Iwasaki, I., 1973. *Trans SME/AIME*, **254**, 323-328.

O'Dell, C.S., Dooley, R.K., Walker G.W. and Richardson, P.E., 1984. Proc. Intl. Symp. Electrochem. in Mineral and Metal Process. I (Eds. P.E. Richardson, S. Srinivasan and R. Woods). ECS: Pennington (NJ), 81-95.

O'Dell, C.S., Walker, G.W. and Richardson, P.E., 1986. *J. App. Electrochem.*, **16**, 544-554.

Pang, J. and Chander S., 1993. Proceedings of XVIII International Mineral Processing Congress, Sydney, 669-677.

Pazhianur, R.R., 1999. Dissertation, Virginia Polytech. Insti. And State Univ. Virginia (USA).

Persson, I., 1994. *J. Coord. Chem.*, **32**, 261-342.

Pillai, K.C. and Bockris, J.O'M., 1984. *J. ECS.*, **131**, 568-572.

Plaksin, I.N. and Shafeev, R.Sh., 1963. *Bull IMM*, **72**, 715-722.

Plaskin, I.N. and Bessonov, S.V., 1957. Proc. 2nd Intl Cong. on Surf Act. (Ed. J.H. Schulman). **3**, 361-367.

Plaskin, I.N., 1959. *Min. Engg.*, **March**, 319-324.

Poling, G.W, and Leja, J., 1963. *J. Phy. Chem*, **67**, 2121-2126.

Ralston, J., 1991. *Minl Engg.* **4(7-11)**, 859-878.

Rao, S.R., 1969. *Sepn Sci.*, **4(5)**, 357-411.

Rastas, J.K., Sten P.M. and Leppinen, J.O., 1990. *Coll Surf.*, **29(4)**, 249-255.

Richardson, P.E. and Walker, G.W., 1985. Proceedings of the XVth International Mineral Processing Congress, Cannes. **2**, 198-210.

Richardson, P.E., and Eldelstein, D.L., 1978. Information Circular 8818. USBM. 72-99

Richardson, P.E., and Maust, E.E., Jr., 1976. Flotation – Gaudin Memorial Volume (Ed. M.C. Fuerstenau). AIME: New York. **1**, 364.

Richardson, P.E., and O' Dell, C.S., 1984. Proc. Intl. Symp. Electrochem. in Mineral and Metal Process. I (Eds. P.E. Richardson, S. Srinivasan and R. Woods). ECS: Pennington (NJ), 132-151.

Salamy, S.G. and Nixon, J.C., 1953. Recent Developments in Mineral Dressing. IMM. 503-516..

Salamy, S.G. and Nixon, J.C., 1954. *Aust J. Chem.* **7**, 146-156.

Senior, G.D., Shannon, L.K. and Trahar, W.J., 1994. *IJMP*, **42**, 169-190.

Steininger, J., 1968. *Trans SME*, **Mar**, 34-42.

Sutherland, K.L. and Wark, I.W., 1955. Principles of Flotation. AusIMM.

Szeglowski, Z., Czarnecki, J., Kowal, A. and Pomianowski, A., 1977. *Trans IMM*, C115-C118.

Taggart, A.F. and Arbiter, N., 1943. *Trans AIME*, **153**, 500.

Taggart, A.F. and Arbiter, N., 1944. *Mining Technology*, **May**, No.1.

Taggart, A.F., 1945. Handbook of Mineral Dressing. John Wiley: New York.

Taggart, A.F., del Guidice, G.R.M. and Ziehl, O.A., 1934. *Trans AIME.* **112**, 348.

Taggart, A.F., Taylor, T.C. and Ince, C.R., 1930. *Trans AIME.* **87**, 285.

Tao, D.P., Li, Y.Q., Richardson, P.E. and Yoon, R.-H., 1994., *Coll. Surf. (A)*, **93**, 229-239.

Tolun, R. and Kitchener, J.A., 1964. *IMM*, 313-322.

Toperi, D. and Tolun, R., 1969, *IMM*, C191-C197.

Trahar, W.J., 1984. Principles of Mineral Flotation, The Wark Symp. AusIMM.

Wadsworth, M.E., Conrady, R.G. and Cook, M.A., 1951. *J. Phy. Chem.* **55**, 1219.

Walker, G.W., Stout, III, J.V. and Richardson, P.E., 1984. *IJMP*, **12**, 55-72.

Walker, G.W., Walters, C.P., and Richardson, P.E., 1986. *IJMP*, **18**, 119-137.

Wark, I.W. and Cox, A.B., 1934a. *Trans AIME*, **112**, 189.

Wark, I.W. and Cox, A.B., 1934b, *Trans AIME*, **112**, 245.

Wark, I.W. and Cox, A.B., 1934c, *Trans AIME*, **112**, 267.

Winter, G. and Woods, R., 1973. *Sepn Sci.*, **8(2)**, 261-267.

Woods, R. 1976, Flotation – Gaudin Memorial Volume (Ed. M.C. Fuerstenau). AIME: New York. **1**, 198-333.

Woods, R., 1971, *J. Phy. Chem.*, **75(3)**, 354-362.

Woods, R., 1988. Reagents in Mineral Technology (Eds. P. Somasundaran and B.M. Moudgil). Marcel Dekker: New York. Ch 2., 39-78.

Woods, R., Basilio, C.I., Kim D.S., and Yoon, R.-H., 1992. *J. Electroanal. Chem. Interf. Electrochem*, **328**, 179-194.

Woods, R., Basilio, C.I., Kim, D.S. and Yoon, R.-H., 1994. *IJMP*, **42**, 215-233.

Woods, R., Chen, Z. and Yoon, R.-H., 1997. *IJMP*, **50**, 47-52.

Woods, R., Young, C.A. and Yoon,R.-H., 1990. *IJMP*, **30**, 17-33.

Table 1.1. List of Sulfide Minerals

Mineral	Chemical Composition
Aresonpyrite	FeAsS
Bornite	Cu_5FeS_4
Chalcocite	Cu_2S
Chalcopyrite	$CuFeS_2$
Covellite	CuS
Galena	PbS
Marcasite	FeS_2
Molybdenite	MoS_2
Orpiment	As_2S_3
Pentlandite	$(Fe_{4.5},Ni_{4.5})S_8$
Pyrite	FeS_2
Pyrrhotite	$Fe_{1-x}S$, Fe_7S_8, $FeS_{1.15}$
Realgar	AsS
Sphalerite	ZnS
Stibnite	Sb_2S_3

Table 1.2. Correlation between rest potentials and xanthate (KEX) oxidation products. (Allison et al., 1972).

($X_2 + 2e \rightarrow 2X^-$, $E^0 = -0.06V$, $E_r = 0.13$ V at pH = 7 and $[X^-] = 6.25 \times 10^{-4}$ M)

Mineral	**Rest Potential (V)**	**Product**
Sphalerite	-0.150	NPI
Stibnite	-0.125	NPI
Realgar	-0.120	NPI
Orpiment	-0.100	NPI
Galena	+0.060	MX
Bornite	+0.060	MX
Chalcocite	+0.060	NPI
Covellite	+0.050	X_2
Chalcopyrite	+0.140	X_2
Molybdenite	+0.160	X_2
Pyrrhotite	+0.210	X_2
Pyrite	+0.220	X_2
Arsenopyrite	+0.220	X_2

NPI = No Positive Identification, MX = Metal Xanthate, X_2 = Dixanthogen

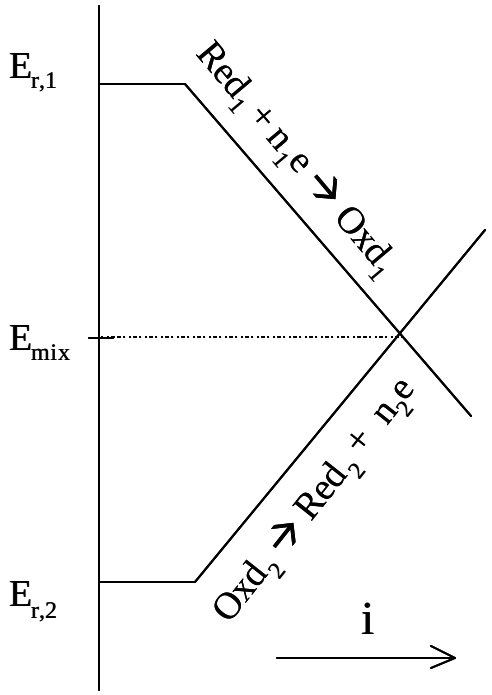

Figure 1.1. Evans diagram showing a mixed potential mechanism for two redox processes with different reversible potentials (Reactions [1.3a]-[1.3]).

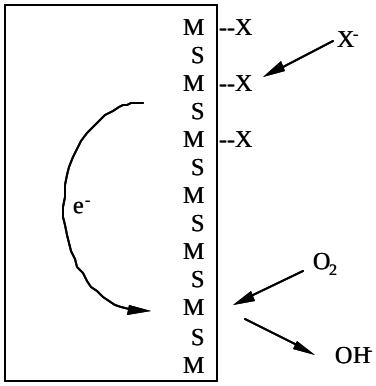

1.1.1.d.Anodic

$X^- \rightarrow X_{ads} + e$

1.1.1.e.Cathodic

$O_2 + 2H_2O + 4e \rightarrow 4OH^-$

1.1.1.f.Overall

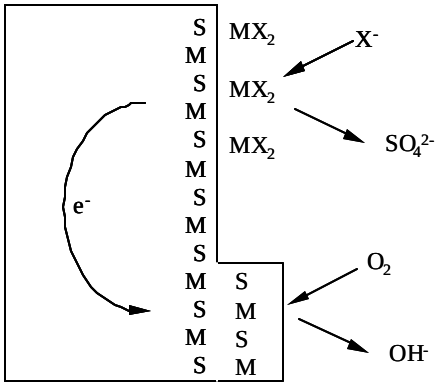

1.1.1.a.Anodic

$2X^- + MS + 4H_2O \rightarrow MX_2 + SO_4^{2-} + 8H^+ + 2e$

1.1.1.b.Cathodic

$O_2 + 2H_2O + 4e \rightarrow 4OH^-$

1.1.1.c.Overall

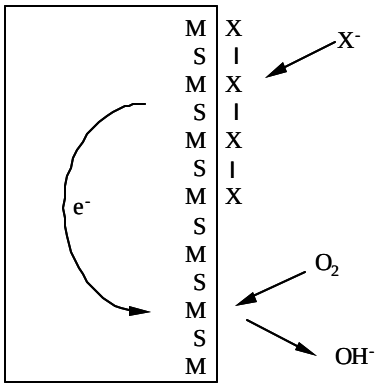

1.1.1.g.Anodic

$2X^- \rightarrow 2X_2 + 2e$

1.1.1.h.Cathodic

$O_2 + 2H_2O + 4e \rightarrow 4OH^-$

1.1.1.i. Overall

Figure 1.2. Schematic representation of xanthate adsorption on a sulfide mineral by:
(a) chemisorption (Reaction [1.7]),
(b) metal xanthate formation (Reactions [1.8] and [1.9]), and
(c) dixanthogen formation (Reaction [1.10]).

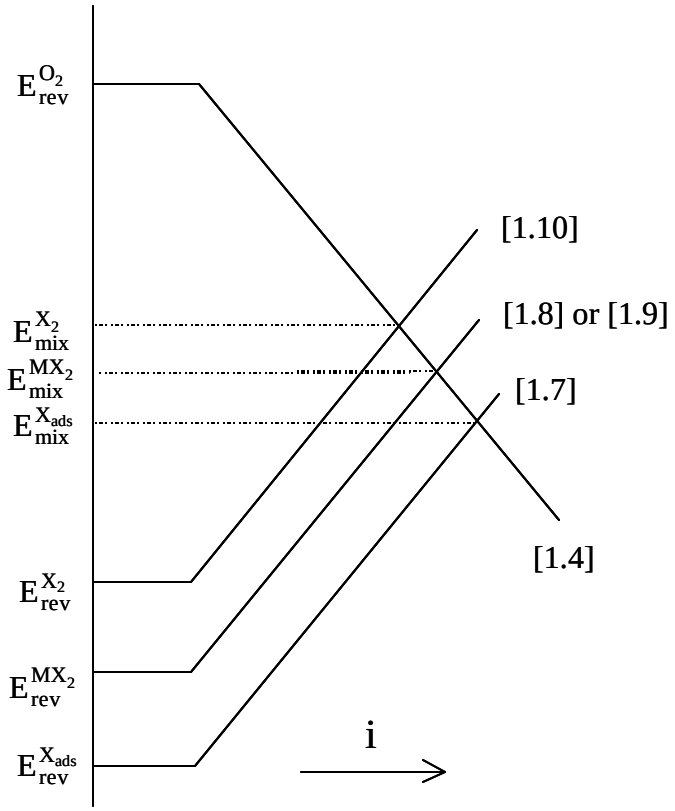

Figure 1.3. Evans diagram showing mixed potential mechanism for the adsorption of xanthate (Reactions [1.7] – [1.10]) coupled with the reduction of oxygen (Reaction [1.4]). The schematic representation of adsorption mechanism is shown in Figure 1.2. The subscripts 'rev' and 'mix' stand for reversible and mixed potentials.

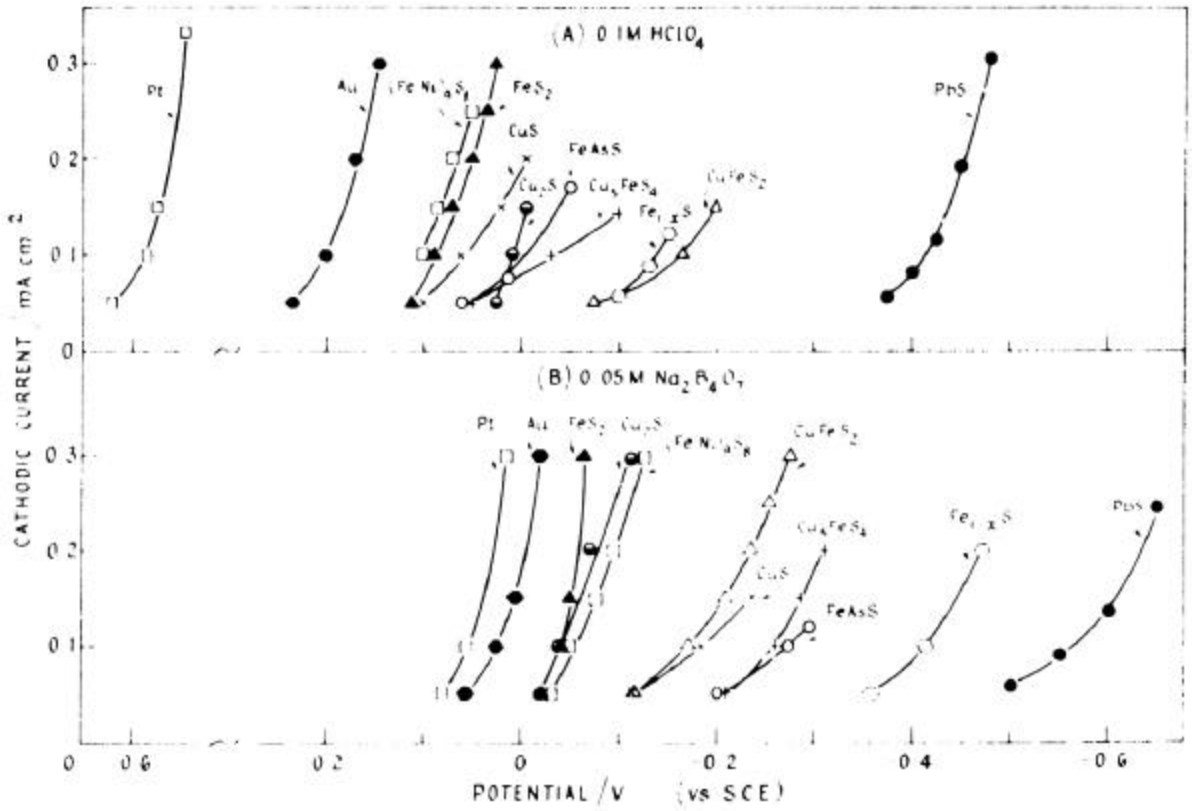

Figure 1.4. Cathodic currents for the oxygen reduction on various sulfide minerals and noble metals in (a) acidic and (b) alkaline solutions (Rand, 1977).

CHAPTER 2

ELECTROCHEMICAL IMPEDANCE SPECTROSCOPY (EIS) OF PYRITE

2.1. INTRODUCTION

2.1.1. General

Pyrite is one of the most abundant sulfide minerals in the earth's crust. It is associated with other metallic and non-metallic sulfide minerals, and coal. Except where it is used to manufacture sulfuric acid or to promote leaching of other sulfides, its existence in other minerals is a severe problem; therefore, its removal from coal or other sulfides is desired. Pyrite has generated numerous electrochemical and semiconducting studies because of several reasons: the need to separate from other sulfide minerals (Majima, 1969; Janetski et al., 1977; Leppinen et al., 1988; Zhu et al, 1991), the need to desulfurize coal (Meyers, 1977; Sinha and Sinha, 1985; Yoon et al., 1991; Zhu et al, 1991; 1994; Tao, 1994; Yoon et al., 1994a and b), minimization of acid mine drainage (Doyle, 1990; Doyle and Mirza, 1990), leaching (Peters and Majima, 1968) and electrowinning (Everett, 1982).

The need for separation from other sulfide minerals and coal arises mainly due to two reasons: acid mine drainage and acid rain. The exposure of pyrite to air and water during mining, milling and concentration leads to the production of acid and hence, contamination of local water bodies. The combustion of pyrite with coal in electric utility plants leads to the emission of sulfur dioxide (SO_2). The presence of pyrite in other sulfide minerals leads to lower concentrate grade and incurs higher costs of controlling SO_2 emissions from smelters. It is well known that presence of SO_2 leads to acid rains.

One of the most effective methods of separation of sulfides is froth flotation. Although coal is hydrophobic, while pyrite is hydrophilic, the separation using froth flotation has been proven difficult due to significant flotation of pyrite. The separation becomes more difficult in mixed sulfide systems. The self-induced flotation of pyrite is related to two reasons: (a) superficial oxidation of pyrite during mining, milling, transportation, and preparation of concentrates (Ball and Richard, 1976; Hamilton and Woods, 1981; Buckley and Woods, 1987; Buckley and Riley, 1991; Yoon et al, 1991) and (b) incomplete liberation of pyrite from coal (Yoon et al., 1991).

The superficial oxidation of pyrite (and other sulfide minerals) leads to a sulfur-rich surface. The nature of sulfur rich surface has been a subject of controversy. Woods and his colleagues (1981, 1984, 1985 and 1987) suggested that the oxidation leads to elemental sulfur and possibly metal deficient sulfide ($Fe_{1-x}S_2$). In either case, the surface is sufficiently hydrophobic to be floated without collector. Mycroft et al (1990), Yoon et al. (1991) and Zhu et al. (1991) have suggested the formation of iron polysulfides (FeS_n, n>2) as the hydrophobic oxidation product on the surface. On the other hand, Chander and his coworkers (1987 and 1991) suggested formation of hydrophilic iron oxide/hydroxide over the sulfur-rich layer on pyrite, which can be removed by simple abrasion or stirring of solution (Yoon et al., 1991; Richardson and Walker, 1985; Walker et al., 1986; Ahlberg et al., 1990); or by complexing reagents, e.g., EDTA (Ahlberg et al., 1990; Pang and Chander, 1992; Chander et al., 1992).

Oxidation of pyrite has been studied extensively (Woods and his colleagues, 1975, 1981, 1984, 1985 and 1987; Biegler, 1976; Chander and his coworkers, 1987, 1988, 1990, 1991 and 1992; Ahlberg et al., 1990; Mycroft et al., 1990; Yoon et al., 1991; Zhu et al., 1991; Chmielewski and Nowak, 1992a and b) using electrochemical techniques and spectroscopy. However, most of the previous studies were carried out on surfaces that had been polished. Polishing is known to cause pre-oxidation and introduction of lattice defects affecting electron transfer processes, which may lead to unambiguous results (Tao et al, 1993a and b, 1994; Li, 1994; Tao, 1994; Mendiratta et al., 1996). Therefore, a technique was developed at Center for Coal and Minerals Processing in which the effects of polishing could be avoided by creating fresh surfaces in situ (Li, 1994; Tao, 1994; Tao et al., 1994). The procedure for creating fresh surfaces in situ is described in the experimental section.

2.1.2. Chronoamperometry Of Pyrite

The studies at Center for Coal and Minerals Processing showed that when fresh surfaces of pyrite are suddenly created by fracture in an aqueous solution, the instantaneous open circuit potential measured at fracture is several hundred millivolts (~300 mV) more negative than the final rest potential (Li, 1994; Tao; 1994; Tao et al., 1994). It was shown also that if the potential of a given pyrite electrode was held at the potential the electrode instantaneously assumed at fracture, no oxidation or reduction currents were observed. Figure 2.1 shows the chronoamperometry curves obtained with freshly fractured pyrite electrodes (from Peru) at pH 4.6 (Li, 1994; Tao et al., 1994). The holding potentials of the electrodes are given on the curves.

Prior to fracture, the electrodes were held at these potentials for approximately 15 minutes to allow for residual currents to reach constant values. Following fracture, a spike was observed in chronoamperometry curves. It is believed that this initial spike was the result of combination of charging a new double layer and faradaic oxidation (or reduction). The decay in current after the spike represents faradaic reaction. Fracture also caused a decrease in the area of an electrode; therefore, the steady current after fracture was smaller than that before fracture. This is evident from the curves obtained at -0.1 and -0.2 V in pH 4.6 solution in Figure 2.1 (Tao, 1994).

As expected, more positive potentials caused an increase in oxidizing currents, while more negative potentials caused an increase in reduction currents. The most significant feature is the existence of a unique potential where there are no oxidation or reduction currents following fracture. At this potential, the newly created surface of pyrite is non-reactive. Therefore, this potential is referred as to the stable potential. The stable potentials measured with electrodes made from pyrite samples from Peru and Spain and coal-pyrite samples from China were 0 V at pH 4.6 and -0.28 V at pH 9.2 (Li, 1994; Tao, 1994, Tao et al., 1994).

Figure 2.2 shows the E_h-pH diagram for the pyrite-H_2O system (Kocabag, 1990), in which the two stable potential values determined in the present work are plotted. Although the stable potentials are located within the region where pyrite is supposed to be stable thermodynamically, the mineral is stable only along the line connecting the two stable potentials. At potentials above this line, pyrite becomes oxidized, forming possibly sulfur-rich surfaces and, hence, rendering the mineral hydrophobic. Since there are no thermodynamic data for these oxidation products, the E_h-pH diagram given in Figure 2.2 shows a large stability region for pyrite.

The significance of the chronoamperometry technique developed lies not only in obtaining a fresh unreacted surface, but also in maintaining it. This is achieved by holding it at its stable potential which lies in the domain of thermodynamically stability of pyrite.

2.1.3. Electrochemical Impedance Spectroscopy

(a) Double Layer Capacitance

When an electrode is inserted in an electrolyte, it creates an anisotropy in the interphase/contact region, known as phase boundary. This causes a rearrangement of charges, ions and dipoles, and the electrode surface gets charged. In order to maintain electroneutrality, the solution is charged with equal amount of opposite charge. The redistribution of charges leads

to development of electrical double layer and the potential difference across the interface (Bockris and Reddy, 1970).

According to the Stern model (Bockris and Reddy, 1970; Bard and Faulkner, 1980; Adamson, 1990), the double layer on the solution side consists of several layers: Inner Helmholtz Layer (IHL), Outer Helmholtz Layer (OHL), and Gouy-Chapman (G-C) Diffusion Layer. The first row, IHL, consists of specifically adsorbed and solvent molecules (in general, water dipoles). The specifically adsorbed molecules can be either neutral molecules or anions or certain large cations. The specifically adsorbed ions are generally considered to be unsolvated, and the locus of their centers defines the position of the inner Helmholtz plane (IHP). According to rough calculations by Bockris and Reddy (1970), about 70% of the surface is hydrated and constitutes primary hydration sheath. The next layer consists of hydrated ions and locus of their center is called as Outer Helmholtz Plane (OHP). Since there are only water molecules between IHP and OHP, it constitutes secondary hydration sheath, which is weakly bound to the electrode surface. Historically, double layer represents the two charged layers: electrode surface and OHP. Since they have equal and opposite charge, the electrical equivalent of the situation is a capacitor and hence the term "double layer capacitance". The charge of electrode surface, q_{ES} is given by:

$$q_{ES} \approx -q_{OHP} \qquad [2.1]$$

where, q_{OHP} is the excess charge density at the OHP.

However, the charge at the OHP is slightly less than that on the electrode surface. Although the charged electrode surface attracts solvated ions, the influence of thermal motions are comparable at distances slightly beyond OHP. At distances far from the OHP (and the surface), thermal forces take over and maintain electroneutrality. Therefore, near the OHP, charges walk randomly away from the OHP and are dispersed into the solution. The excess charge density decreases with distance from the electrode and potential falls of asymptotically. This layer essentially represents G-C Diffusion Layer. The schematic representation of ions and potential distribution is shown in Figure 2.3 (Bockris and Reddy, 1970; Bard and Faulkner, 1980).

As it can be seen from Figure 2.3, the potential decreases linearly within the IHP and OHP, whereas it decreases almost exponentially in G-C Diffusion Layer. Therefore, the charge on the electrode surface q_{es} can be given by:

$$q_{ES} = q_{IHP} + q_{OHP} + q_{G-C} \qquad [2.2]$$

where, subscripts IHP, OHP and G-C refer to corresponding layers. The total capacitance of the electrical double layer, C_{DL}, is given by series combination of Helmholtz capacitance, C_H, and diffusion capcitance, C_G as follows (Bockris and Reddy, 1970):

$$\frac{1}{C_{DL}} = \frac{1}{C_H} + \frac{1}{C_G} \qquad [2.3]$$

Since most of the sulfide minerals are semiconductor, another term is introduced in the double layer capacitance owing to diffuse charge region (the Garrett-Brattain Space Charge) inside an intrinsic semiconductor. Figure 2.4 shows the excess charge distribution and potential variation for a semiconductor in an electrolyte. In such case, the observed capacitance is resultant of two capacitors in series: the space charge capacitor, C_{SC}, and the double layer capacitance in the solution phase (Bockris and Reddy, 1970):

$$\frac{1}{C_{obs}} = \frac{1}{C_{SC}} + \frac{1}{C_{DL}} = \frac{1}{C_{SC}} + \frac{1}{C_H} + \frac{1}{C_G} \qquad [2.4]$$

In a strong electrolyte solution $C_G \gg C_H \gg C_{SC}$, therefore the measured capacitance is given by $C_{obs} \approx C_{SC}$. Double layer capacitance measurements can provide information on adsorption and desorption phenomena, film formation processes at the electrode, and the degradation and integrity of organic coatings.

(b) Polarization/Charge Transfer Resistance

When an electrode in placed in an electrolyte, it undergoes two types of processes: faradaic and nonfaradaic. Faradaic processes are governed by Faraday's law of directly proportionality between extent of reaction and amount of electricity. Such processes involve transfer of charge across the electrode-electrolyte interphase and cause either oxidation or reduction (Bard and Faulkner, 1980). Nonfaradaic processes do not involve transfer of charge through interphase due to thermodynamic or kinetic restrictions; however, adsorption and desorption of electrode surface may take place depending upon potential and/or solution composition (Bard and Faulkner, 1978).

For electrochemical studies, although usually faradaic processes are of more significance, nonfaradaic processes can also effect interpretation of electrochemical data. The simplest example of nonfaradaic processes is ideal polarized electrodes (IPE), which serve their function as reference electrodes in electrochemical studies. As mentioned earlier, the faradaic processes are governed by Faraday's law. Therefore, when an electrode is polarized (i.e., an overpotential

is applied), either oxidation (loss of electrons at positive overpotential) or reduction (gain of electrons at negative overpotential) occurs depending upon the extent of polarization and the electrolyte conditions (Bard and Faulkner, 1980). However, the electrode-electrolyte interphase, which is also acting as a capacitor (section 2.1.3.a.), offers a resistance to the transfer of electrons/charges occurring due to the polarization. Such a resistance is known as the charge transfer, R_{CT}, (or polarization, R_p) resistance. The significance of charge transfer resistance lies in the fact that for corrosion type processes, it is inversely proportional to the rate of reaction (Bard and Faulkner, 1980, Chapter 4). Therefore, an electrode-electrolyte interphase consists of a parallel combination of charge transfer resistance, R_{CT}, and doble layer capacitance, C_{DL}. These components may be in combination (usually in series) with other resistances (e.g., solution resistance) and capacitances present in an electrochemical system.

(c) Electrochemical Impedance Theory

As described in previous sections, a sulfide mineral electrode in an electrolyte can be represented by an array of resistors and capacitors. There exists another uncompensated resistance due to the solution between the reference electrode and the working electrode, called as solution resistance, R_Ω. It is more or less an artifact of the electrochemical cell design. Therefore, An electrochemical cell can be represented by a pure electronic circuit (de Levie and Popíšil, 1969; Bockris and Reddy, 1970; Bard and Faulkner, 1980; McCann and Badwal, 1982; Chander et al., 1988; Pang et al., 1990; Xiao and Mansfeld, 1994). The resistance and capacitance, jointly known as impedance, can be studied using electrochemical impedance spectroscopy (EIS).

Figure 2.5(a) shows the simplest equivalent circuit is given by a parallel combination of charge transfer resistance, R_{CT}, and double layer capacitance, C_{DL}, in series with solution resistance, R_Ω. For a resistor, R. the impedance equals its resistance. For a capacitor, C, its impedance equals $-j/\omega C$ (ω is the angular frequency of the ac voltage). For the series circuit of a resistor, R, and a capacitor, C, the impedance can be expressed by

$$Z = R - j/\omega C \qquad [2.5]$$

For a parallel RC circuit,

$$\frac{1}{Z} = \frac{1}{R} + \frac{1}{-j/\omega C} = \frac{1}{R} + j\omega C \qquad [2.6]$$

or,

$$Z = \frac{R}{1 + j\omega CR} \qquad [2.7]$$

or,

$$Z = \frac{R}{1 + \omega^2 C^2 R^2} - \frac{j\omega CR^2}{1 + \omega^2 C^2 R^2} \qquad [2.8]$$

For the circuit shown in Figure 2.5(a),

$$Z = R_\Omega + \frac{R_{CT}}{1 + \omega^2 C_{DL}^2 R_{CT}^2} - \frac{j\omega C_{DL} R_{CT}^2}{1 + \omega^2 C_{DL}^2 R_{CT}^2} \qquad [2.9]$$

where the real and the imaginary components are as follows:

$$Z_r = R_\Omega + \frac{R_{CT}}{1 + \omega^2 C_{DL}^2 R_{CT}^2} \qquad [2.10]$$

$$Z_i = -\frac{\omega C_{DL} R_{CT}^2}{1 + \omega^2 C_{DL}^2 R_{CT}^2} \qquad [2.11]$$

Elimination of ω from this pair of equations yields (Southampton Electrochemistry Group, 1985):

$$\left(Z_r - \left(R_\Omega + \frac{R_{CT}}{2} \right) \right)^2 + Z_i^2 = \left(\frac{R_{CT}}{2} \right)^2 \qquad [2.12]$$

Hence $-Z_i$ vs. Z_r should give a circular plot centered at $Z_r = R_\Omega + R_{CT}/2$ and $-Z_i = 0$, and having a radius of $R_{ct}/2$. Figure 2.5(b) depicts the result, where R_Ω R_{CT} and C_{DL} can be obtained. The format of data representation as shown in Figure 2.5(b) is known as a complex impedance plane plot or a Cole-Cole plot. The most commonly used name is Nyquist plot. Figure 2.6 gives the Nyquist plots for various simple electronic circuits.

Another way of representing electrochemical data is known as the Bode plot. Figure 2.7 represents the data in Figure 2.5(b) in the Bode plot format. For a Bode plot, the absolute impedance, Z, and phase shift, θ, is plotted against log of angular frequency, ω and are given by:

$$Z = \sqrt{Z_r^2 + Z_i^2} \qquad [2.13]$$

$$\tan\theta = -\frac{Z_i}{Z_r} \qquad [2.14]$$

The distinct advantage of the Bode plot is that the relationship with frequency is visible explicitly and capacitance can be calculated directly. Secondly, it is useful to identify processes

which produce multiple semicircles when plotted as Nyquist plots. However, the dependence of the plots and calculated values of capacitances on R_Ω is a serious drawback in Bode plots.

(d) Warburg Impedance

In a diffusion-controlled system, the Warburg impedance represents resistance to mass transfer. The equivalent circuit for diffusion controlled electrochemical system is shown in Figure 2.8(a), where Z_w represents the Warburg impedance. The Warburg impedance is given by:

$$Z_W = \frac{\sigma}{\omega^{1/2}} - j\frac{\sigma}{\omega^{1/2}} \qquad [2.15]$$

where, σ, the Warburg coefficient, is given by:

$$\sigma = \frac{RT}{\sqrt{2D}An^2F^2}\left(\frac{1}{M_O^b} + \frac{1}{M_R^b}\right) \qquad [2.16]$$

where, A is the electrode area, D is the diffusion coefficient for species in solution, and M_O^b and M_R^b are bulk concentrations of reactant and product, respectively.

Similar to Equations [2.9] – [2.11], the real and imaginary component can be written as (Bard and Faulkner, 1980):

$$Z_r = R_\Omega + \frac{R_{CT} + \sigma\omega^{-1/2}}{(C_{DL}\sigma\omega^{1/2} + 1)^2 + \omega^2 C_{dl}^2 (R_{CT} + \sigma\omega^{-1/2})^2} \qquad [2.17]$$

$$Z_i = \frac{\omega C_{DL}(R_{CT} + \sigma\omega^{-1/2})^2 + \sigma\omega^{-1/2}(C_{DL}\sigma\omega^{1/2} + 1)}{(C_{DL}\sigma\omega^{1/2} + 1)^2 + \omega^2 C_{DL}^2 (R_{CT} + \sigma\omega^{-1/2})^2} \qquad [2.18]$$

At high frequencies, Equations [2.17] and [2.18] are reduced to Equations [2.10] and [2.11], respectively and yield a semicircular shape (Equation [2.12]). Al low frequencies ($\omega \rightarrow 0$), Equations [2.17] and [2.18] can be re-arranged to:

$$Z_r = R_\Omega + R_{CT} + \sigma\omega^{-1/2} \qquad [2.19]$$

$$Z_i = 2\sigma^2 C_{DL} + \sigma\omega^{-1/2} \qquad [2.20]$$

As it can be seen that the real and imaginary components are linearly proportional to $\omega^{-1/2}$ and their slope is equal to the Warburg coefficient, σ. After eliminating ω from both the equations, one can get:

$$Z_i = Z_r - R_\Omega - R_{CT} + 2\sigma^2 C_{DL} \qquad [2.21]$$

Therefore, the Nyquist plot at low frequencies would be linear and have a unity slope. The

Nyquist plot for Warburg impedance system is shown in Figure 2.8(b). In this plot, both the kinetically controlled (semicircular, high frequency) and mass transfer controlled (linear, unity slope, low frequency) regions are displayed. According to SEC (1985), The relative size of R_{CT} and Z_w at any given frequency is a measure of the balance between kinetic and diffusion control.

The presence of Warburg impedance can also be verified from Bode plots and Randles plot (plot of Z_r or Z_i vs. $\omega^{-1/2}$). The Warburg impedance is indicated by a slope of –½or –¼ of the linear portion in a Bode plot format and by presence of linearity and same slope for real and imaginary components in a Randles plot (Equations [2.19] and [2.20]).

(e) Constant Phase Element (CPE)

For a perfectly flat electrode, the impedance of the electrode-electrolyte interface is given by the resistances, capacitances and Warburg impedance described in earlier sections. However, for a rough electrode, a frequency dependent term has been often observed, which is referred as to Constant Phase Element (CPE). The impedance of CPE is given by:

$$Z_{CPE} = 1/Y_0 (j\omega)^n \qquad [2.22]$$

where Y_0 is the admittance, also known as CPE coefficient and n is referred as to CPE exponent and is used to separate real and imaginary component of Z_{CPE}. Usually, but not always, n varies between ½and 1.

The frequent occurrence of CPE in electrochemical processes has generated numerous studies and physical interpretations on it. The first interpretation was made by de Levie (1965) to describe infinite pore model for n = ½ Le Méhauté and his coworkers (1989) made first attempt to describe CPE behavior in terms of fractals. Since then, there have been innumerous studies conducted to explain CPE in terms of roughness (Scheider, 1975; Rammelt and Reinhard, 1990, de Levie, 1990) and fractals (Pajkossy and Nyikos, 1990; Hernández-Creus et al., 1993; Sapoval et al., 1993).

The Equation [2.22] can also be considered as a general dispersion equation (Boukamp, 1989). For n = 0, it represents a resistance with $R = 1/Y_0$, for n = 1 a capacitance with $C = Y_0$ and for n = ½it represents a Warburg impedance with $\sigma = 1/Y_0$. Chander et al. (1988), Pang et al. (1990) and Chielewski and Nowak (1992a and b) observed CPE for electrochemical studies and collector flotation of pyrite, which was attributed to the surface roughness.

(f) Electrochemical Impedance Spectroscopy Technique

Ohm's law for AC measurements at a non-zero frequency can be written as:

$$E = I \times Z \qquad [2.23]$$

where, E and I are potential and current, respectively. Z is defined as impedance and measured in ohms (Ω). For an AC circuit, which may include resistors, inductors and capacitors, current is shifted in time with respect to potential. However, for a purely resistive circuit (without capacitors and inductors), both current and potential should stay in phase.

Therefore, when an AC signal is applied to the mineral electrode, it acts an AC electrical circuit with resistors and capacitors due to solution-surface phenomena and diffusion. For applied signal E:

$$E(t) = E_0 \sin(\omega t) \qquad [2.24]$$

the electrode-electrolyte interphase responds with current, I:

$$I(t) = I_o \sin(\omega t + \theta) \qquad [2.25]$$

where ω is the frequency in radians $= 2\pi f$ and θ is the phase shift in radians (Equation [2.14]). The impedance, Z, for the electrochemical system can be given by:

$$Z = \frac{E(t)}{I(t)} = \frac{E_0 \sin(\omega t)}{I_0 \sin(\omega t + \theta)} \qquad [2.26]$$

Using complex number convention, Equation [2.26] can be rewritten as:

$$Z = \frac{E_r + jE_i}{I_r + jI_i} = Z_r + jZ_i \qquad [2.27]$$

where Z_r and Z_I are real and imaginary components given by Equations [2.10] and [2.11] (or [2.17] and [2.18]), respectively. The total impedance, Z, is given by Equation [2.13].

2.2. OBJECTIVE

The objective of the present investigation was to use Electrochemical Impedance Spectroscopy (EIS) to study the oxidation and reduction characteristics of pyrite. It is well known that on ideal semiconducting electrodes, such as pyrite and galena, EIS can provide fundamental information on reaction kinetics and on the basic semiconducting properties of electrodes (Chander and his coworkers, 1987, 1988, 1990, 1991 and 1992; Schumann et al., 1987; Chmielewski and Nowak, 1992a and b). The electrodes were fractured in situ in order to obtain fresh and unoxidized surface for the present study.

2.3. EXPERIMENTAL

2.3.1. Samples And Electrode Preparation

Cubic crystals of pyrite from Peru were obtained from Ward's Scientific Co. and cubic crystals from Spain were obtained from Geoscience Resources. No visible impurities were present in the pyrite samples.

Using a low speed diamond saw, pyrite samples were cut into thin rods of dimensions of approximately 3 × 3 × 10 mm. A copper wire was attached to one of the 3 × 3 faces using conducting silver epoxy and/or indium solder. The electrical contact was covered with non-conducting epoxy, Torr Seal (Varian). The conductivity of the contact was tested using an ohmmeter before further preparation of the samples.

The samples were mounted in a glass (Pyrex) tube (OD = 8mm, ID = 6mm) using same non-conducting epoxy. The epoxy was also used to cover approximately one half of the electrode; the other half protruded out and was in contact with electrolyte when inserted in electrochemical cell. Figure 2.9(a) show the electrode assembly. The electrode was inserted in to the electrochemical cell described below and sealed using an O-ring. Fresh surface was created when electrode was fractured in situ by blowing a sharp tap on the protruding half through a cell port.

2.3.2. Electrochemical Cell

A standard three-electrode cell was modified in order to accommodate pyrite electrodes and allow it to be fractured through a port. The cell is shown in Figure 2.9(b). The sides were made from Teflon. One side had an optical window, which was used for photoelectrochemical studies (Li, 1994), and ports for counter (platinum) electrode and reference electrode (Figure 2.9(c)). A saturated calomel electrode (SCE) was used as the reference electrode,which was attached to main assembly using Luggin-Haber capillary as shown in Figure 2.9(b). The potentials were converted to standard hydrogen scale by adding adding 0.245 V. The other side contained only one port for the working electrode (pyrite). The working electrode was sealed with an O-ring.

The main body of the cell was made of Pyrex glass. It contained two ports, one of which was used as nitrogen inlet. The second port was used to fracture samples and it also served as the gas outlet

2.3.3. Procedure

The solutions were deoxygenated prior to each experiment by sparging it with nitrogen for approximately half an hour. The electrode was inserted using specially designed holder and sealed with an O-ring. Care was taken to avoid spillage of experimental solution. All the three electrodes in the cell were connected to the potentiostat and computer. The mineral electrode was conditioned at it stable potential: 0 V at pH 4.6 and –0.28 V at pH 9.2. During the conditioning, approximately after 2-3 minutes, the electrode was fractured in situ to generate fresh surface. In order to do so, a glass rod was inserted through gas outlet port and a sharp tap on the rod would result in fracture of exposed mineral specimen exposing new surface to electrolyte.

Impedance spectroscopy was carried out immediately following the fracture. For impedance spectroscopy at other potentials, the electrode was first conditioned at pre-determined potential for two minutes. In order to study the effect of polishing, the fractured electrode was wet polished at 600 and 1200 grit silicon carbide paper, 0.3 μm α-alumina and 0.05 μm γ-alumina micrpolish.

2.3.4. Solutions

The experiments were carried out in pH 4.6 and pH 9.2 buffer solutions. The buffer solution were prepared in double distilled de-ionized water using reagent grade chemicals. The composition of buffers is:

pH 4.6 0.05 M Acetic Acid (CH_3COOH) + 0.05 M Sodium Acetate (CH_3COONa)

pH 9.2 0.05 M Sodium Borate ($Na_2B_4O_7$)

2.3.5. Equipment

The electrochemical impedance spectroscopy system consisted of a 5208 Lock-in Analyzer connected to a computer through a Model 273 Potentiostat, both manufactured by EG&G Princeton Applied Research. The potentiostat was controlled by Model 388 software provided by EG&G. The impedance spectra was obtained over a frequency range of 10^{-2} Hz to 10^{-5} Hz using single-sine and multiple-sine waveforms: the former for the range of 5 to 100 KHz; the latter for the range of 0.01 to 6 Hz. The signal amplitude was 5 mV peak to peak. The amplitude of signal was kept small in order to keep perturbation minimal without irreversibly changing the surface product.

2.4 RESULTS AND DISCUSSION

2.4.1. Effect Of Oxidation

Figure 2.10 shows the Nyquist plots of the freshly fractured pyrite (Spanish) electrodes obtained at pH 4.6 and at oxidizing potentials. At the stable potential (0 V), the spectrum was obtained immediately after fracture. At higher potentials, the spectra were obtained after holding the electrodes at the respective potentials for two minutes. At high frequencies (lower left portions of each curve), the impedance is predominantly real and all the curves intercept the real impedance axis at about 40 ohms. This component represents the series resistance (R_Ω in Figure 2.5) of the sample and electrolyte, and is independent of the reactions at the interface. R_Ω can also be directly calculated from the Bode impedance plot (Figure 2.11). The lower right plateau on the Bode impedance plot intercepts the impedance axis at the value of $R_\Omega \approx 40$ ohms.

The Nyquist plots were nearly linear at the stable potential. Little changes were observed in the impedance curve in the potential range of 0 to 0.645 V. Only at potentials above 0.645 V, the Nyquist plots assumed the well-known semicircular shape which is characteristic of the electrode reactions controlled by the charge transfer resistance (R_{CT} in Figure 2.5) rather than the Warburg impedance (Figure 2.8) that is characteristic of diffusion controlled electrode processes (Section 2.1.3). The semicircles were slightly depressed with the origin located below the real axis, and the diameter decreased with increasing potential.

In general, a linear slope of a Nyquist plot is characteristic of reaction(s) where mass-transfer (Warburg impedance) controls the reaction rate and the electron transfer process is fast. However, this generalization does not seem to apply to the data obtained at potentials in the range of 0 to 0.645 V (Figure 2.10). This could be explained by the following observations.

(a) The slope of the impedance curves in Nyquist plots (Figure 2.10) is non-unity (~2.4-2.6), whereas Warburg impedance suggests unity slopes (Equation [2.21], Figure 2.8(b)).

(b) The slope measured for linear portion in Bode impedance plots (Figure 2.11) is in the range of –0.67 to –0.70. For Warburg impedance, the slopes should be either -½or -¼.

(c) The Randles plot (Figure 2.12) shows that although the curves for real (solid) and imaginary (open) impedances at 0 (square), 0.245 (circle) and 0.645 V (up-tri) are almost linear, they have different slopes, whereas the Equations [2.19] and [2.20] suggest that they should have equal slopes (= σ).

Thus, an alternative explanation for the linear behavior at potentials between 0 and 0.645 V in Figure 2.10 may be that the charge transfer resistance is extremely large. This is also suggested by asymtotical curves in the Bode impedance plot (Figure 2.11). The linear region in Nyquist plot may represent a small portion of a semicircle with a very large radius. This is equivalent to saying that the charge transfer resistance at the pyrite electrode is so large that it behaves almost like a blocking electrode, while the behavior at potentials >0.645 V is that of an electrode process controlled by charge transfer, with the charge transfer resistance decreasing with increasing potential.

The impedance behavior of pyrite is consistent with the flotation behavior observed by Tao et al. (1994) and Yoon et al., (1996). Figure 2.13 (Tao et al., 1994) shows the flotation recovery of pyrite at different potentials using microflotation-electrochemical cell. At pH 4.6, flotation commences at 0 V, the stable potential where freshly created pyrite surfaces begin to oxidize. The flotation recovery drops at approximately 0.65 V, the potential at which impedance curves begin to assume semicircular shape. As described earlier, linear impedance curves below 0.645 V are equivalent to semicircles with large diameter, i.e., R_{CT}. Since, R_{CT} is inversely proportional to the rate of reaction, it indicates that the reactions below 0.645 V proceed slowly. Due to slow rate of reaction, the hydrophilic layers of iron oxidation (hydroxides) products have sufficient time to diffuse away leaving hydrophobic sulfur species on the surface leading to its flotation. At higher oxidizing potentials (>0.645 V), the rate of reaction is fast enough to replenish the diffused iron oxidation products (e.g., $Fe(OH)_3$) rendering surface hydrophilic leading to low flotation recovery (Tao et al., 1994; Yoon et al., 1996).

2.4.2. Effect Of Reduction

Figure 2.14 shows similar Nyquist plot obtained with another pyrite electrode from the same source (Spain). At the stable potential (0 V), the spectrum was obtained immediately after fracture. At lower potentials (-0.105 to -0.605 V), the spectra were obtained after two minutes of polarization. The almost linear Nyquist behavior at the stable potential is characteristic of a blocking electrode or diffusion controlled process. However, similar to impedance plots at oxidizing potential, the slopes of the linear region in the Nyquist plot are ~2.4-3.0 and in the Bode impedance plot (Figure 2.15) vary between –0.70 to –0.73. Also, the slopes for real and imaginary impedances in the Randles plot (Figure 2.16) are not equal. This suggests that the linearity observed in the Nyquist plots is not due to the Warburg impedance.

With progressive reduction, the semicircular behavior characteristic of a reduction process controlled by the charge transfer resistance is observed, with the charge transfer resistance decreasing with increasing reduction potential in the range of -0.105 to -0.605 V. At more negative potentials, the Nyquist plots develop into semicircles that are also depressed with the origin below the real Z axis. The behavior during reduction is qualitatively similar to the behavior observed with progressive oxidation

2.4.3. Cyclic Voltammetry Of Pyrite

Figures 2.10 and 2.14 indicate that pyrite is nearly inert over a wide potential range from ca. -0.5 V to 0.7 V, i.e., over a potential range of approximately 1.2 V. This behavior, and the obvious decrease in charge transfer resistance that occurs with aggressive oxidation and reduction, can be explained by considering the cyclic voltammogram of pyrite at pH 4.6 as shown in Figure 2.17. The voltammogram establishes that aggressive oxidation of pyrite occurs at potentials more positive than 0.75 V while aggressive reduction occurs at potentials more negative than the -0.6 V. At potentials corresponding to aggressive oxidation and reduction, the impedance spectra have the classical semicircular behavior characteristic of electrode reactions controlled by charge transfer processes.

The insert in Figure 2.17 shows a voltammogram for pyrite obtained over a narrower range of potentials and with increased current sensitivity. It is apparent that there are a number of reactions that occur on pyrite over the potential range where the impedance plots indicate the electrode is nearly inert. The reactions evident on the voltammogram of the insert may represent processes that are limited to about a monolayer. These processes give current peaks on dynamic voltammograms, but are not expected to give persistent or continuous currents during steady state polarization. Thus, during steady state polarization experiments, as employed to obtain the impedance spectra, the electrode processes responsible for these reactions are not expected to contribute to the charge transfer resistance. The reactions occurring on the voltammogram shown in the insert are also irreversible, as a large overpotential is required to reduce the oxidation products. If one applies an AC signal to the electrode within the range of potentials where pyrite only undergoes surface reactions, the first positive going cycle may drive the oxidation reaction, producing more of the surface product. However, it requires an overpotential larger than 5 mV to reduce this product. Therefore, after the first few cycles, no further reactions should occur. Thus, surface limited reactions should not directly contribute to the charge transfer

resistance measured by an AC signal. However, the surface products may introduce additional resistance or capacitance elements into the equivalent circuit. Overall, pyrite exhibits an impedance behavior of an inert electrode over a wide range of potentials, where the formation and reduction of oxidation products on the surface are irreversible.

2.4.4. Effect Of pH

Impedance experiments for freshly fractured pyrite electrodes were conducted in pH 9.2 buffer solution. Spectra were obtained at the stable potential (-0.28 V) and after progressive oxidation between -0.28 V and 0.75V (Figure 2.18) and reduction at potential between -0.28 V and -1.0 V (Figure 2.19). Similar to the behavior observed at pH 4.6, the Nyquist impedance plots were nearly linear over a wide range of potentials (-0.80 to 0.40 V), establishing again that pyrite is nearly inert to small amplitude AC signals over a wide potential range. It is not until the potential reaches approximately -1.0 V during reduction and 0.5 V during oxidation that the impedance plots assume semicircular shapes characteristic of reactions controlled by the charge transfer processes. These results are consistent with the behavior of pyrite in pH 4.6 buffer solution except that the potential range over which the electrode is nearly inert shifts to more negative values. The shift with pH (~65 mV/pH) is consistent with the expected shift in the thermodynamic potential for oxidation and reduction reactions with pH (~59 mV/pH).

The flotation results at pH 9.2 are also consistent with impedance spectroscopy. As it can be seen from Figure 2.13 that flotation commences at –0.2 V, near stable potential where fresh pyrite surfaces begin to oxidize. The flotation recovery drops at approximately 0.4 V. The relatively high recovery corresponds to oxidizing potentials, where pyrite acts an inert electrode with large R_{CT}. Similar to results obtained at pH 4.6, the reactions in this potential range are slow enough to let hydrophilic iron oxidation product diffuse and render surface floatable. At high potentials, iron oxidation products remain on the surface decreasing its flotation recovery.

2.4.5. Effect Of Polishing

To study the effect of polishing on EIS spectra, fractured electrodes were progressively wet-polished using 600 and 1200 grit silicon carbide paper followed by polishing with 0.3 μm α-alumina and 0.05 μm γ-alumina powders. After each polishing, the impedance spectra were obtained at -0.60, 0 and 0.85 V. The results are compared with those obtained with fractured electrode.

Figure 2.20 shows the Nyquist plots for freshly fractured and polished electrodes at 0V. As it can be seen from the figure, the shape of the impedance curves at 0 V is almost linear, even for polished electrodes. Although polishing may cause pre-oxidation of surface, slightly oxidized pyrite surface near 0 V also behaves as inert electrode as observed from impedance spectra at oxidizing potentials (Figure 2.10). Therefore, no significant differences were observed for freshly fractured and polished electrodes at 0 V.

Figure 2.21 (a) and (b) show the Nyquist plots for the fractured and polished electrode that were obtained at –0.60 V and 0.85 V, respectively, at pH 4.6. The diameter of the semicircular impedance plots, i.e., the charge transfer resistance, decreases in going from the fractured electrode to finer grades of polishing, except for the 0.05 μm micropolish. The change in magnitude of the impedance due to polishing reflects, for a large part, changes in the surface area of the electrodes. If it is assumed that a part of the capacitive impedance is due to the double layer in the solution, then the capacitance should vary as:

$$C_{DL} = \varepsilon A/d \qquad [2.28]$$

where ε is the dielectric constant, A the area, and is d the effective thickness of the double layer. The capacitive impedance will then be given by:

$$X_C = -j/\omega C_{DL} = -(j/\omega\varepsilon)(d/A) \qquad [2.29]$$

where, ω is the angular frequency of the AC signal.

Similarly, the resistive component of the impedance depends on A through the relation:

$$X_R = R = (\rho d/A) \qquad [2.30]$$

where, ρ is the resistivity.

Thus, for simple electrolyte-solid interfaces, the magnitude of the imaginary and real components should decrease with increasing area. It is apparent from Figures 2.21 (a) and (b) that the fractured electrode has the smallest area and that the area increases with polishing in the order 600>1200>0.3. However, the impedance plots cannot be normalized by the area such that they are coincident over the entire frequency range. The changes that cannot be accounted for by changes in surface area may be attributed to changes in surface roughness, or possibly to polishing induced defect levels in the space charge region of pyrite. Electronic state associated with defects could change the charge transfer resistance by providing additional electronic levels in the surface region for charge transfer reactions, or charge storage in such states may offer an additional interfacial capacitance.

Several equivalent circuits have been considered in an attempt to model the data of Figures 2.20 – 2.21, using Boukamp's equivalent circuit software (Boukamp, 1989) to analyze the data. Figure 2.22 shows two of the simplest circuits that account for many of the features of the impedance spectra. In this figure, R_Ω is the series resistance due to the solution, sample and electrical connections, R_{CT} is the charge transfer (polarization) resistance of the surface in parallel with C_T which is the capacitance of the freshly fractured interface. R_{CT} is inversely related to the surface reaction rate, while C_T consists of the space charge and Helmoltz layer capacitance (Equation [2.4]: $C_T = C_{obs}$). Table 2.1 shows the impedance values calculated for the equivalent circuits to model the data of impedance plots in Figures 2.20 – 2.21.

Not surprisingly, the calculated capacitance values depend on the frequency. Frequency dependent interfacial capacitance, known as CPE, is usually interpreted in terms of the surface roughness (Section 2.1.3.e). When n=0.5, Z_C would be equivalent to the Warburg impedance, however, analysis of the data shows that n varies from 0.71 to 0.92 depending on the methods of polishing employed. Chander and his coworkers (1988 and 1990) and Chmielewski and Nowak (1992a and b) have also observed CPE in electrochemical studies and collectorless flotation of pyrite and attributed CPE to surface roughness with other factors, such as diffusion, etc.

The simple circuit of Figure 2.22(a) accounts reasonably well for the fractured electrode and for electrodes polished at 600 and 1200 grit. For electrodes polished with 0.3 and 0.05 μm micropolishes, however, another RC circuit in series with the simple circuit provides a better fit with the data shown in Figure 2.22(b). This indicates that the fine polishing induces either formation of a product layer on the surface or changes in local electronic states in the space charge region, as represented by the R_X-C_X circuit. These defects can act as traps for charge carriers and will cause a decrease in the impedance (increase in the capacitance), as observed for impedance plots after polishing with 0.05 μm micropolish.

2.5. CONCLUSIONS

EIS was carried out to study the reodx processes of pyrite and following conclusions were drawn:

1. The charge transfer (or polarization) resistance, R_{CT}, decreases with increase in oxidation (positive going) and reduction (negative going) potentials. Since R_{CT} is inversely

proportional to rate of reaction, it indicates that the rate of reaction increases with progressive oxidation and reduction.

2. The rate of reaction at moderate and high oxidizing potentials is consistent with flotation results obtained by Tao et al., (1994) and Yoon et al. (1996).
   (a) At moderate oxidizing potentials (0 to 0.4 V), the rate of reaction is slow enough to allow diffusion of hydrophilic iron-oxidation products leaving hydrophobic sulfur-rich layers on the pyrite surface. The sulfur-rich layers render pyrite hydrophobic and cause its collectorless (self-induced) flotation at moderate oxidizing potentials.
   (b) At high oxidizing potential (>0.65 V), the rate of reaction is fast enough to replenish iron-oxidation products, which do not have sufficient time to diffuse away. The iron-oxidation products render the surface hydrophilic, thereby reducing its flotation recovery.
3. Pyrite exhibits an impedance behavior of nearly inert electrode to a small AC signal (~5 mV) over a range of approximately 1.1 V. This is because of the irreversibility of the reaction products to small overpotentials (~5 mV).
4. The range of potential at which pyrite exhibits inert behavior is approximately –0.5 to 0.7 V at pH 4.6 and –0.8 V to 0.4 V at pH 9.2. The shift with pH (~65 mV/pH) is consistent with the expected shift in the thermodynamic potential for oxidation and reduction reactions with pH (~59 mV/pH).
5. For freshly fractured and polished pyrite electrodes, equivalent circuits were developed using Boukamp's software. It was observed that micropolishing introduces an addition R-C pair in addition to R_{Ω}, R_{CT} and C_{DL}. The capacitances calculated were frequency dependent, also referred as to CPE. The frequency dependence was attributed to the surface roughness due to fracture and polishing.
6. Polishing of the mineral surface changes the polarization resistance and hence, the rate of reaction. This could be due to following reasons:
   (i) increase in the surface area,
   (ii) formation of product layers on the surface, and
   (iii) creation of defects in the space charge region.

2.6 REFERENCES

Adamson, A.W., 1990. Physical Chemistry of Surfaces, 5th Ed. Wiley: New York.

Ahlberg, E., Forssberg, K.S.E., and Wang, X., 1990. *J. App. Electrochem.*, **20**, 1033-1039.

Ball, B. and Rickard, R.S., 1976. Flotation – Gaudin Memorial Volume (Ed. M.C. Fuerstenau). AIME: New York. **1**, 458-484.

Bard, A.J. and Faulkner, L.R., 1980. Electrochemical Methods : Fundamentals and Applications. Wiley: New York.

Biegler, T., 1976. *J. Electroanal. Chem. Interf. Electrochem*, **70**, 265-275.

Biegler, T., Rand, D.A.J. and Woods, R., 1975. *J. Electroanal. Chem. Interf. Electrochem*, **60**, 151-162.

Bockris, J.O'M. and Reddy, A.K.N., 1970. Modern Electrochemistry. Plenum: New York. **2**.

Boukamp, B.A., 1989. Equivalent Circuit – Impedance Data Analysis. University of Twente: Netherlands.

Buckley, A.N. and Woods, R., 1984. Proc. Intl. Symp. Electrochem. in Mineral and Metal Process. I (Eds. P.E. Richardson, S. Srinivasan and R. Woods). ECS: Pennington (NJ), 286-302.

Buckley, A.N. and Woods, R., 1987. *Applied Surface Science*, **27**, 437-452.

Buckley, A.N. and Woods, R., 1991. *Surf. Interf. Anal.*, **17**, 655-659.

Buckley, Hamilton and Woods, 1985. Flotation of Sulfide Minerals (Ed. K.S.E. Forssberg). 41-60.

Chander, S. and Briceno, A., 1987. *Minerals and Metall. Process.*, **4**, 171-176.

Chander, S. and Zhou., R., 1991 *Minerals and Metall. Process*. **8**, 91-96

Chander, S., 1991. *IJMP*, **33**, 121-134.

Chander, S., Briceno, A. and Pang, J., 1992. SME Annual Meeting, Phoenix (AZ). SME: Littleton (CO). Preprint No. 92-240.

Chmielewski, T. and Nowak, P. 1992a. *Physicochem. Problems of Miner. Process.*, **25**, 59-67.

Chmielewski, T. and Nowak, P. 1992b. *Source unknown.*, 149-157.

de Levie, R. and Popíšil, L., 1969. *J. Electroanal. Chem. Interf. Electrochem*, **22**, 277-290.

de Levie, R., 1965. *Electrochim. Acta*, **10**, 395.

de Levie, R., 1990. *J. Electroanal. Chem. Interf. Electrochem*, **281**, 1.

Doyle, F.M. and Mirza, A.H., 1990. Proc. Western Reg. Symp. on Min. and Minl. Process. Wastes (Ed. F.M. Doyle). SME: Littelton (CO). 43-51.

Doyle, F.M., 1990. Sulphide Deposits: Their Origin and Process. (Eds. P.M.J. Gray et al.). IMM: London. 301-310.

Everett, P.K., 1982. Hydrometall. Research, Dev. and Plant Practice (Eds. K. Osseo-Aasre and J.D. Miller). AIME: Warrendale (PA). 165.

Hamilton, I.C. and Woods, R., 1981. *J. Electroanal. Chem. Interf. Electrochem*, **118**, 327-343.

Hernández-Creus, A., Bolzan, A.E., Carro, P., Gonzalez, S., Salvarezza, R.C. and Arvia, A.J., 1993. *Electrochim. Acta*, **38(11)**, 1545-1549.

Kocabag, D., Shergold, H.L. and Kelsall, G.H., 1990a. *IJMP*, **29**, 195-210.

Kocabag, D., Shergold, H.L. and Kelsall, G.H., 1990b. *IJMP*, **29**, 211-219.

Le Méhauté, A., 1989. *Electrochim. Acta*, **34(4)**, 591-592 and references therein.

Leppinen, J.O., Basilio C.I., and Yoon, R.-H., 1988. Proc. Intl. Symp. Electrochem. in Mineral and Metal Process. II (Eds. P.E. Richardson and R. Woods). ECS: Pennington (NJ). 49-65.

Li, Y. 1994. Dissertation, Virginia Polytech. Insti. And State Univ. Virginia (USA).

McCann, J.F. and Badwal, S.P.S., 1982. *J. ECS*. **129(3)**, 551-559.

Mendiratta, N.K., Yoon, R.-H. and Richardson, P.E., 1996. Proc. Intl. Symp. Electrochem. in Mineral and Metal Process. IV (Eds. R. Woods, F.M. Doyle and P.E. Richardson). ECS : Pennington (NJ). 155-166.

Meyers, R.E., 1977, Coal Desulfirization. Marcel Dekker: New York (NY).

Mycroft, J.R., Bancroft, G.M., McIntyre, N.S., Lorimer, J.W. and Hill, I.R., 1990. *J. Electroanal. Chem. Interf. Electrochem*, **292**, 139-152.

Pajkossy, T. and Nyikos, L., 1990. *Phy. Review B*, **42(1)**, 709-719.

Pang, J., Briceno, A. and Chander, S., 1990. *J. ECS*, **137(11)**, 3447-3455.

Peters, E. and Majima, H., 1968. *Can. Metall. Quart.*, **7(3)**, 111-117.

Richardson, P.E. and Walker, G.W., 1985. Proceedings of the XVth International Mineral Processing Congress, Cannes. **2**, 198-210.

Sapoval, B., Gutfraind, R., Meakin, P., Keddam, M. and Takenouti, H., 1993. *Phys. Review E*, **48(5)**, 3333-3344.

Sinha, A.K. and Sinha, K.M., 1985. *Minl. Metall. Process.*, **Nov**, 203.

Southampton Electrochemistry Group, 1985. Instrumental methods in Electrochemsitry. Ellis Horwood Ltd.

Tao, D.P., Li, Y.Q., Richardson, P.E. and Yoon, R.-H., 1994., *Coll. Surf. (A),* **93**, 229-239.

Woods et al., 1987. *IJMP*, **20**, 109-120.

Woods, R. 1981, *PCIL*, **200**, 200.

Woods, R., 1975. *PCIL*, **100**, 100.

Table 2.1. The Impedance Values Calculated for the Equivalent Circuits for the Impedance Plots in Figures 2.20-2.21.

Electrode Condition	Impedances								
	0 V			-0.60 V			0.85 V		
	R_{CT}	Y_0 ($\times 10^{-6}$)	n	R_{CT}	Y_0 ($\times 10^{-6}$)	n	R_{CT}	Y_0 ($\times 10^{-6}$)	n
Freshly Fractured	1.3×10^{20}	17.5	0.76	4650	27.5	0.73	893	17.6	0.74
600 grit S-C paper	1.0×10^{20}	37.1	0.84	2950	35.1	0.78	487	21.2	0.85
1200 grit S-C paper	1.5×10^{20}	30.8	0.75	4530	34.2	0.78	556	25.4	0.79
0.3 μm micropolish	1.4×10^{4}	19.0	0.75	4070	28.0	0.84	531	19.0	0.92
”	116	27.8	0.71	69	42.0	0.77	111	63.7	0.70
0.05 μm micropolish	4.0×10^{4}	20.7	0.86	3060	30.8	0.85	426	22.8	0.91
”	91	28.9	0.72	60	63.6	0.74	92	132.4	0.63

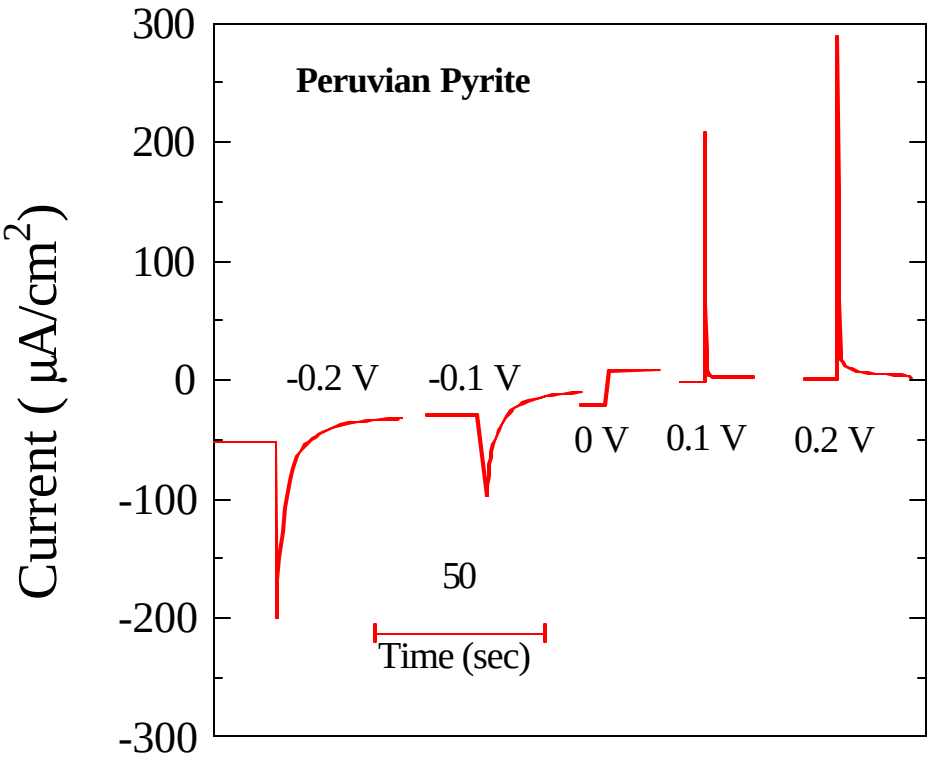

Figure 2.1. Chronoamperometry curves of pyrite fractured at different potentials at pH 4.6 (Li, 1994).

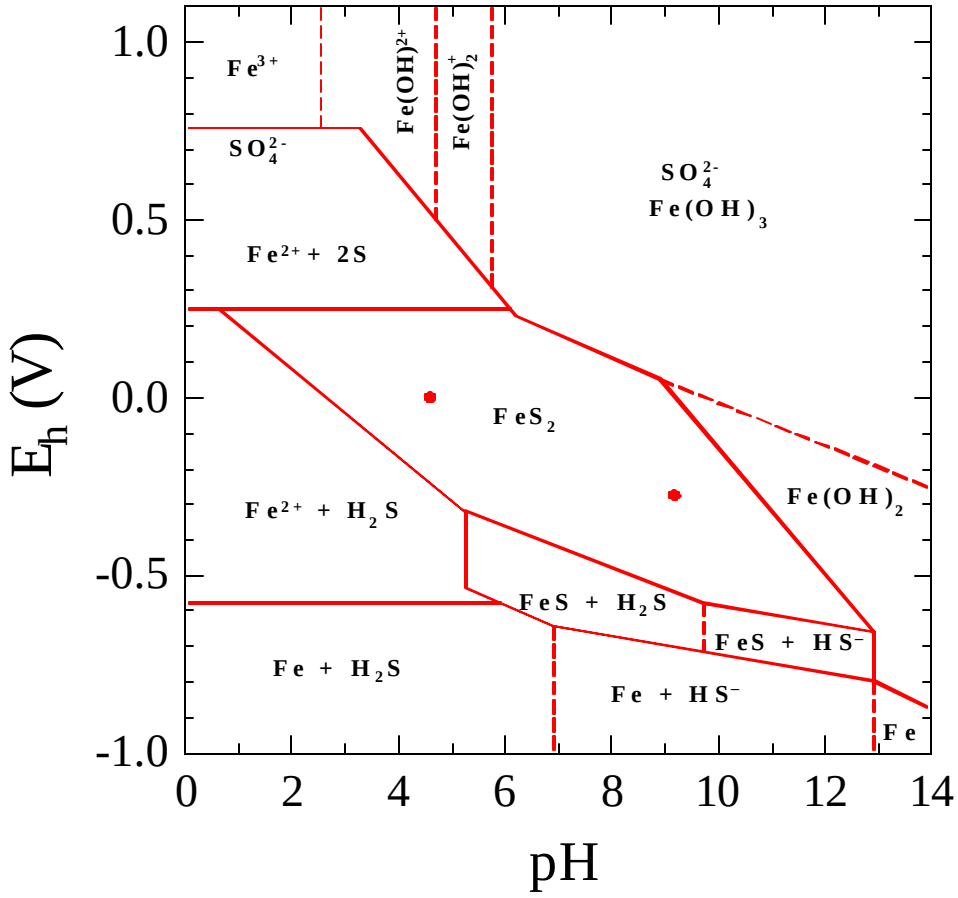

Figure 2.2. E_h – pH diagram for FeS_2 – H_2O system at 25 ^{0}C and for 10^{-5} M dissolved species. The two points in the stability region of FeS_2 represent stable potentials at pH 4.6 and 9.2 (Kocabag et al., 1990; Li, 1994; Tao, 1994).

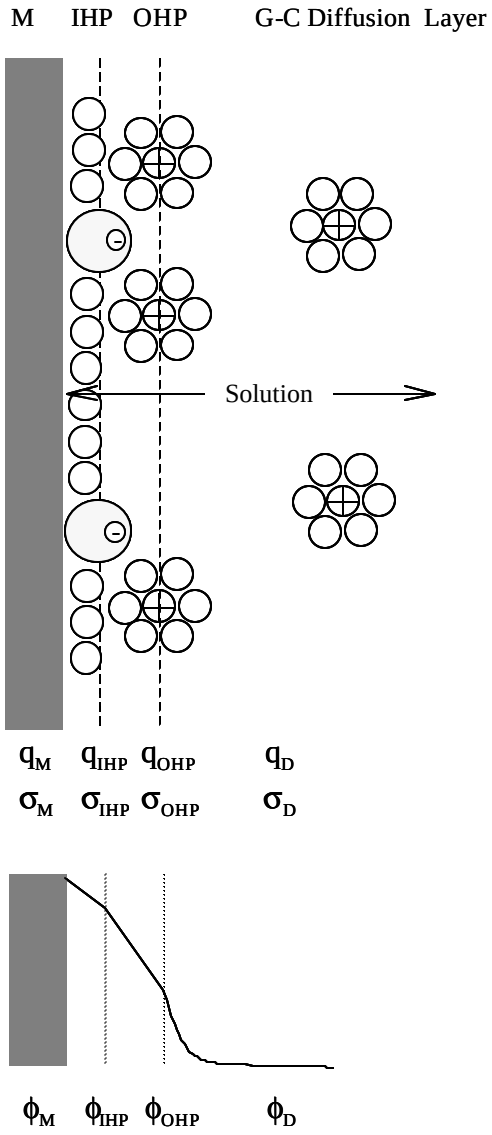

Figure 2.3. Double layer model for a metal in an electrolyte showing the distribution of ions in Inner Helmoltz Plane (IHP), Outer Helmoltz Plane (OHP), and Gouy-Chapman (G-C) Diffusion Layer. The potential (ϕ) is decays linearly in Helmoltz planes and exponentially in diffusion layer. q and σ represent the surface charge and charge density (Bockris and Reddy, 1970; Bard and Faulkner, 1980).

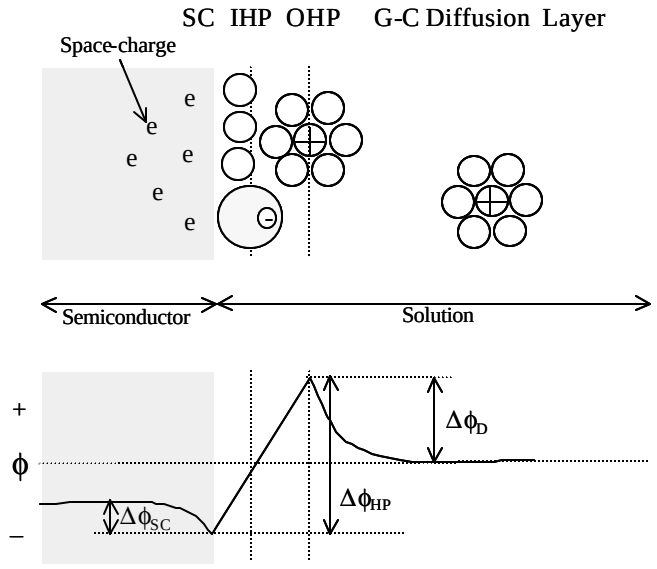

Figure 2.4. Excess charge distribution and variation of potential (ϕ) in the Garrett-Brattain space charge region and the double layer for a semiconductor in an electrolyte (Bockris and Reddy, 1970).

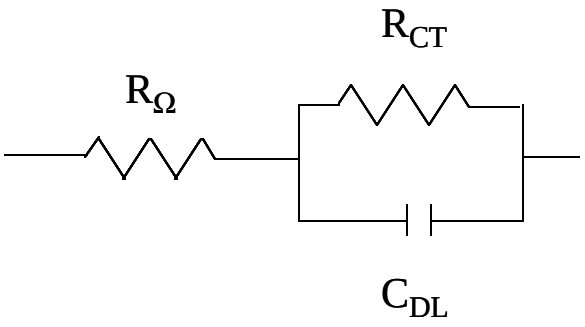

(a)

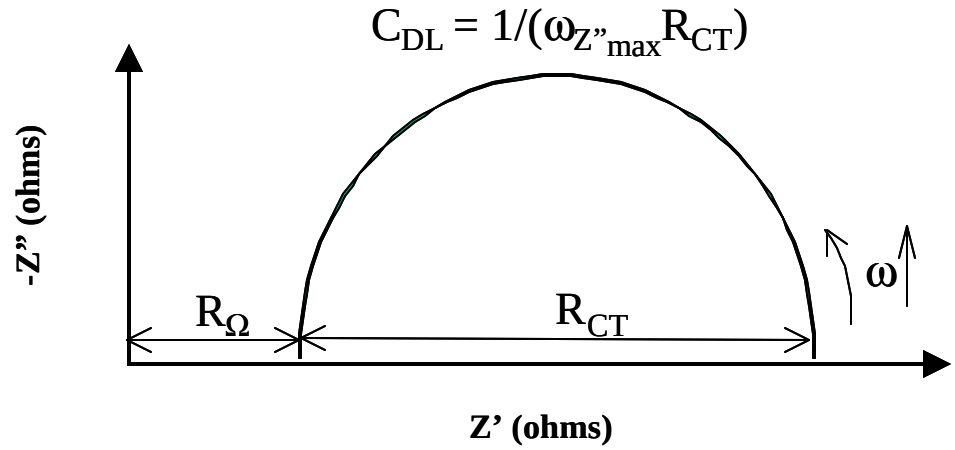

(b)

Figure 2.5. (a) An equivalent circuit for simple electrochemical cell
(b) The Nyquist plot for equivalent circuit in part (a).

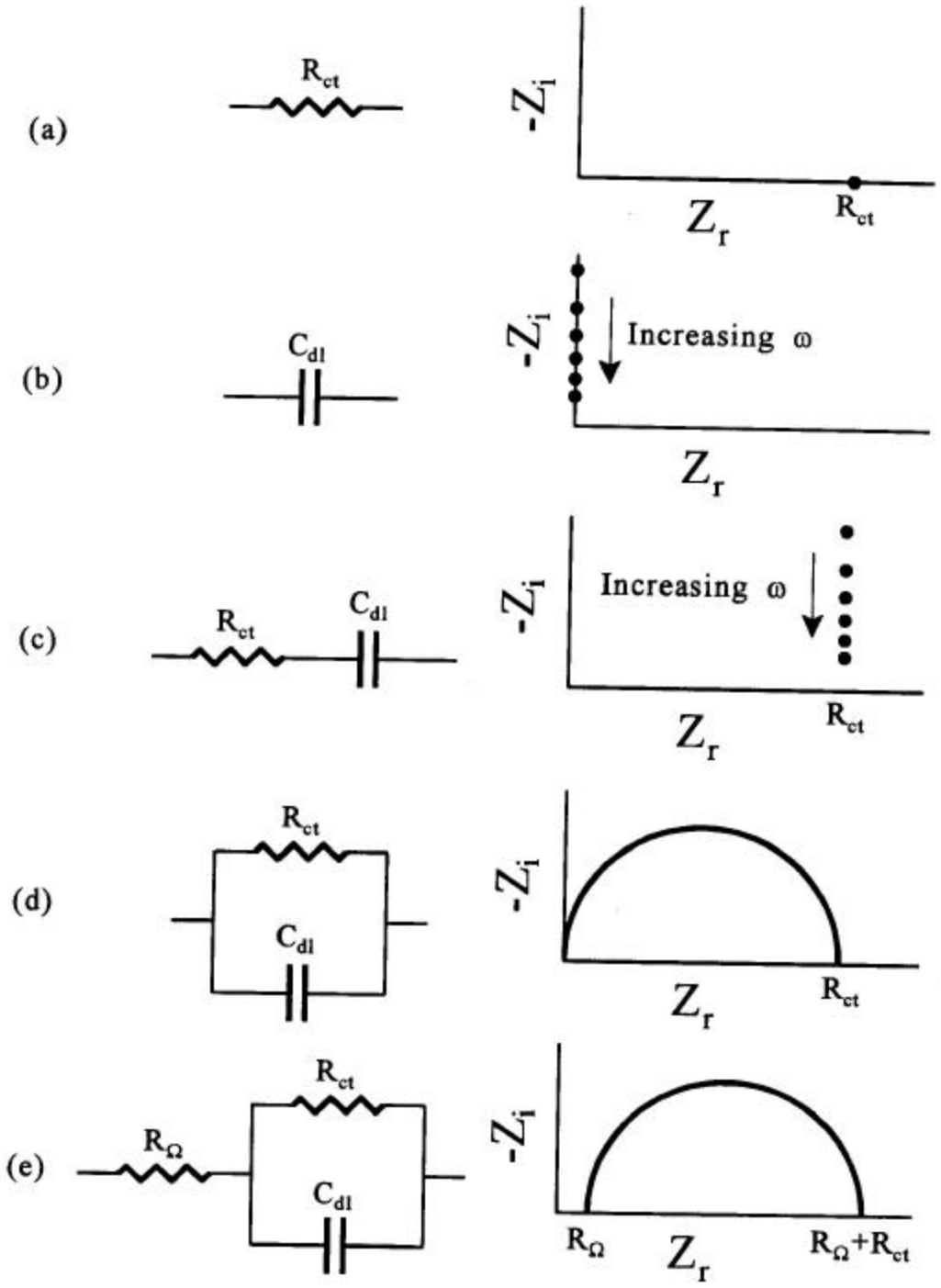

Figure 2.6. Various equivalent circuit and their Nyquist plots.

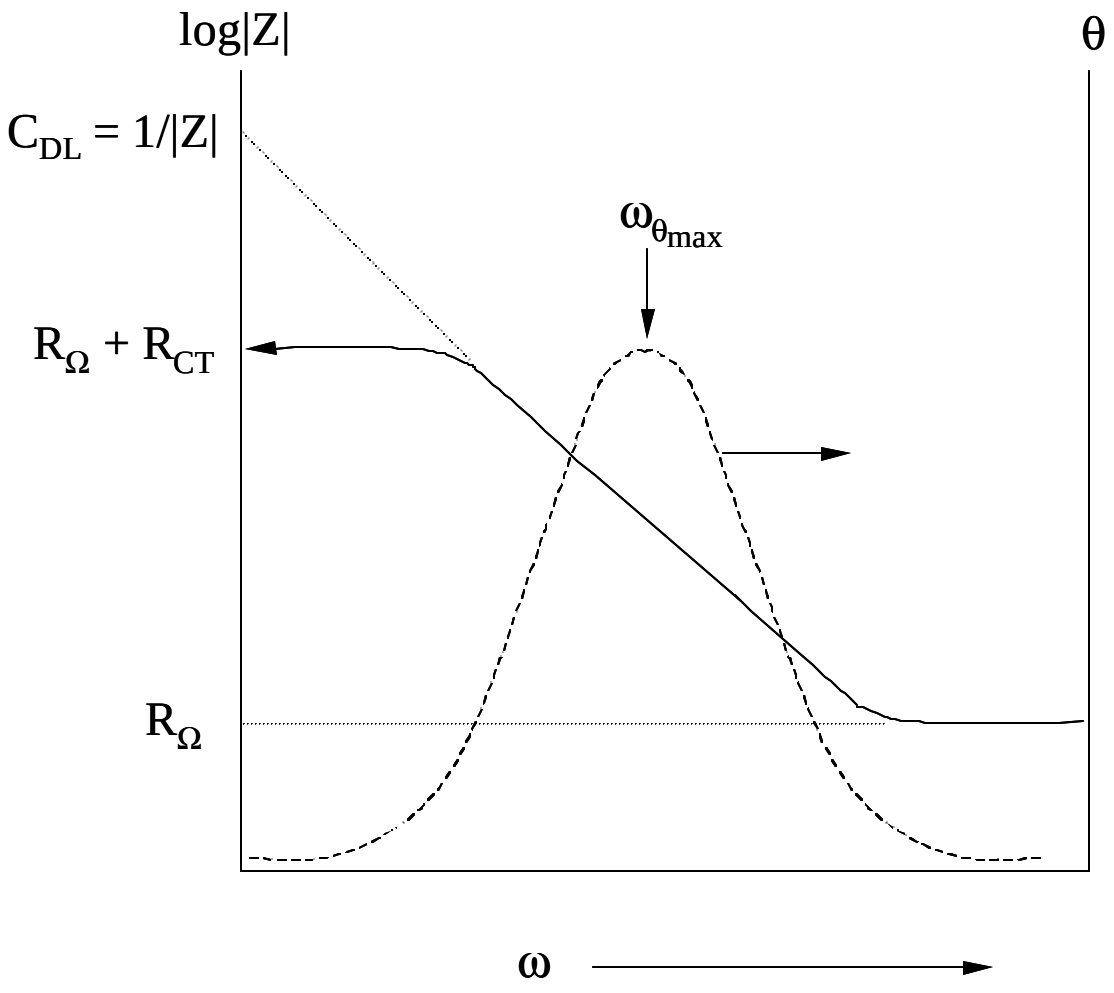

Figure 2.7 The Bode plot representation of equivalent circuit shown in Figure 2.5(a).

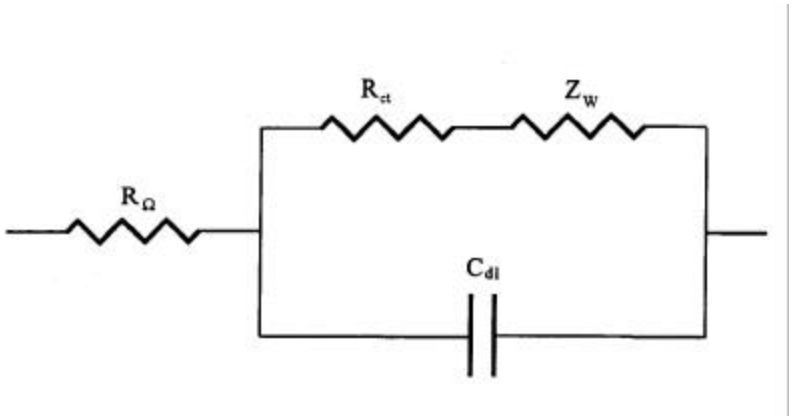

(a)

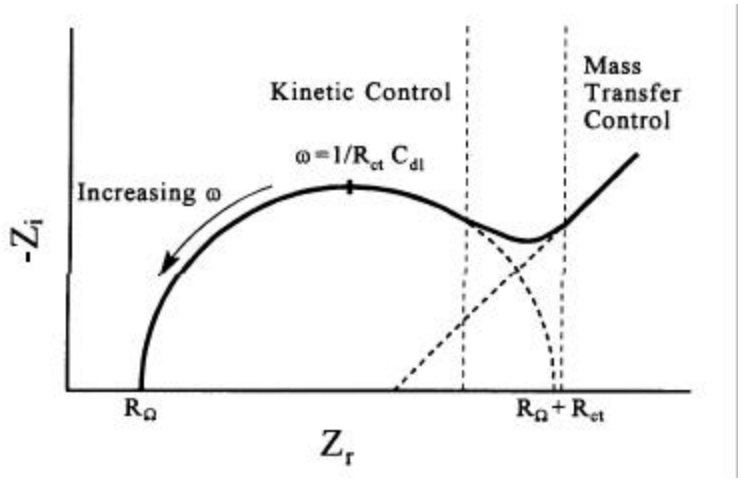

(b)

Figure 2.8 (a) An equivalent circuit for an electrochemical cell with Warburg impedance.
(b) The Nyquist plot for the equivalent circuit in part (a). (Bard and Faulker, 1980; Southhampton, 1985)

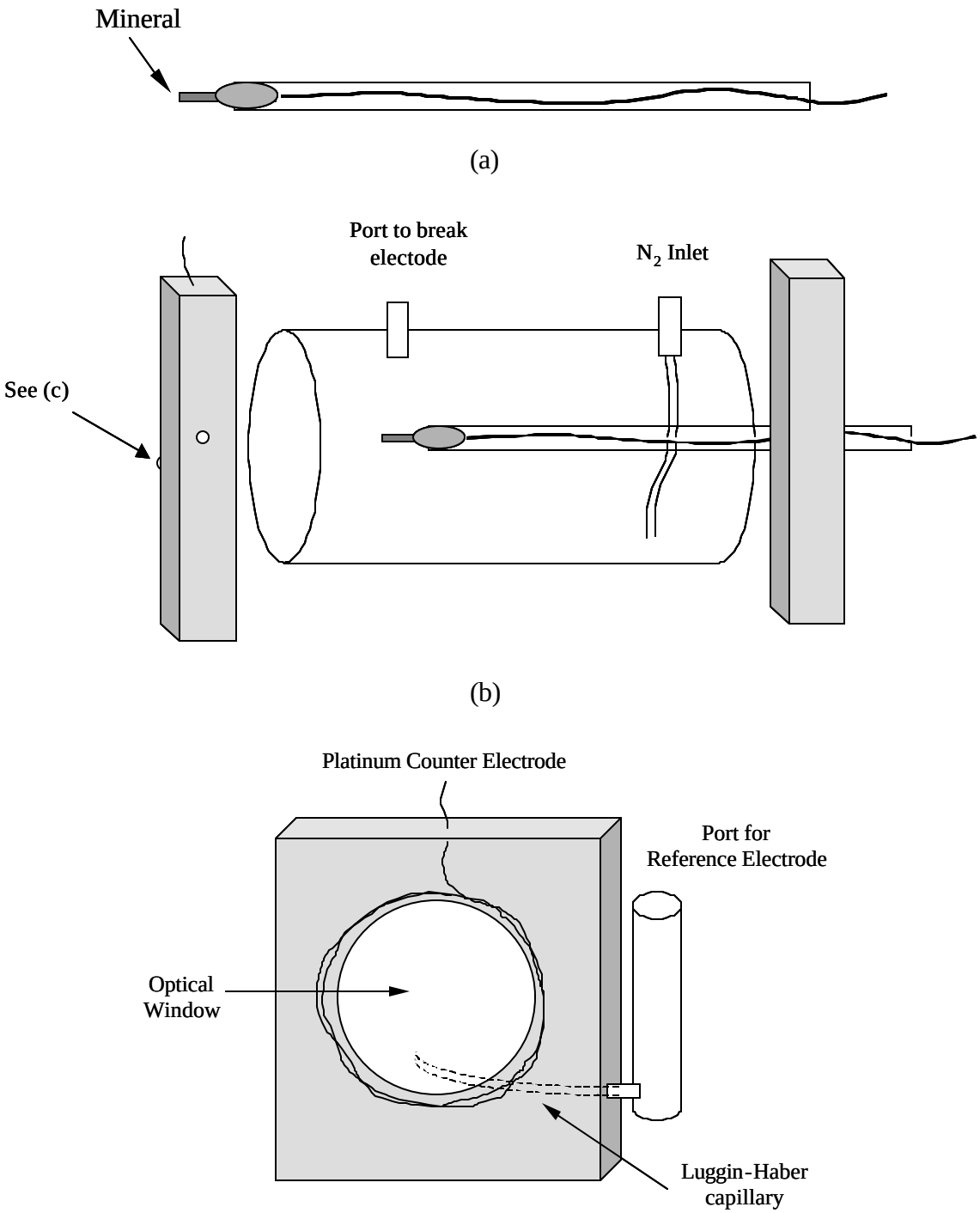

Figure 2.9 Electrochemical Setup: (a) Electrode, (b) and (c) Electrochemical Cell.

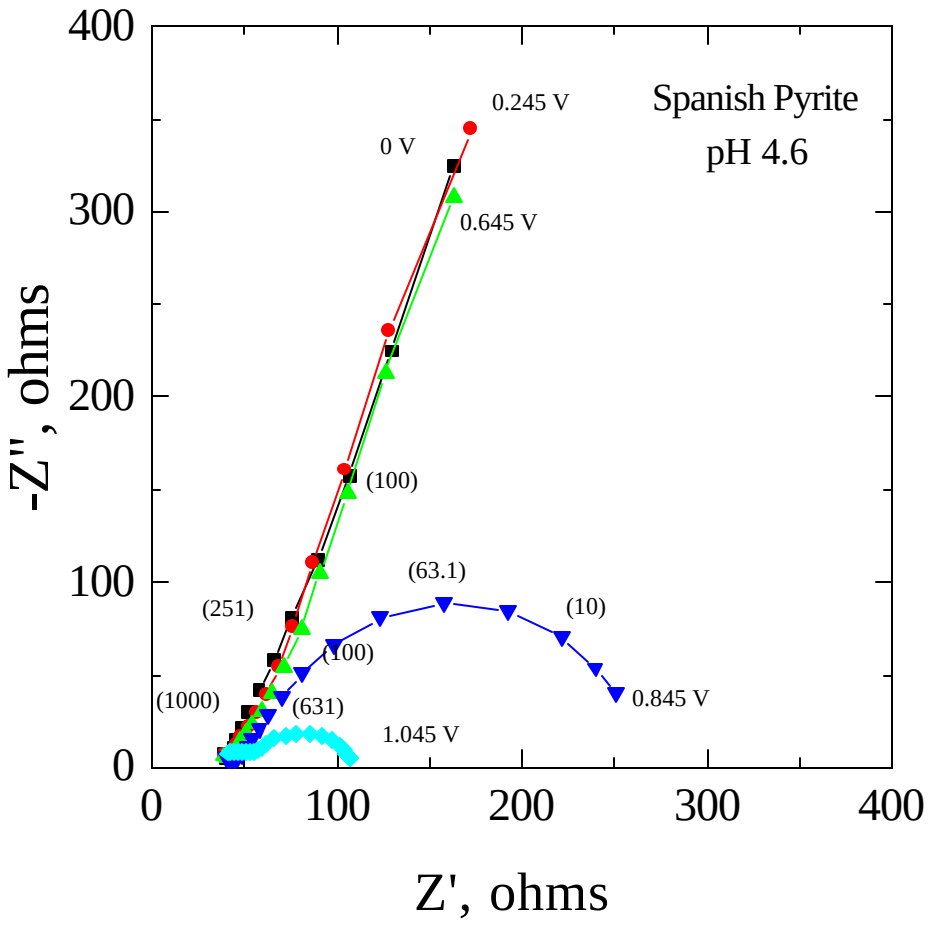

Figure 2.10 Nyquist plots for the Spanish pyrite sample in pH 4.6 solution at the stable potential (0 V SHE) and at oxidizing potentials. The numbers in parentheses represent the AC frequencies in Hz.

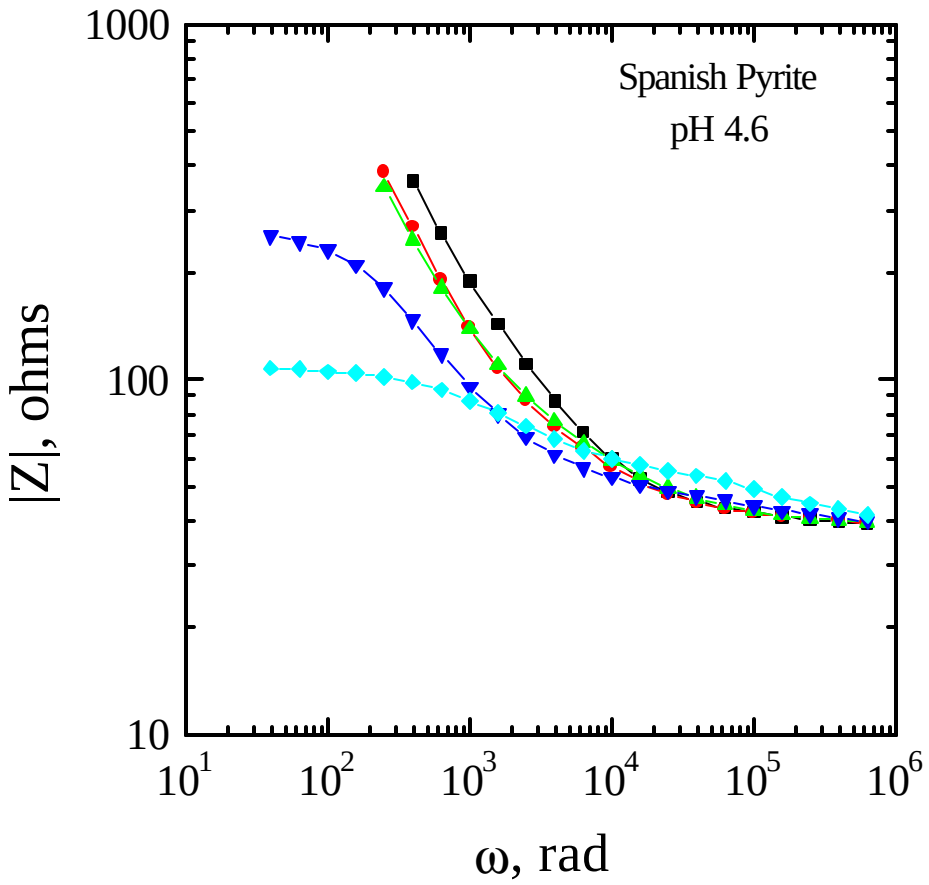

Figure 2.11. Bode plots for the Spanish pyrite sample in pH 4.6 solution at the stable potential (0 V SHE) and at oxidizing potentials.

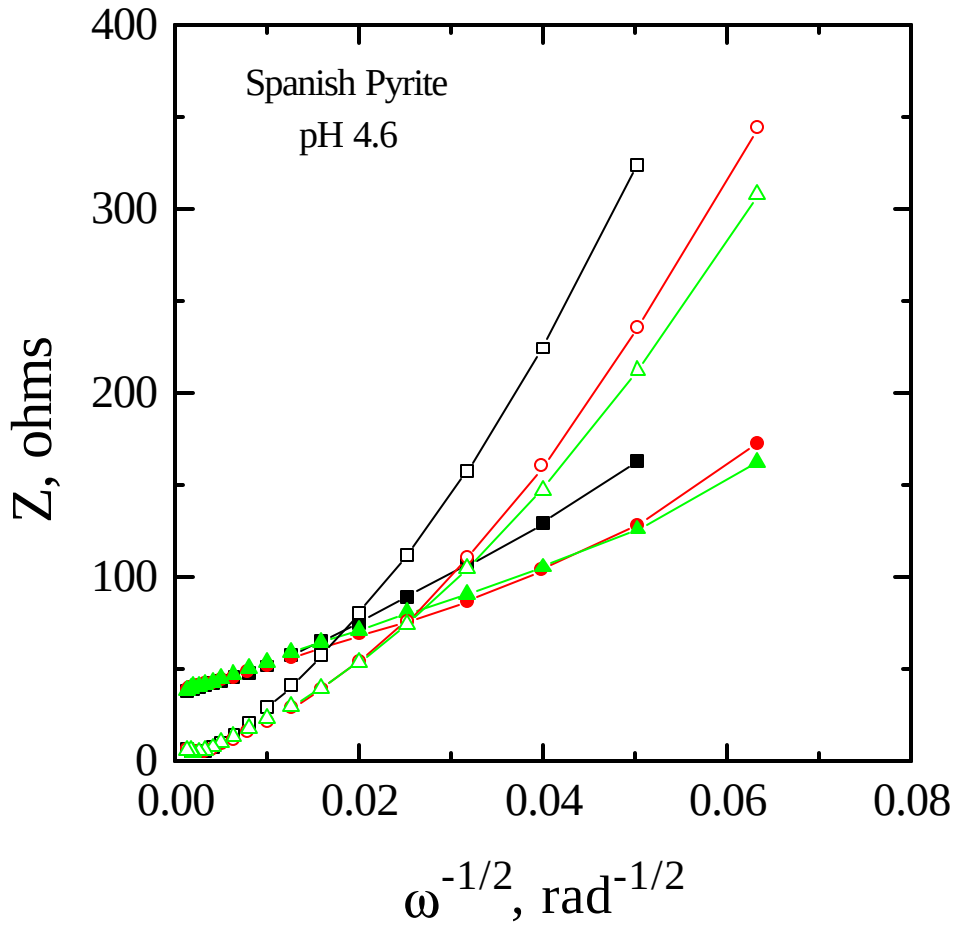

Figure 2.12. Randles plots for the Spanish pyrite sample in pH 4.6 solution at the stable potential (0 V SHE) and at oxidizing potentials.

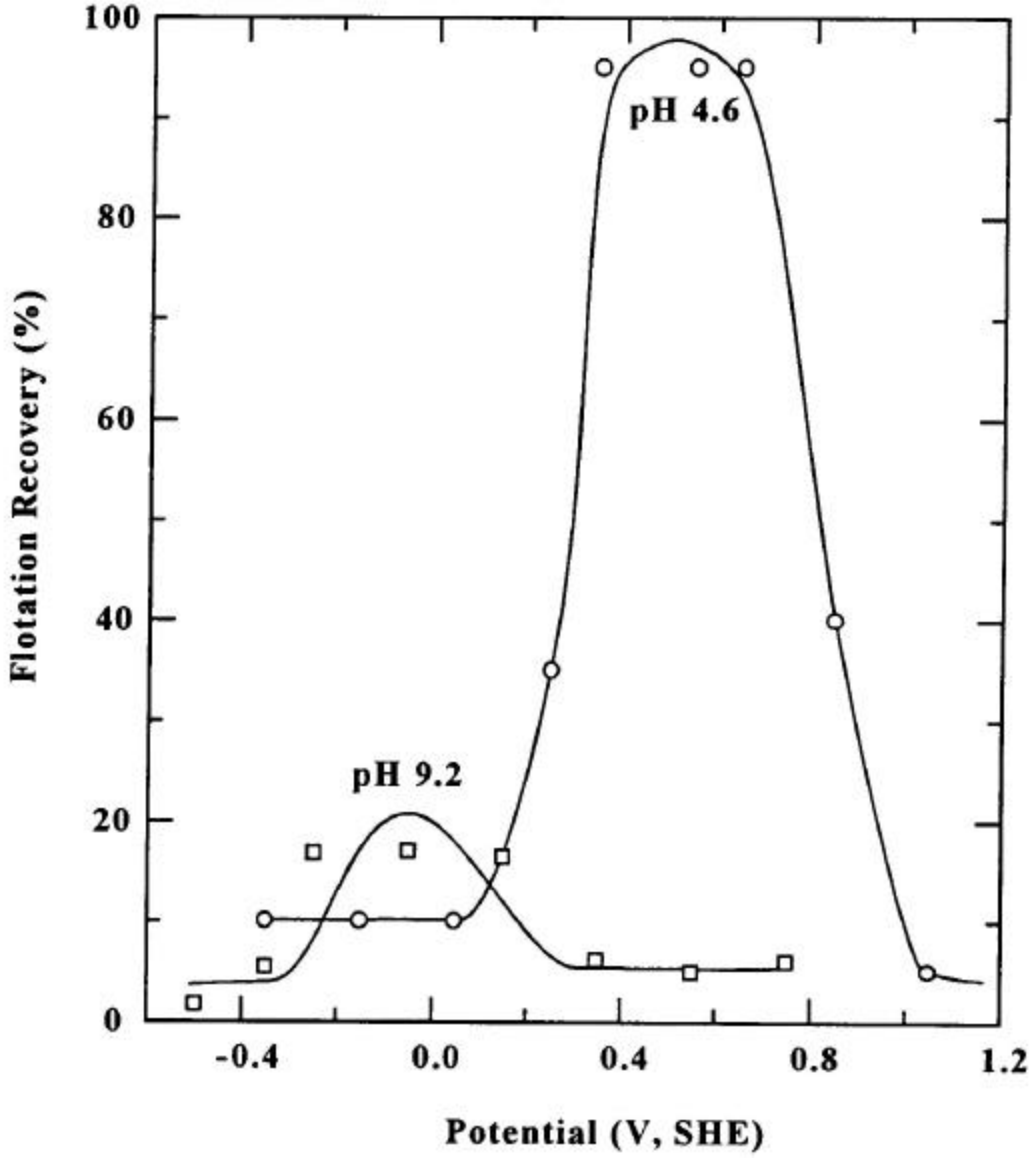

Figure 2.13 Flotation recovery of freshly ground pyrite as a function of potential at pH 4.6 and 9.2 (Tao, 1994).

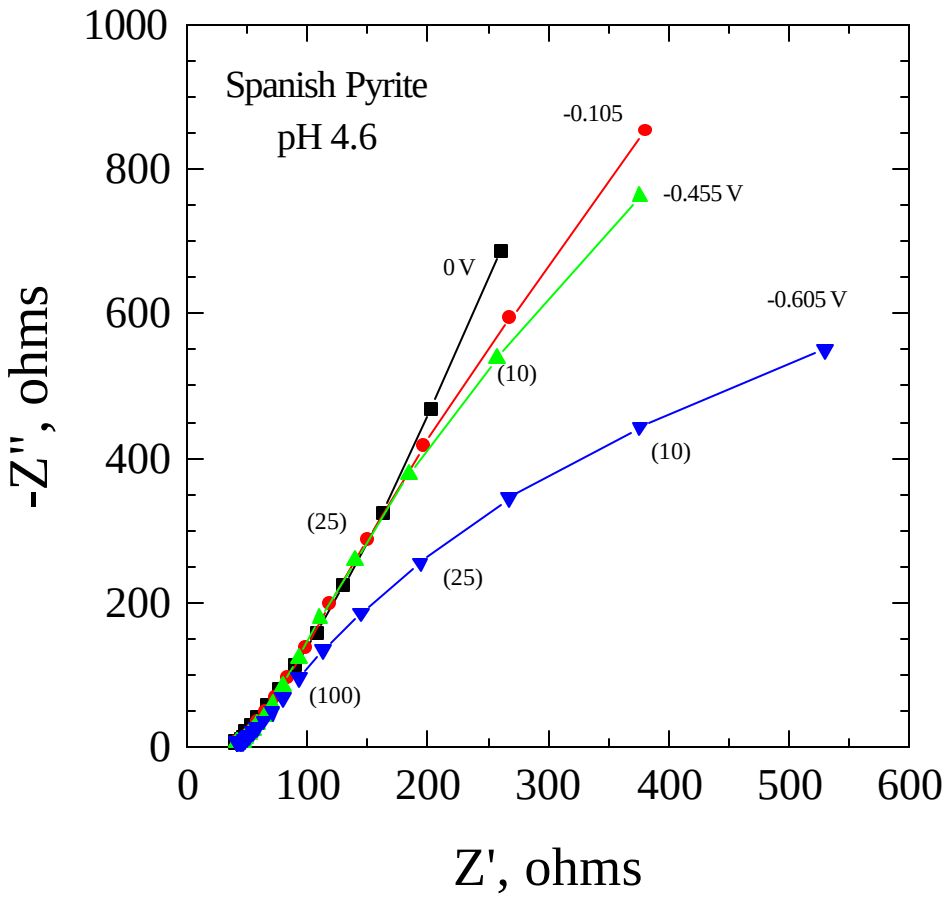

Figure 2.14 Nyquist plots for the Spanish pyrite sample in pH 4.6 solution at the stable potential (0 V SHE) and at reducing potentials. The numbers in parentheses represent the AC frequencies in Hz.

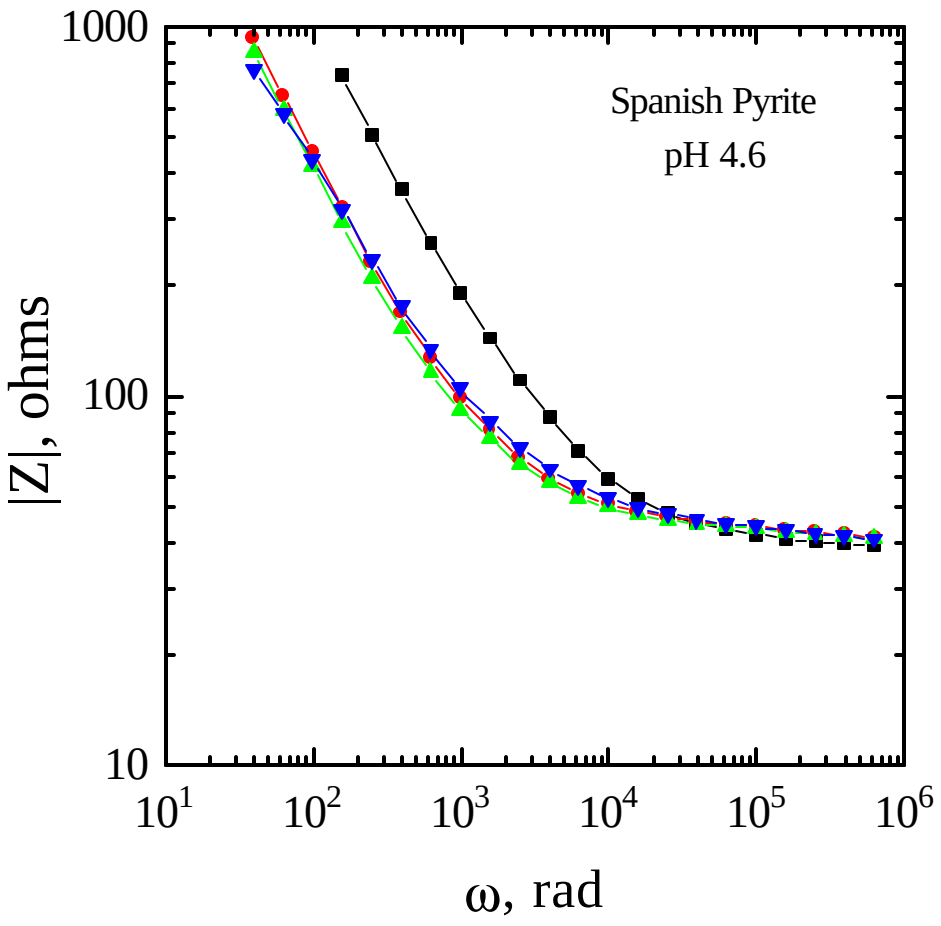

Figure 2.15 Bode plots for the Spanish pyrite sample in pH 4.6 solution at the stable potential (0 V SHE) and at reducing potentials.

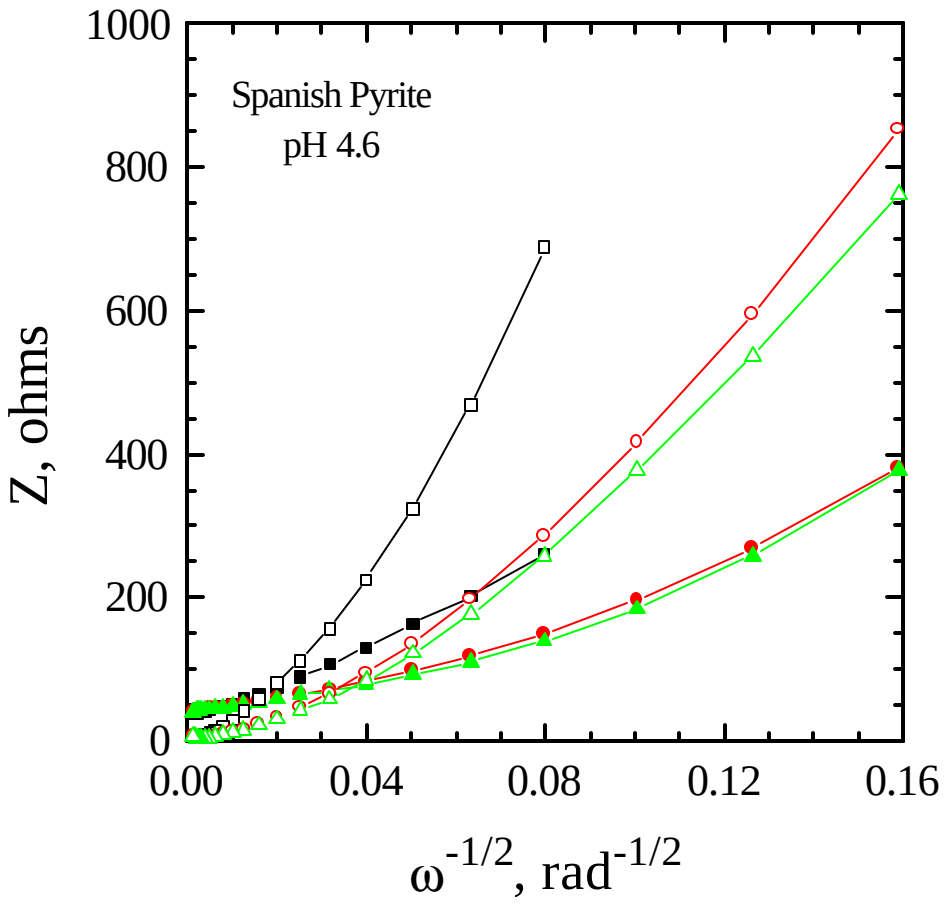

Figure 2.16. Randles plots for the Spanish pyrite sample in pH 4.6 solution at the stable potential (0 V SHE) and at reducing potentials.

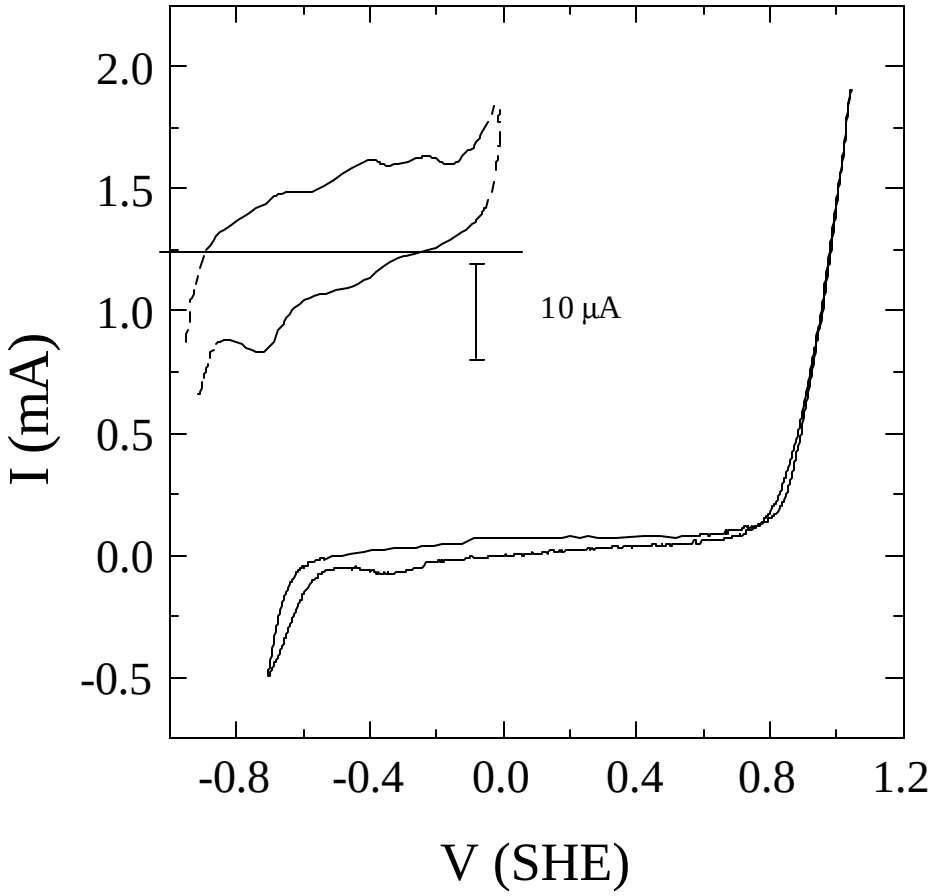

Figure 2.17. Cyclic voltammogram for Spanish pyrite at pH 4.6. Insert shows the voltammogram obatined at a higher current sensitivity

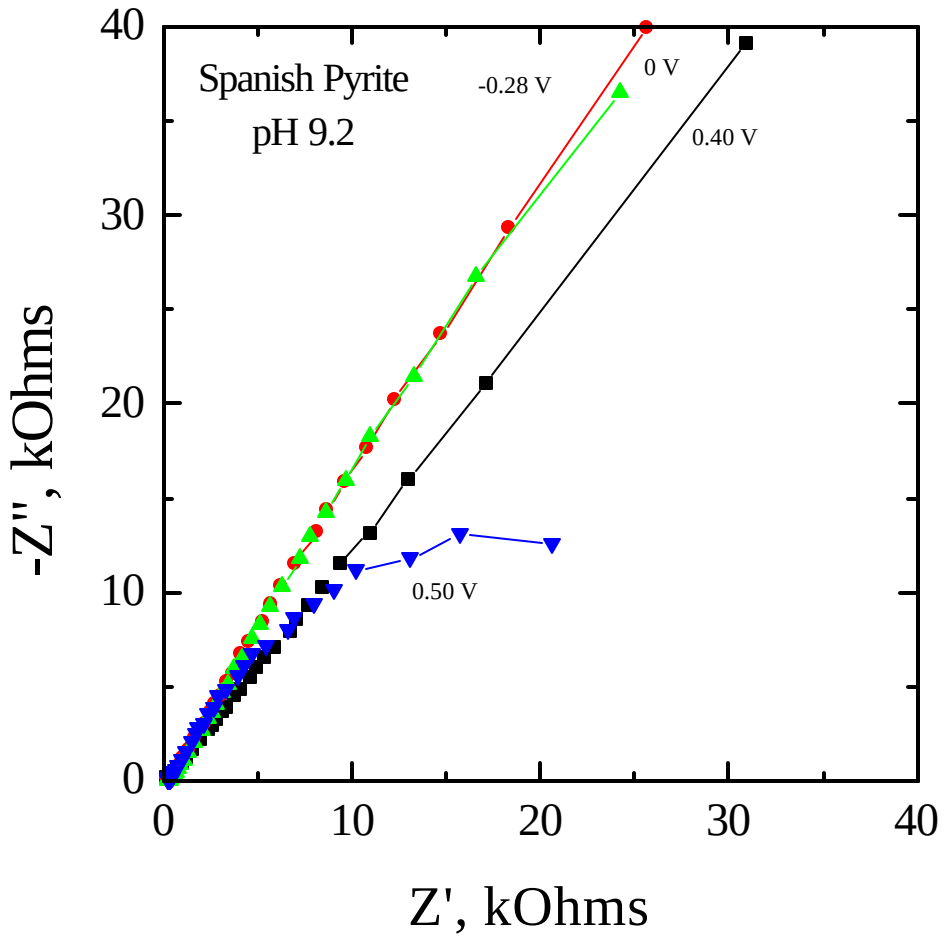

Figure 2.18 Nyquist plots for the Spanish pyrite sample in pH 9.2 solution at the stable potential (-0.28 V SHE) and at oxidizing potentials.

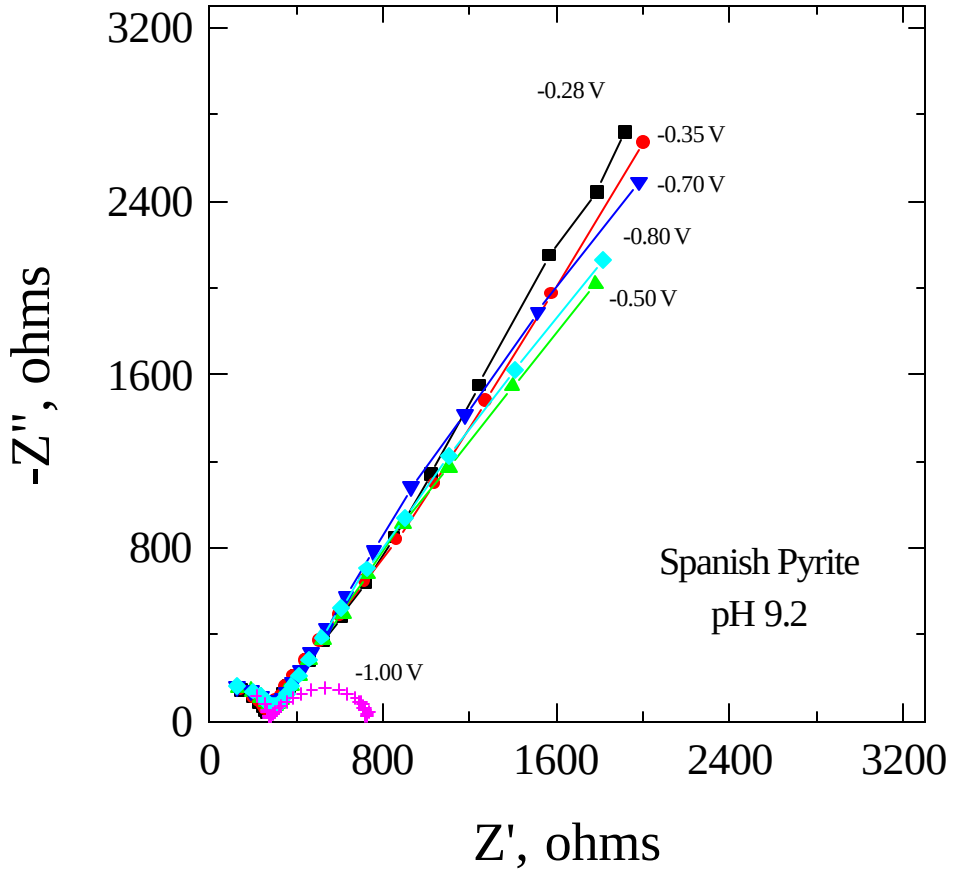

Figure 2.19 Nyquist plots for the Spanish pyrite sample in pH 9.2 solution at the stable potential (-0.28 V SHE) and at reducing potentials.

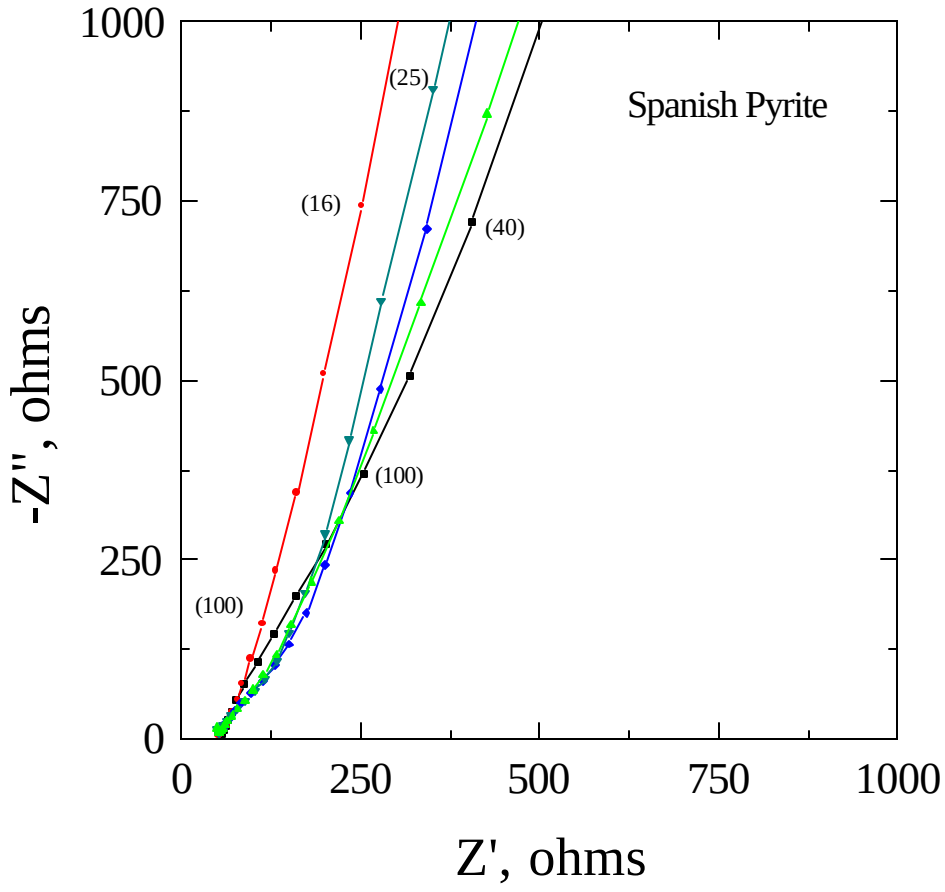

Figure 2.20. Nyquist plots for the Spanish pyrite sample at pH 4.6: (■) fractured at 0 V; polished using 600 (●) and 1200 (▲) grit silicon-carbide paper followed by micropolishing using 0.3 μm α-alumina (◆) and 0.05 μm γ-alumina (▼) and subsequently oxidized at 0.85 V.

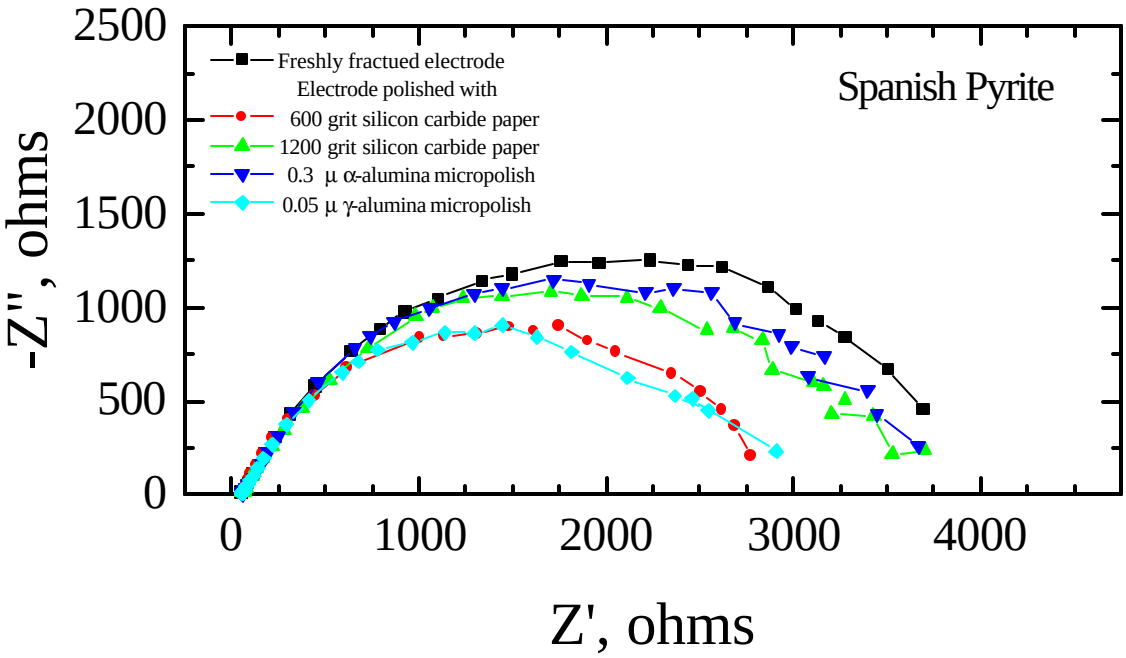

(a)

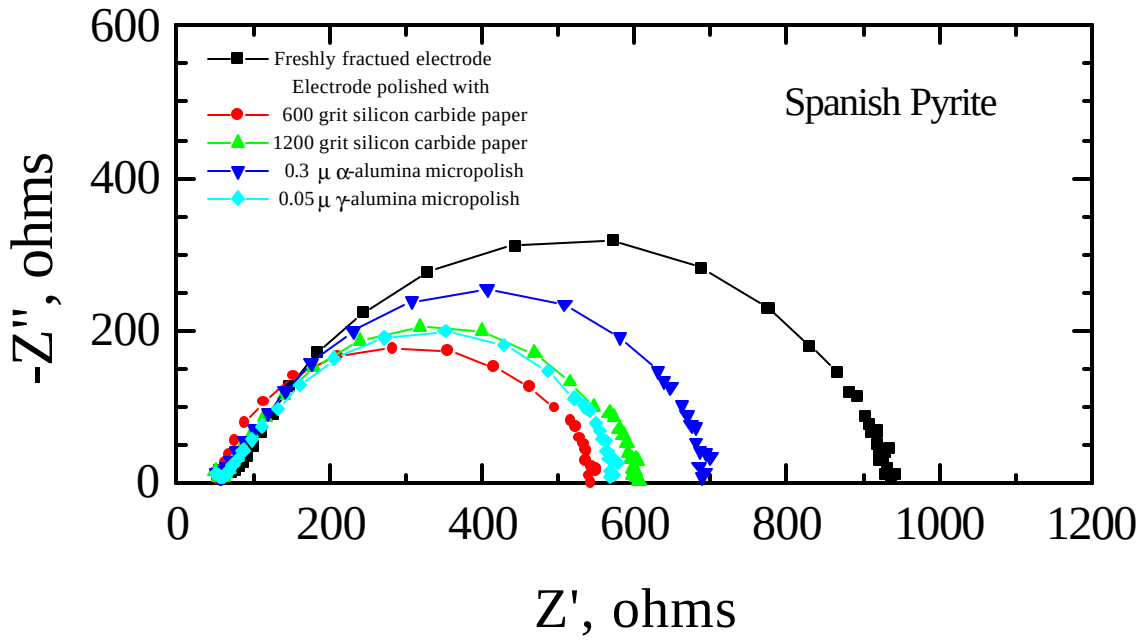

(b)

Figure 2.21. Nyquist plots for the Spanish pyrite sample at pH 4.6: (■) fractured at 0 V and polarized at (a) –0.6 V and (b) 0.85 V; polished using 600 (●) and 1200 (▲) grit silicon-carbide paper followed by micropolishing using 0.3 μm α-alumina (♦) and 0.05 μm γ-alumina (▼) and subsequently polarized.

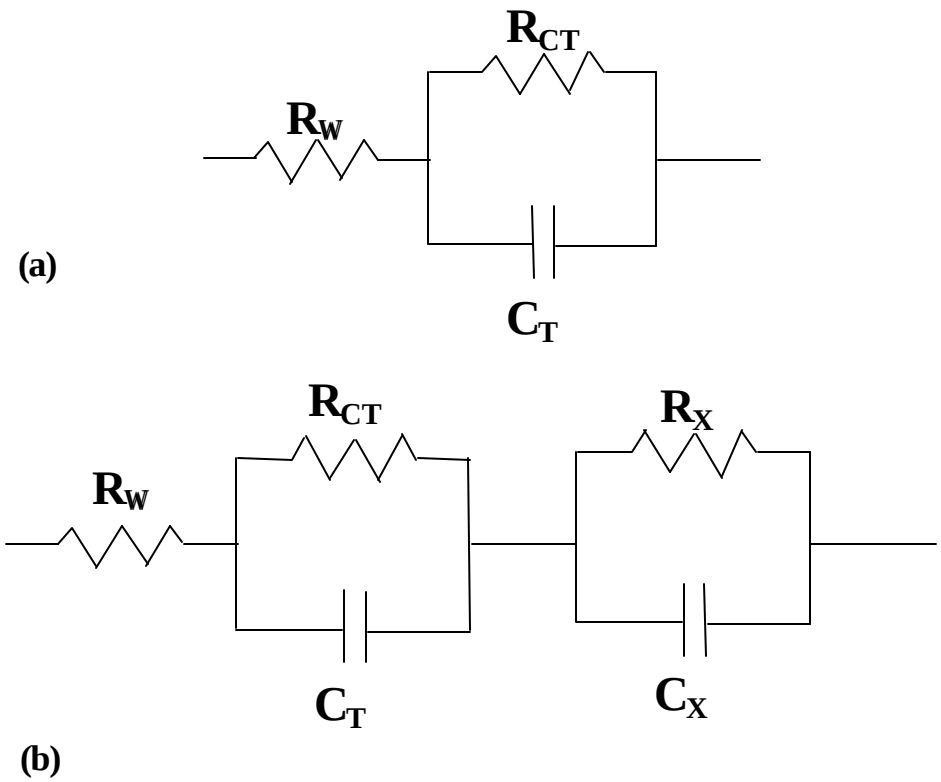

Figure 2.22 The schematic diagrams of equivalent electrical circuits for (a) simple electrochemical system, and (b) simple electrochemical system coupled with an additional R-C pair.

CHAPTER 3

ROLE OF FERRIC IONS IN XANTHATE ADSORPTION ON CHALCOPYRITE AND COPPER ACTIVATED SPHALERITE.

3.1 INTRODUCTION

3.1.1. History

In order to improve the performance of flotation circuits at the Red Dog, Alaska, electrochemical studies were carried out using an electrochemical probe, especially designed for the stated purpose. One of the most interesting discoveries made from the survey was that the despite the low amounts of oxygen present in the zinc conditioner (Figure 3.1), electrochemical potentials were sufficiently high to warrant xanthate adsorption (Figure 3.2). The flotation recovery in the zinc circuit was acceptable, although not satisfactory. The solution thermodynamics of the flotation solutions revealed that they were supersaturated with iron. The iron in flotation solution may have been produced from the grinding circuit. It was considered that oxygen was depleted from the pulp due to the oxidation of the iron chips ($Fe^0 \rightarrow Fe(II) \rightarrow Fe(III)$). In such a case, the pulp contains a considerable amount of Fe^{3+} ions in solution (due to mildly acidic pH), which might play the role of an electron scavenger in the absence of oxygen during conditioning.

3.1.2. Xanthate Adsorption

As it has been discussed in Chapter 1 (Section 1.2.1), xanthate adsorption on sulfide minerals is controlled by mixed potential mechanism. Therefore, the oxidation of xanthate on the surface of a sulfide mineral:

$$MS + X^- \rightarrow MX + S^o + e \qquad [3.1]$$

is coupled with a cathodic (reduction) reaction. For the flotation systems, the cathodic reaction is usually given by the reduction of oxygen:

$$O_2 + 4H^+ + 4e \rightarrow 2H_2O \qquad E_r = 1.23 - 0.059pH \qquad [3.2]$$

Ahmed (1978a and b) proposed that although oxygen reduction is necessary for the oxidation of xanthate, both reactions occur at separate sites and the direct reaction between xanthate and oxygen does not cause the xanthate adsorption. This indicates that the role of oxygen is to consume electrons

produced during xanthate oxidation (Reaction [3.1]). Hence, this role may be substituted by other oxidants such as ferric ions:

$$Fe^{3+} + e \rightarrow Fe^{2+} \qquad E_r = 0.77 - 0.059 \times \log([Fe^{2+}]/[Fe^{3+}]) \qquad [3.3]$$

The role of ferric ions as oxidant can be elucidated by Evans diagram (Figure 3.3). In the figure, the mixed potential is given by $E_{MX}^{O_2}$ the presence of oxygen, whereas E_{MX}^{Fe} is the mixed potential in the presence of ferric ions (and the absence of oxygen).

(a) Chalcopyrite

Allison et al. (1972) reacted chalcopyrite with xanthate (methyl through hexyl) and extracted dixanthogen using carbon disulfide. This was consistent with the results obtained by Woods (1976, Reagents book), who also stated that dixanthogen is the product of interaction between xanthate and oxygen on chalcopyrite surface. However, lower homologues of cuprous xanthate (CuX) are insoluble in carbon disulfide; therefore, they may not have been detected by Allison et al. (1972). Further work done by Richardson and his colleagues (1985, 1986) and Roos et al. (1988, 1990) shows that there is a weak to moderate flotation of chalcopyrite below the reversible potential of dixanthogen formation $\left(E_{X_2}^r\right)$. This was attributed to the formation of cuprous xanthate according to following reaction:

$$CuFeS_2 + X^- \rightarrow CuX + FeS_2 + e \qquad E^0 = -0.096 \text{ V} \qquad [3.4]$$

The reversible potential, E_h, for reaction [3.4] at $[X^-] = 2 \times 10^{-5}$ *M* is -0.340 V. However, the flotation of chalcopyrite below reversible potential for xanthate formation has also been attributed to its collectorless flotation (Gardner and Woods, 1979; Leppinen et al., 1989).

Leppinen et al. (1989) conducted FTIR studies and concluded that CuX forms at the potentials above $E_{X_2}^r$ and co-exists with X_2. At higher potentials, CuX may form *via* CuS, an oxidation product of chalcopyrite (Leppinen et al., 1989):

$$CuFeS_2 + 3H_2O \rightarrow CuS + Fe(OH)_3 + S + 3H^+ + 3e$$

$$E^0 = 0.547 \text{ V} \qquad [3.5a]$$

$$CuS + X^- \rightarrow CuX + S + e \qquad E^0 = -0.112 \text{ V} \qquad [3.5b]$$

The overall reaction may be give by:

$$CuFeS_2 + 3H_2O\ X^- \rightarrow CuX + Fe(OH)_3 + 2S + 3H^+ + 3e \qquad [3.5]$$

Roos et al. (1990) showed that the flotation above $E^r_{X_2}$ decreases with a decrease in CuX indicating that X_2 coexists with CuX and is not sufficient alone. However, Woods (1976, 1994), Heyes and Trahar (1977), Trahar (1984), Richardson and Walker (1985), Walker et al. (1986) and Leppinen et al. (1989) showed that the flotation is maximum when dixanthogen is present at the surface near or above $E^r_{X_2}$. The oxidation of xanthate to dixanthogen is given by:

$$2X^- \rightarrow X_2 + 2e \qquad E_h = -0.060 - 0.059 \times \log[X^-] \qquad [3.6]$$

(b) Copper Activated Sphalerite

The activation of sphalerite by metal ions such as Cd(II), Pb(II), Ag(II), and especially Cu(II) has been studied extensively (Ralston and Healy, 1980a,b; Ralston et al., 1981; Richardson et al., 1994; Yoon et al., 1995; Kartio et al., 1996; Yoon and Chen, 1996; Chen and Yoon, 1997, 1999, 2000). Despite studies for more than four decade, there are many uncertainties regarding the mechanism and activation products. It has been shown that the activation product and mechanism depend upon various factors such as pH, potential, time and extent of the reaction. The generalized form of the activation of ZnS with Cu(II) can be written as:

$$\underline{y\text{ZnS}} + x\text{Cu}^{2+} \rightarrow \underline{(y\text{-}x)\text{ZnS}.x\text{Cu}^{+}\text{S}^{-}} + x\text{Zn}^{2+} \qquad [3.7]$$

where underlined species represents the surface species. In alkaline pH solution, cupric and zinc ions may be considered to be the respective hydroxides, viz., $Cu(OH)_2$ and $Zn(OH)_2$ (Finkelstein, 1997).

Although the form of Cu on the surface is a debatable issue, it has been consistently shown that Cu(I) is the dominant form, which may penetrate deeper into the lattice (Perry et al., 1984, cecile, 1985, Buckley et al., 1989a; Kartio et al., 1996; Prestidge et al., 1997). However, Cu(II) is also detected at alkaline pH, which converts to Cu(I) with time (Perry et al., 1984; Prestidge et al., 1997). Nevertheless, the latest studies done by Yoon and his colleagues confirm that the activation product on the surface of cooper-activated sphalerite is CuS-like, where the valence state of Cu is 1+. For detailed information, the reader is referred to Finkelstein (1997) and Chen (1998).

If the activation product is assumed to be CuS-like, then the adsorption of xanthate can be given by:

$$\text{CuS} + \text{X}^- \rightarrow \text{CuX} + \text{S}^o + \text{e} \qquad [3.8]$$

3.2. OBJECTIVE

The purpose of the present investigation was to study the possible role of Fe^{3+} ions in the flotation of sulfide minerals. Initially, galvanic coupling experiments were conducted using two separate cells connected through a salt bridge, one with a mineral electrode immersed in a xanthate solution and the other with a platinum electrode immersed in a ferric chloride ($FeCl_3$) solution. Later experiments were conducted using a single cell, in which a mineral electrode is exposed to xanthate with and without Fe^{3+} ions. The tests were conducted using activated sphalerite and chalcopyrite.

3.3 EXPERIMENTAL

3.3.1. Materials

(a) Sample

Specimen-grade sphalerite (Santander, Spain) was obtained from the Ward's Natural Science Est., Inc. It contains 0.035% Fe, 0.012% Cu and <0.001% Pb by weight, and has a resistivity of 10^{10} ohm-cm. Chalcopyrite (of unknown purity) from Rico, Colorado, was also obtained from Ward's Natural Science Est., Inc.

(b) Reagents

All the solutions used were prepared in double-distilled deionized water using reagent grade chemicals, with the following compositions:

pH 2.0 buffer: 0.01 M HCl and 0.05 M KCl

pH 4.6 buffer: 0.05 M CH_3COOH and 0.05 M CH_3COONa

pH 6.8 buffer: 0.05 M NaH_2PO_4 and 0.025 M NaOH

Ferric ion solutions were prepared by dissolving $FeCl_3$ in pH 2.0 buffer solution. Xanthate solutions were prepared by dissolving freshly purified potassium ethyl xanthate (KEX) in deoxygenated double-distilled deionized water. All of the solutions were deoxygenated before use.

3.3.2. Apparatus and Procedure

(a) Electrochemical Experiment

Figure 3.4 shows the galvanic coupling cell designed for contact angle measurements. The cell consisted of two compartments connected by a salt bridge. The working electrode was placed in one

compartment (Cell 1), while the counter (platinum) electrode was placed in the other compartment (Cell 2). The two electrodes were galvanically connected with each other. Galvanic currents were measured by means of a zero-resistance ammeter (Keithley 485 autoranging picoammeter). A standard calomel reference electrode (SCE) was placed in Cell 1 to measure the rest potentials. The Cell 1 was equipped with an optical window to enable contact angle measurements. The measured potentials were converted to the standard hydrogen electrode (SHE) scale, taking the potential of the SCE to be 0.245 V against SHE.

Experiments were also conducted in a single-cell, which consists of the standard three-electrode system. These experiments more closely approximate the conditions for the actual conditioning of ore slurries than those conducted in galvanic coupling cell.

Chalcopyrite electrodes were prepared from specimens cut into cylinders of 6 mm in diameter. A copper wire was attached to one end by means of a conducting carbon paste or an indium solder and encapsulated with epoxy. The electrode was mounted in a glass tubing filled with epoxy, leaving one end of the cylindrical electrode exposed for contact with solution. The electrode surface was renewed before each experiment as follows: surface was wet-polished on 600 grit silicon carbide paper followed by wet polishing using 0.05 μ alumina micropolish; cleaned in a ultrasonic bath for about 5 minutes and wet polished on MASTERTEX® (Buehler) for final cleaning. Surface was rinsed with double distilled de-ionized water between each step. After rinsing with double-distilled water, the electrode was placed in a deoxygenated pH 6.8 buffer solution in Cell 1 with the mineral surface facing down.

Due to the insulating nature of sphalerite, an electrode could not be fabricated in the same manner as with chalcopyrite. Therefore, a surface conducting (SC) electrode was fabricated. A sphalerite chunk with dimensions of 15×10 mm was molded in a glass tube using epoxy resin. A small hole was drilled along the edge of the mineral and a platinum wire was inserted through it (see Figure 3.5). The platinum wire was bent at one end to ensure the electrical contact with the mineral surface, whereas the other end was connected with the copper wire. Sphalerite has been studied extensively at CCMP using carbon paste (Richardson, 1994) and indigenously developed carbon matrix electrode (CMC) (Yoon et al., 1995 & 1996). Preliminary studies with SC electrode showed that sphalerite behaved in a manner similar to carbon paste and CMC electrodes, which will be published elsewhere (Chen, 1998; Chen and Yoon, 1999, 2000).

Before each test, the mineral surface was first cleaned in chloroform to remove the KEX coating left from the previous experiment, and then treated with cyanide to remove the copper left on the surface. Then the mineral surface was renewed in a manner similar to as described for chalcopyrite. The sphalerite electrode was then activated at pH 4.6 in 10^{-4} M $CuSO_4$ solution for 30 minutes. After rinsing with distilled water, the activated sphalerite was placed in a deoxygenated pH 6.8 buffer solution, and the rest potentials were monitored.

(b) Contact Angle Measurements

As a mean of determining the hydrophobicity of the mineral electrodes used in the electrochemical experiments, contact angle measurements were conducted. The electrodes were used in such a way that the surface to be studied was facing downward. Small nitrogen bubbles were generated on the mineral surface using a syringe whose needle was bent upwards. The contact angles were measured through aqueous phase using Rame Hart goniometer. The values reported are the average of 3-5 different measurements done on the same mineral surface under the same conditions. The error for contact angle measurements was ca. $\pm 2^0$.

3.4 RESULTS AND DISCUSSION

3.4.1 Copper-Activated Sphalerite

(a) Separate-Cell Arrangement

A sphalerite electrode was activated in a 10^{-4} M $CuSO_4$ solution prepared in a pH 4.6 buffer solution at open circuit. After 30 minutes of activation, the electrode was taken out of the solution, washed with deionized water and then placed in Cell 1 containing a deoxygenated pH 6.8 buffer solution. The rest potential of the copper-activated sphalerite was measured to be 240 mV, and the contact angle was measured to be 15^o, as shown in Table 3.1. Also, as shown in Table 3.1, when 10^{-4} M KEX was added, the rest potential decreased to 165 mV, because xanthate is a reducing agent. The contact angle remained unchanged upon the xanthate addition, indicating that xanthate does not adsorb in the absence of oxygen. Figure 3.6 shows the rest potentials, contact angles and the galvanic current after activated sphalerite electrode in Cell 1 was connected to platinum electrode in Cell 2 through a zero-resistance ammeter. As, it can be seen from Figure 3.6, the contact angle remained the same

when the sphalerite electrode in Cell 1 was galvanically coupled with the platinum electrode in Cell 2, which contained deoxygenated pH 6.8 buffer solution. Also, the ammeter showed no current flowing, indicating that no galvanic interaction was taking place between the activated sphalerite and the platinum electrode.

When 10^{-4} M $FeCl_3$ was added to Cell 2 containing deoxygenated pH 6.8 buffer solution, a small galvanic current was observed. However, the contact angle and the mixed potential remained essentially the same. The fact that a small current was flowing suggest that a coupled electrochemical reactions occurred, involving an anodic reaction:

$$CuS + X^- \rightarrow CuX + S^o + e \qquad [3.8]$$

and a cathodic reaction:

$$Fe^{3+} + e \rightarrow Fe^{2+} \qquad [3.3]$$

These reactions suggest that Fe^{3+} ions act as the scavenger of the electrons generated from the anodic reaction involving xanthate adsorption. The activation product was assumed to be CuS-like, as shown by Yoon and his co-workers (Kartio et al., 1996; Yoon and Chen, 1996; Chen and Yoon, 1997, 1999, 2000).

The small galvanic current observed at pH 6.8 may be attributed to the fact that Fe^{3+} ion concentration is small at this pH due to the precipitation of $Fe(OH)_3$. Therefore, the pH of the solution in Cell 2 was reduced to 3.2, which resulted in a sharp increase in the galvanic current, as shown in Figure 3.6. The mixed potential measured after the current pulse was 240 mV, and the contact angle increased to 20^o. These results indicate increased amount of xanthate adsorbed on the activated sphalerite surface *via* Reaction [3.8], which in turn can be attributed to the increased concentration of Fe^{3+} ions in Cell 2. When the content of the solution in Cell 2 was replaced by a pH 2.0 buffer solution containing 10^{-4} M $FeCl_3$ solution, a very large pulse of galvanic current was observed. The mixed potential measured after the pulse increased to 253 mV, while the contact angle increased to 37^o.

Experiments were also conducted by changing the concentration of Fe^{3+} ions in deoxygenated pH 2 buffer solution in Cell 2 (Figure 3.6 and Table 3.1). As it can be seen from the Figure 3.6 and Table 3.1, increasing concentration of Fe^{3+} ions increases both the mixed potential and the contact angle. This indicates that xanthate adsorption on activated-sphalerite is highly sensitive to the activity of Fe^{3+} ions.

In order to compare the effect of Fe^{3+} ions on xanthate adsorption with that of oxygen, experiments were conducted by purging the pH 6.8 buffer solution in Cell 2 with air. Galvanic contacts were made between the copper-activated sphalerite in Cell 1 containing 10^{-4} M KEX in pH 6.8 buffer solution and the platinum electrode in Cell 2. The results, given in Table 3.2 as well as plotted in Figure 3.6, show that the longer the aeration time, the higher the mixed potential and the contact angle. After 20 minutes of aeration, the mixed potential of the sphalerite electrode increased to 260 mV and the contact angle to 36^{o}. These results suggest that xanthate adsorbs on activated sphalerite *via* the mixed potential reactions represented by Reactions [3.8] and [3.2], and that the longer the aeration time, the more xanthate adsorbs. Note here that it took 20 minutes of aeration before the contact angle reached 36^{o}. On the other hand, it was almost instantaneous to get a contact angle of 37^{o} at 10^{-4} M $FeCl_3$ at pH 2 (see Figure 3.6). Obviously, Fe^{3+} ions are much better electron scavenger than oxygen from kinetic point of view.

(b) Single Cell

A copper-activated sphalerite electrode was placed in a deoxygenated pH 6.8 buffer solution in a single cell. The rest potential was measured to be 240 mV and the contact angle was 15^{o}. The rest potential decreased to 161 mV when 10^{-4} M KEX was added to the solution. When $FeCl_3$ was added to the xanthate solution, both the mixed potential and the contact angle increased. As shown in Figure 3.7 and Table 3.3, the higher the Fe^{3+} ion concentration, the larger the increases become. Surprisingly, the contact angle becomes as high as 43^{o} at 5×10^{-5} M $FeCl_3$, despite the fact that most of the Fe^{3+} ions should precipitate as $Fe(OH)_3$ at pH 6.8. It is difficult to explain the reason that the contact angles measured in the single cell at pH 6.8 are substantially higher than those measured with the separate-cell arrangement at the same pH. One possible explanation is that the $Fe(OH)_3$ precipitate serves as a reservoir of Fe^{3+} ions that are supplied to the system as they are consumed during the process of xanthate adsorption. This mechanism may be similar to the case of copper activation of sphalerite in alkaline pHs, where $Cu(OH)_2$ precipitate is considered as a reservoir of Cu^{2+} ions (Ralston and Healy, 1980; Jain and Fuerstenau, 1985; Laskowski et al., 1997; Chen and Yoon, 1997).

Table 3.4 shows the results obtained with the Fe^{3+} ions replaced by air. The results are also plotted in Figure 3.7. The aeration of the xanthate solution increased both the mixed potential and the contact angle. The contact angles obtained in the presence of air are comparable to those obtained with

Fe^{3+} ions; however, the potentials were substantially higher. The reason that the mixed potentials for the Reactions [3.8] and [3.3] are lower than those for Reactions [3.8] and [3.2] can be explained by the fact that the reversible potential for Fe^{3+}/Fe^{2+} couple would be substantially lower than the oxygen reduction potential under the experimental conditions employed in the present work. One important observation made during the contact angle measurements was that the copper-activated sphalerite became hydrophobic much more quickly when Fe^{3+} ions are used as oxygen scavengers than the case of using oxygen.

3.4.2. Chalcopyrite

(a) Separate-Cell Arrangement

A chalcopyrite electrode was placed in Cell 1 containing a deoxygenated pH 6.8 buffer solution. As shown in Table 3.5, the rest potential and the contact angle were measured to be 295 mV and 10^o, respectively. When 10^{-4} M KEX was added to Cell 1, the rest potential decreased to 135 mV and the contact angle remained unchanged, indicating that xanthate does not adsorb on chalcopyrite in the absence of an electron scavenger. When the chalcopyrite electrode was galvanically coupled to the platinum electrode in Cell 2 containing a deoxygenated pH 6.8 buffer solution, no current was observed as shown in Figure 3.9, and the contact angle remained unchanged.

When 10^{-4} M $FeCl_3$ was added to the pH 6.8 buffer solution in Cell 2, a small galvanic current was observed, as shown in Figure 3.9. Also, the potential increased to 195 mV and contact angle increased to 18^o (Table 3.5). These changes suggest that xanthate adsorption occurs *via* the following reaction:

$$2X^- \rightarrow X_2 + 2e \qquad E_h = -0.060 - 0.059 \times \log[X^-] \qquad [3.6]$$

coupled with Reaction [3.2]. It has been shown by Leppinen et al. (1989) that Reaction [3.6] occurs at relatively low potentials. At higher potentials, xanthate adsorbs *via* the following reaction:

$$CuFeS_2 + 3H_2O\ X^- \rightarrow CuX + Fe(OH)_3 + 2S + 3H^+ + 3e \qquad [3.5]$$

suggesting that CuX is the hydrophobic species.

The fact that only a small current was observed and that the contact angle was increased only to 18^o may be attributed to the lower concentration of Fe^{3+} ions at pH 6.8. Therefore, the solution in Cell 2 was replaced by a pH 2 buffer solution containing 10^{-4} M Fe^{3+} ions, which resulted in a large galvanic

current, as shown in Figure 3.9. Also, the mixed potential increased to 390 mV and contact angle increased to 31°, as shown in Table 3.5.

Also shown in Table 3.5 is the result of replacing the Fe^{3+} ions in Cell 2 with oxygen. The Cell 2 was filled with a pH 6.8 buffer solution, which was purged subsequently with air for 30 minutes. The result was that the mixed potential increased to 405 mV and contact angle increased to 34°. These results are close to those obtained with 10^{-4} M Fe^{3+} ions in Cell 2. However, the kinetics of xanthate adsorption, as detected by contact angle measurement, was much faster with the Fe^{3+} ions as electron scavengers.

(b) Single-Cell

Table 3.6 shows the results obtained with a chalcopyrite electrode in the single cell containing a deoxygenated pH 6.8 buffer solution. The rest potential was 292 mV and the contact angle was measured to be 8°. When 10^{-4} M KEX was added, the potential decreased to 134 mV, and the contact angle remained the same. When 10^{-4} M $FeCl_3$ was added to the cell, the mixed potential increased to 395 mV, and the contact angle increased to 20°. This value is comparable to that obtained using the separate-cell with the pH of the solution in Cell 2 at 6.8 (see Table 3.5). However, it is considerably lower than the case of using the separate-cell with the pH of the solution in Cell 2 at 2. This can be attributed to the lower activity of Fe^{3+} ions in the single cell at pH 6.8.

When the Fe^{3+} ions in the xanthate solution at pH 6.8 was replaced with 30 minutes of aeration, the chalcopyrite electrode gave a mixed potential of 400 mV and a contact angle of 30°. The mixed potential is comparable to the same measured with the case of separate-cell arrangement; however, the contact angle is slightly lower.

3.5 CONCLUSIONS

1. Galvanic coupling experiments were conducted with a sulfide mineral electrode in Cell 1 containing a xanthate solution and a platinum electrode in Cell 2. The xanthate adsorption, as detected by the changes in contact angle, occurs only when an electron scavenger is present in Cell 2.
2. Both oxygen and Fe^{3+} ions can serve as the scavenger of the electrons generated during the process of xanthate adsorption on sulfide minerals. The results obtained with activated sphalerite and

chalcopyrite show that the kinetics of xanthate adsorption is faster when using the Fe^{3+} ions as the electron scavenger than using air.

3. The xanthate adsorption on activated sphalerite is dependent on the activity of free Fe^{3+} ions present in solution. Thus, the contact angle and the galvanic current increase with decreasing pH of the solution in Cell 2 and with increasing concentration of Fe^{3+} ions in solution.
4. The effects of the Fe^{3+} ions on the xanthate adsorption on chalcopyrite and activated sphalerite were also studied using a single electrochemical cell, which simulates the conditioners that are commonly used to for reagent addition to ore slurries prior to flotation. The experimental data obtained with the single cell gave the same conclusion as that obtained using the separate electrochemical cells, i.e., xanthate can adsorb on sulfide minerals in the absence of oxygen, provided that Fe^{3+} ions are present in solution.
5. The single-cell experiments show that xanthate can adsorb on a copper-activated sphalerite electrode at pH 6.8 at 10^{-4} M $FeCl_3$ in the absence of oxygen, despite the fact that most of the iron are tied-up as $Fe(OH)_3$ at this pH. This finding might be explained by the possibility that $Fe(OH)_3$ precipitate may act as a reservoir for Fe^{3+} ions during the process of xanthate adsorption on the mineral surface.

3.6 REFERENCES

Ahmed, S.M., 1978a. *IJMP*, **5**, 163-174.

Ahmed, S.M., 1978b. *IJMP*, **5**, 175-182.

Allison, S.A., Goold, L.A., Nicol, M.J. and Granville, A., 1972. *Metall Trans.*, **3**, 2613-2618.

Chen, Z. 1998. Dissertation, Virginia Polytech. Insti. And State Univ. Virginia (USA).

Chen, Z. and Yoon, R.-H. 1997. Processing of Complex Ores (Eds. J.A. Finch, S.R. Rao and I. Holubec). CIM: Montrel (Canada). 143-152.

Chen, Z. and Yoon, R.-H., 1999. SME Annual Meeting, Denver, (CO). SME: Littleton (CO).

Chen, Z. and Yoon, R.-H., 2000. *IJMP*, **58** 57-66.

Finkelstein, N.P., 1997. *IJMP*, **52**, 81-120.

Gardner, J.R. and Woods, R., 1979b. *J. Electroanal. Chem. Interf. Electrochem*, **100**. 447-459. 1979

Jain, S. and Fuerstenau, D.W., 1985. Flotation in Sulfide Minerals, (Ed. K.S.E. Forssberg), 159-174.

Kartio, I.J., Basilio, C.I. and Yoon, R.-H. 1996. Proc. Intl. Symp. Electrochem. in Mineral and Metal Process. IV (Eds. R. Woods, F.M. Doyle and P.E. Richardson). ECS: Pennington (NJ). 25-37.

Laskowski, J.S., Liu, Q. and Zhan, Y., 1997, "Sphalerite Activation: Flotation and Electrokinetics Studies", Minerals Engg. 10, 787-802.

Laskowski, J.S., Liu, Q. and Zhan, Y., 1997. *Minerals Engg.*, **10**, 787-802.

Leppinen, J.O., Basilio, C.I. and Yoon, R.-H., 1989. *IJMP.*, **26**, 259-274.

Perry, D.L., Tsao, L. and Taylor, J.A., 1984. . Proc. Intl. Symp. Electrochem. in Mineral and Metal Process. I (Eds. P.E. Richardson, S. Srinivasan and R. Woods). ECS: Pennington (NJ), 169-184.

Prestidge, C.A., Skinner, W.M., Ralston, J. and Smart, R., 1997. *App Surf Sci.*, **108**, 333-344.

Ralston, J. and Healy, T.W., 1980a. *IJMP*, **7**, 175-201.

Ralston, J. and Healy, T.W., 1980b. *IJMP*, **7**, 203-217.

Ralston, J., Alabaster, P. and Healy, T.W., 1981. **7,** 279-310.

Richardson, P.E. and Walker, G.W., 1985. Proceedings of the XVth International Mineral Processing

Congress, Cannes. **2**, 198-210.

Richardson, P.E., Hu, Q., Finkelstein, N.P. and Yoon, R.-H., 1994. *IJMP*, **41**, 71-76.

Roos, J.R., Celis, J.P. and Sundarsono, A.S., 1988. *IJMP*, **24**, 91-110.

Roos, J.R., Celis, J.P. and Sundarsono, A.S., 1990. *IJMP*, **28**, 231-245.

Trahar, W.J., 1984. Principles of Mineral Flotation, The Wark Symp. AusIMM.

Walker, G.W., Walters, C.P., and Richardson, P.E., 1986. *IJMP*, **18**, 119-137.

Woods, R., "Electrochemistry of Sulfide Flotation", 1976, Flotation, M.C. Fuerstenau (Ed.), A.M. Gaudin Memorial Volume, AIME, Volume 1, 198-333.

Yoon R.-H., Chen Z., Finkelstein, N.P. and Richardson, P.E., 1995. XIX Intl Min. Process. Conference, SME.

Yoon, R.-H. and Chen Z., 1996. Proc. Intl. Symp. Electrochem. in Mineral and Metal Process. IV. (Eds. R. Woods, F.M. Doyle and P.E. Richardson .), ECS: Pennington (NJ). 38-47.

Table 3.1. Effects of Fe^{3+} Ions on the Mixed Potentials and the Contact Angles of Copper-Activated Sphalerite Electrodes.

Cell 1	Cell 2		Chalcopyrite	
pH 6.8 buffer solution	pH 2 buffer solution	Rest Potential (mV)	Mixed Potential (mV)	Contact Angle
-	-	240	-	15^o
10^{-4} M KEX	-	165	-	15^o
10^{-4} M KEX	1×10^{-5} M Fe^{3+}	-	170	25^o
10^{-4} M KEX	4×10^{-5} M Fe^{3+}	-	220	30^o
10^{-4} M KEX	9×10^{-5} M Fe^{3+}	-	255	38^o

Table 3.2. Effects of Oxygen on the Mixed Potentials and the Contact Angles of Copper-Activated Sphalerite Electrodes.

Cell 1	Cell 2		Copper-Activated Sphalerite	
pH 6.8 buffer solution	pH 6.8 buffer solution	Rest Potential (mV)	Mixed Potential (mV)	Contact Angle
-	-	240	-	15^o
10^{-4} M KEX	-	165	-	15^o
10^{-4} M KEX	Air (2 min.)	-	181	26^o
10^{-4} M KEX	Air (5 min.)	-	209	29^o
10^{-4} M KEX	Air (20 min.)	-	260	36^o

Table 3.3. Effects of the Fe^{3+} Ions on the Mixed Potentials and the Contact Angles of Copper-Activated Sphalerite Electrodes at pH 6.8.

Single Cell		Copper-Activated Sphalerite		
pH 6.8 buffer solution		Rest Potential (mV)	Mixed Potential (mV)	Contact Angle
-	-	240	-	15^o
10^{-4} M KEX	-	161	-	15^o
10^{-4} M KEX	10^{-5} M Fe^{3+}	-	163	26^o
10^{-4} M KEX	2×10^{-5} M Fe^{3+}	-	165	40^o
10^{-4} M KEX	5×10^{-5} M Fe^{3+}	-	173	43^o

Table 3.4. Effects of Oxygen on the Mixed Potentials and the Contact Angles of Copper-Activated Sphalerite Electrodes at pH 6.8.

Single Cell		Copper-Activated Sphalerite		
pH 6.8 buffer solution		Rest Potential (mV)	Mixed Potential (mV)	Contact Angle
-	-	240	-	15^o
10^{-4} M KEX	-	161	-	15^o
10^{-4} M KEX	Air (2 min.)	-	202	30^o
10^{-4} M KEX	Air (5 min.)	-	225	40^o
10^{-4} M KEX	Air (20 min.)	-	245	47^o

Table 3.5. Effect of Fe^{3+} Ions and Oxygen on the Mixed Potentials and the Contact Angles of Chalcopyrite Electrodes.

Cell 1	Cell 2	Chalcopyrite		
pH 6.8 buffer solution	(Buffer Solution)	Rest Potential (mV)	Mixed Potential (mV)	Contact Angle
-	-	295	-	10^{o}
10^{-4} M KEX	-	135	-	10^{o}
10^{-4} M KEX	10^{-4} M Fe^{3+} (pH 6.8)	-	195	18^{o}
10^{-4} M KEX	10^{-4} M Fe^{3+} (pH 2)	-	390	31^{o}
10^{-4} M KEX	Air (30 min.) (pH 6.8)	-	405	34^{o}

Table 3.6. Effects of Fe^{3+} Ions and Oxygen on the Mixed Potentials and the Contact Angles of Chalcopyrite Electrodes.

Single Cell		Chalcopyrite		
pH 6.8 buffer solution		Rest Potential (mV)	Mixed Potential (mV)	Contact Angle
-	-	292	-	8^{o}
10^{-4} M KEX	-	134	-	8^{o}
10^{-4} M KEX	10^{-4} M Fe^{3+}	-	395	20^{o}
10^{-4} M KEX	Air (30 min.)	-	400	30^{o}

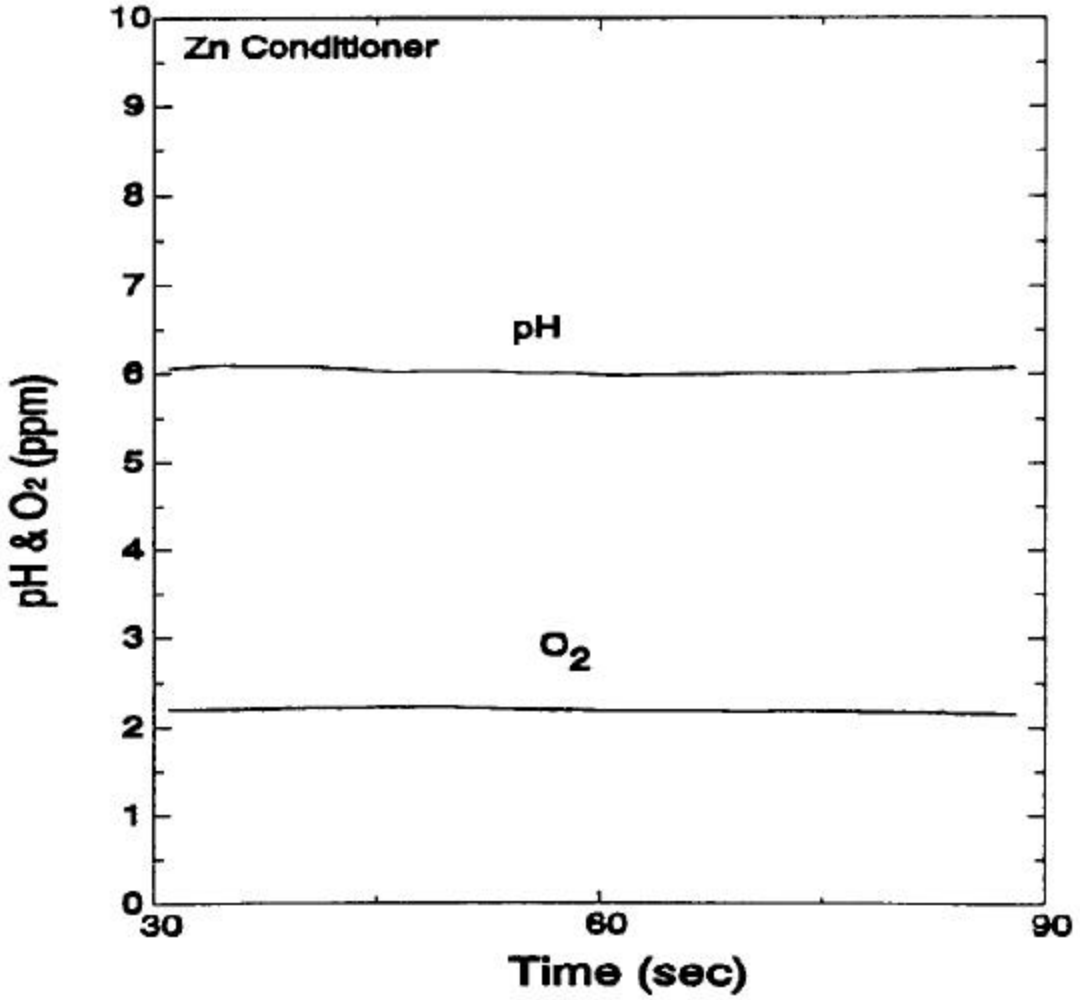

Figure 3.1 O_2 levels measured in Red Dog Zinc Conditioner.

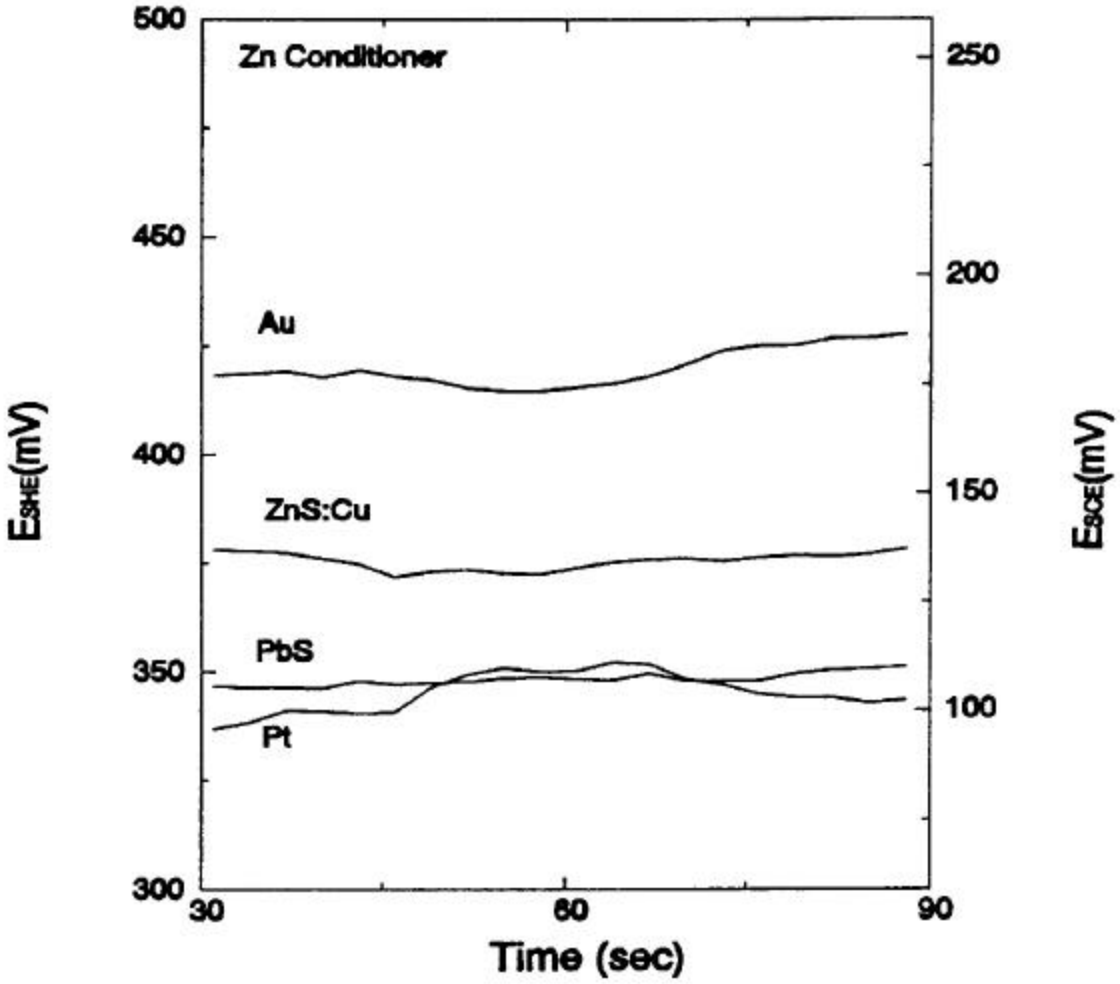

Figure 3.2 Potential measured in Red Dog Zinc Conditioner.

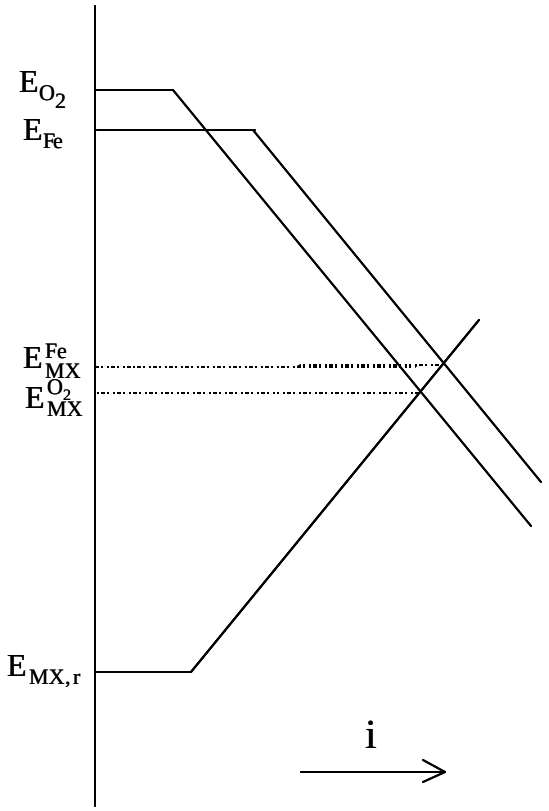

Figure 3.3. Evan's diagram showing mixed potential mechanism for the adsorption of xanthate coupled with either oxygen reduction (E_{MX}^{O2}) or ferric ions (E_{MX}^{Fe}).

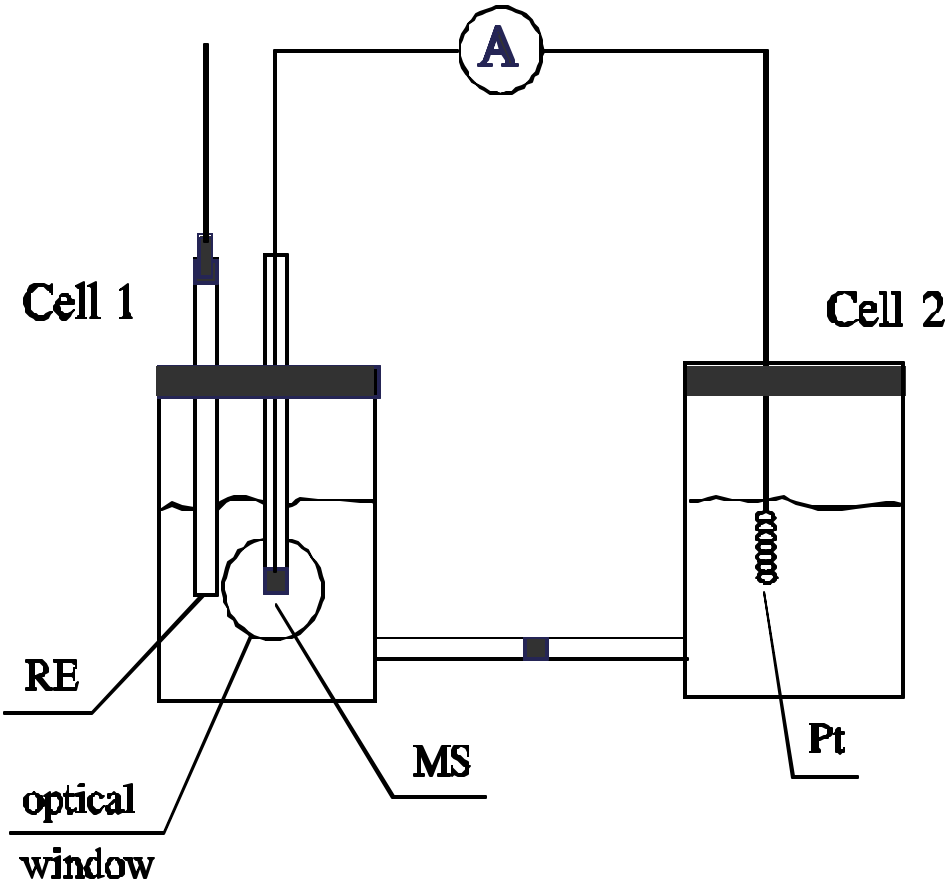

Figure 3.4 Schematic illustration of the electrochemical apparatus for galvanic coupling experiments and contact angle measurements.

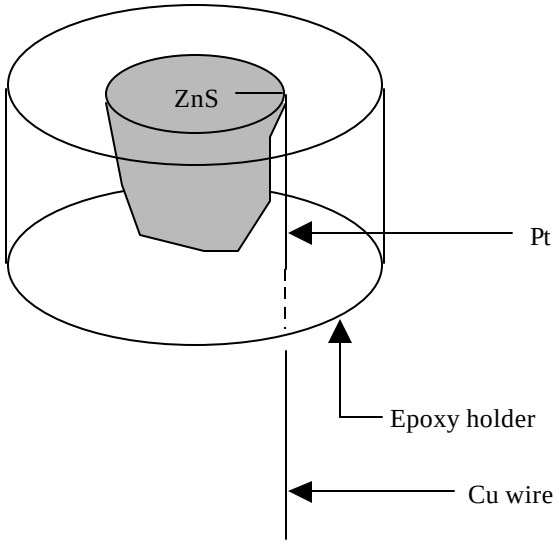

Figure 3.5 Schematic illustration of surface conducting (SC) electrode.

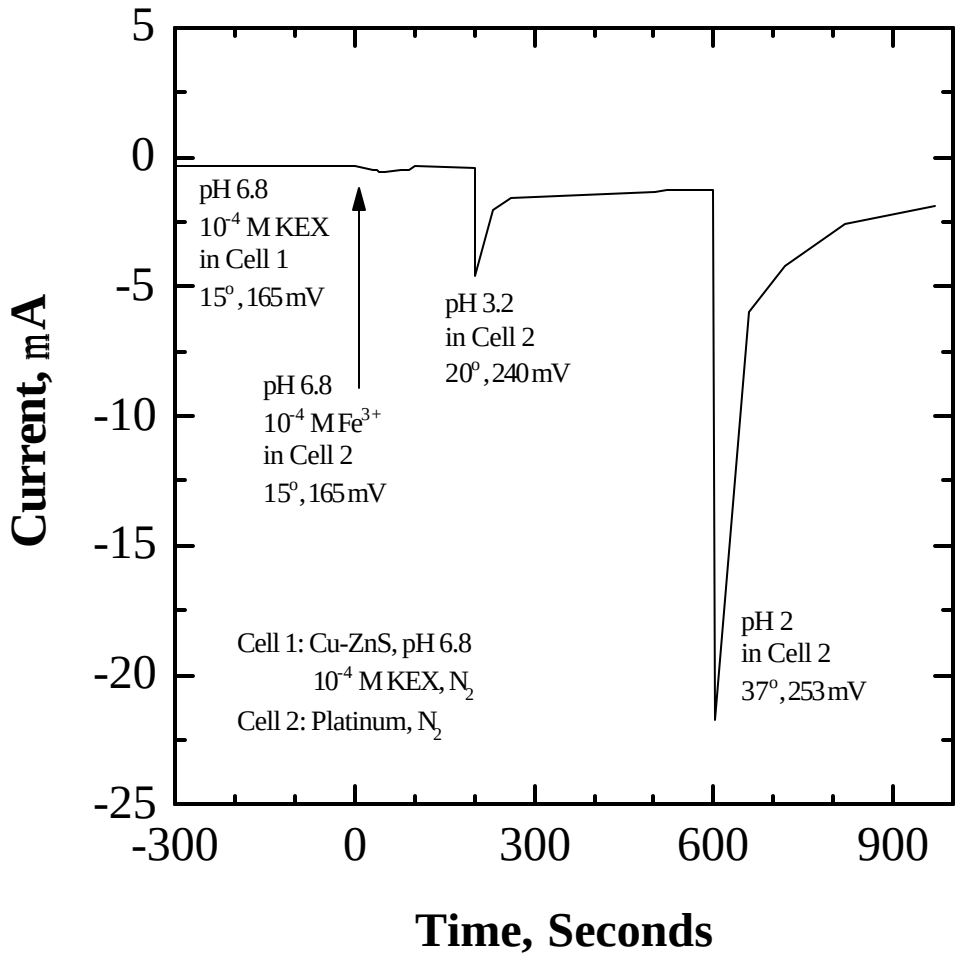

Figure 3.6 Galvanic coupling current between a copper-activated sphalerite electrode in Cell 1 containing 10^{-4} M KEX solution at pH 6.8 and a platinum electrode in Cell 2 containing 10^{-4} M $FeCl_3$ at different pHs.

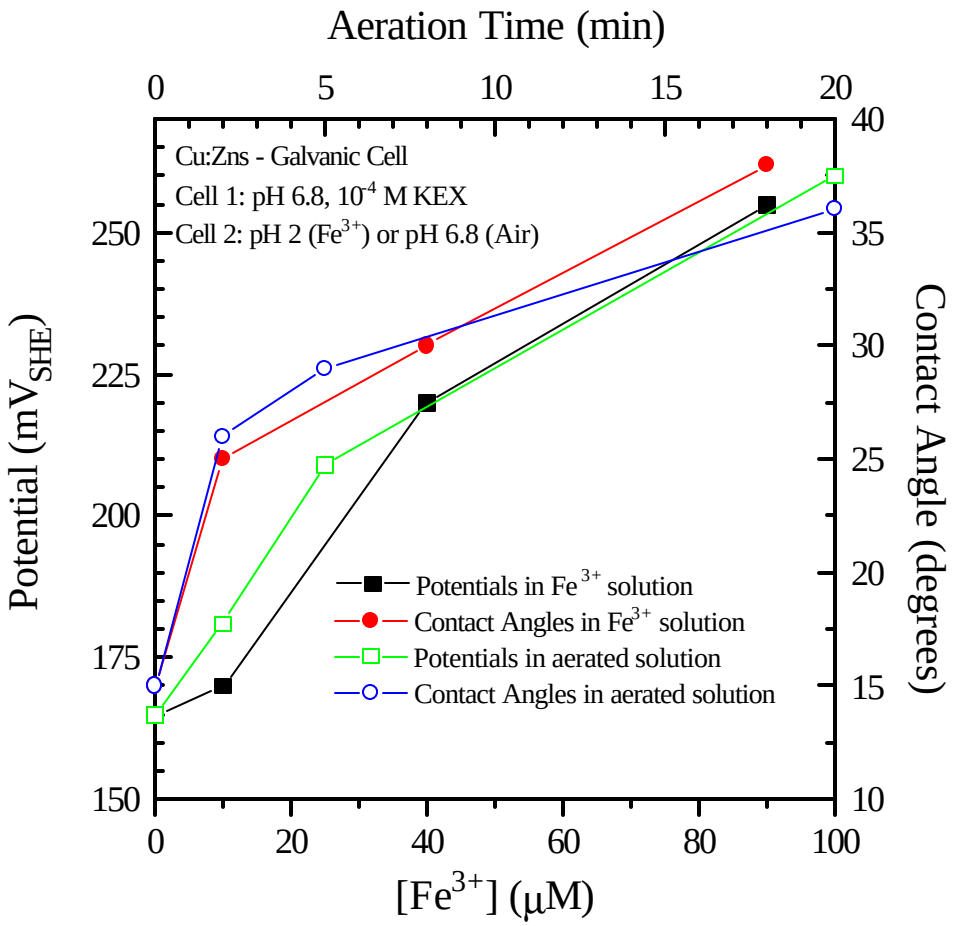

Figure 3.7 Effect of Fe^{3+} and aeration on mixed potential and contact angle for copper-activated sphalerite in galvanic coupling cell.

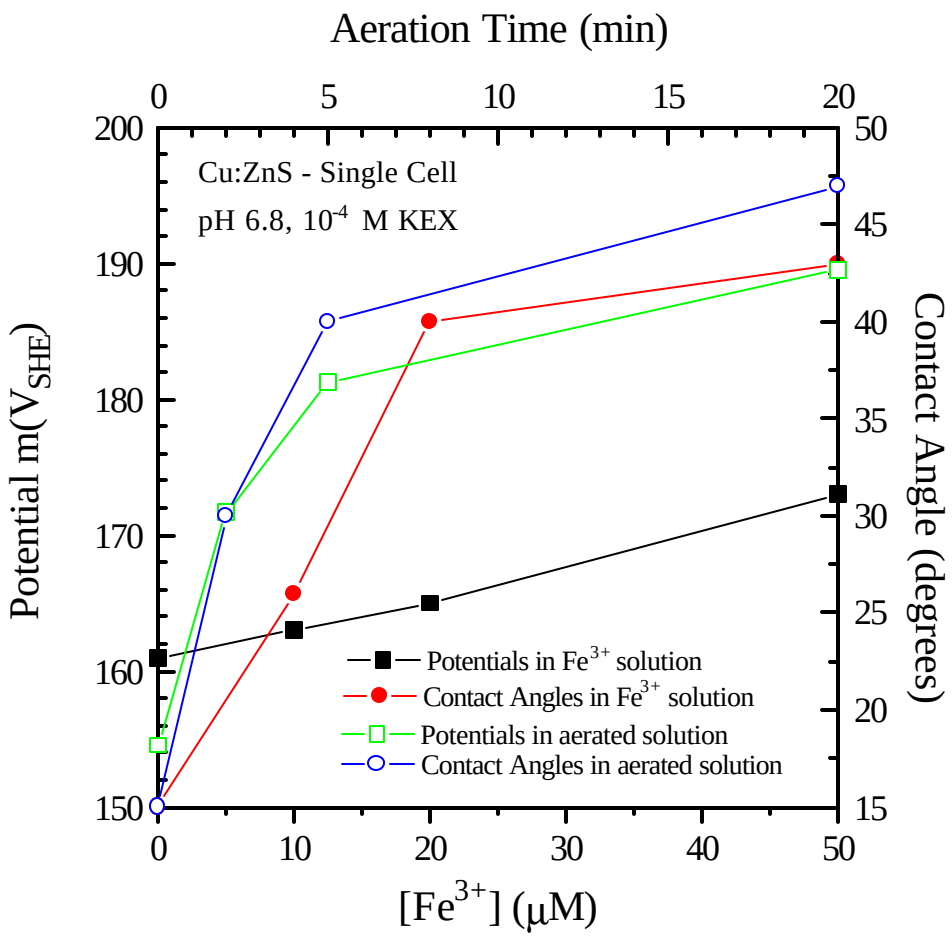

Figure 3.8 Effect of Fe^{3+} and aeration on mixed potential and contact angle for copper-activated sphalerite in single cell.

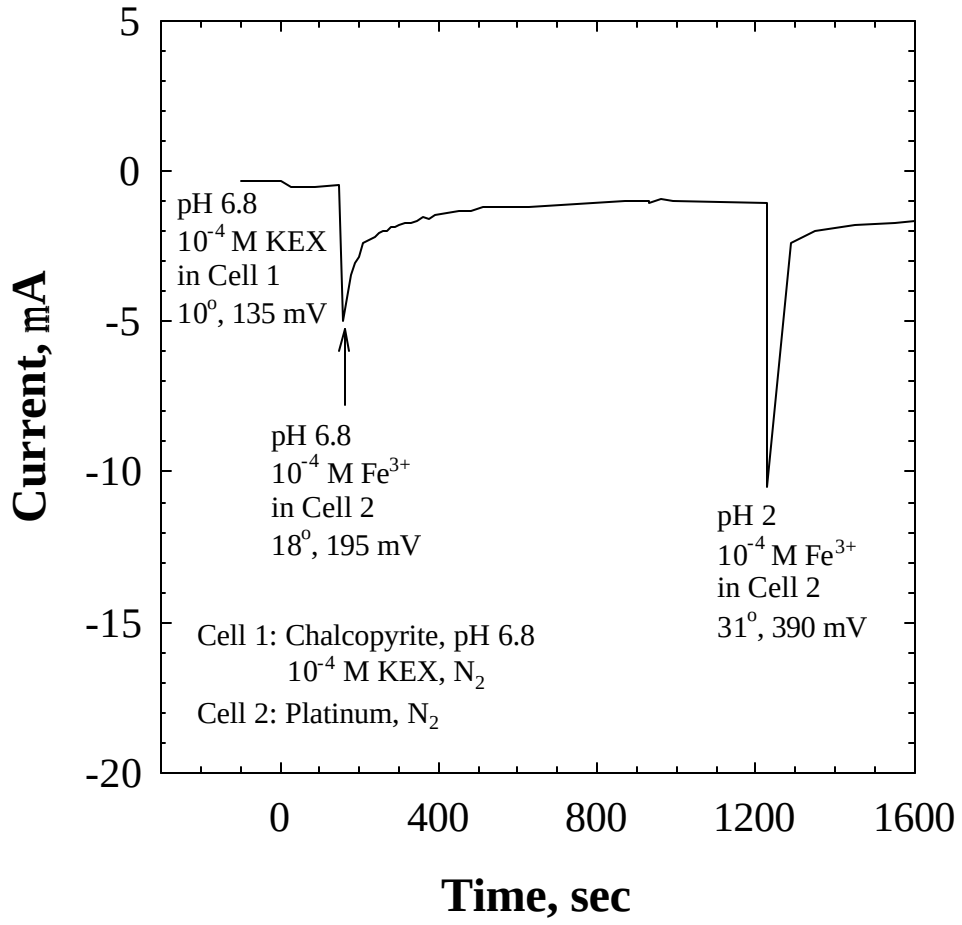

Figure 3.9 Galvanic coupling current between a chalcopyrite electrode in Cell 1 containing 10^{-4} M KEX solution at pH 6.8 and a platinum electrode in Cell 2 containing 10^{-4} M $FeCl_3$ at different pHs.

CHAPTER 4

ESTIMATION OF ACTIVATION ENERGY FOR ADSORPTION OF ETHYL XANTHATE ON SULFIDE MINERALS FROM TAFEL STUDIES

4.1. INTRODUCTION

The energy of activation is an important parameter in understanding the kinetics of any reaction mechanism. The most commonly used technique of measuring activation energy is to measure changes in a reaction system, such as disappearance of reactants or appearance of products. The changes can be monitored through various analytical techniques, such as titration, turbidity, Ultra-Violet/Visible Spectroscopy and a variety of absorbance and reflectivity tests. However, electrochemists have used potentiodynamic polarization techniques such as Tafel plots to determine activation energies for reactions, which are primarily electrochemical in nature. The advantage of Tafel studies over analytical techniques is essentially the speed and ease of the experimentation. However, the analysis of data requires more rigorous scrutiny than analytical techniques.

4.1.1. Use of Tafel Studies to Estimate Activation Energies

Tafel plots have gained immense utilization in corrosion studies. The corrosion parameters, such as polarization resistance, corrosion rate (in terms of current), Tafel slopes and energy barriers (activation energies) can easily be extracted from Tafel plots. The Tafel plots are the extension of Evans diagram developed to elucidate corrosion by Evans and his colleagues (1932, 1947 and 1963) and Petrocelli (1950). Both Evans diagram and Tafel plots are also known by a common name, "polarization curves".

Polarization curves have been commonly used for estimating activation energies in corrosion processes, for example, iron in sulfuric acid (Finley and Myers, 1970); tungsten in alkaline phosphate solution (El-Basiouny and Hefny, 1980); copper, silver and gold in perchloric acid (Frese and Stimming, 1986); gallium in acidic sulfate solutions (Jang et al., 1989); mild steel in seawater (Pandya et al., 19??); platinum in phosphoric acid (Gileadi, 1987; Clouser et al., 1993). The Arrhenius form of the rate equation is used to estimate the heat of activation:

$$i = A \exp\left(-\frac{\Delta H^*}{RT} \right) \qquad [4.1]$$

where, i is the current density and represents the rate of reaction under study, A is the frequency factor.

Bockris and his colleagues (Years) and Conway and his colleagues (Years) have led the research into the area of studying Tafel behavior of hydrogen evolution reaction (H.E.R) on various metals (including mercury) in different organic and inorganic solvents.

(a) Sulfide minerals:

As described in Chapter 1, the adsorption of thiol collectors on sulfide minerals is a mixed potential, corrosion-type process. Previously, polarization curves have been used to establish mixed potential theory in sulfide flotation. Salamy and Nixon (1953, 1954) used polarization curves to establish mixed potential on mercury using various flotation reagents (xanthates, cyanide ions). Following their work, Tolun and his colleagues (Tolun and Kitchener, 1964; Toperi and Tolun, 1969) studied galena in aqueous xanthate system, whereas Majima and his colleagues (Majima and Takeda, 1968; Peters and Majima, 1968) studied pyrite in aqueous xanthate solutions.

Tafel studies were also conducted by various researchers in order to study oxygen reduction of sulfides (e.g., pyrite, galena) and metals (e.g., gold, platinum). Briss and Damjanovic (1987) studied oxygen evolution reaction (OER) on platinum to examine the dependence of OER on pH and oxide film thickness. Similarly, Parthasarathy et al. (1992) and Grgur et al. (1997) studied oxygen reduction on platinum in order to establish temperature dependence of kinetics. Polarization curves have also been used to study the oxygen reduction on sulfide by Biegler et al. (1975), Biegler (1976), Rand (1977), Pillai and Bockris (1984) and Ahlberg and Broo (1996a, b, c, 1997). Although some of their experiments were carried out in the presence of xanthate, the results and discussion were primarily focused on oxygen reduction mechanism and rate determining step (Section 1.2.3) (Pillai and Bockris, 1984; Ahlberg and Broo, 1996b).

4.1.2. Interaction between Xanthate and Sulfide Minerals

In order to optimize separation of sulfide minerals, numerous studies have been carried out on the interaction of sulfide minerals and collectors, such as xanthate. The studies generated not only the valuable thermodynamic data, but also provided a detailed insight into the surface products. However, the interactions between sulfide and collector are more complex than what have been investigated. Despite some groundbreaking studies, the controversies still exist over

the exact nature of the surface product. Moreover, only few studies have attempted to measure the kinetic parameters (rate of reaction and heat of activation) of the sulfide-collector interactions.

(a) Pyrite

Although it has been established that dixanthogen (X_2) is the species responsible for hydrophobicity and flotation of pyrite, the controversy exists due to the presence of ferric xanthate (FeX_3) and ferric-hydroxy xanthate ($FeOHX_2$ and $Fe(OH)_2X$) species on the pyrite surface. Depending upon the conditions and techniques used to investigate, almost all the forms of xanthate have been reported to be responsible for the hydrophobicity of pyrite (Ball and Rickard, 1976).

Gaudin et al (1934) extracted ferric xanthate into benzene when pyrite was crushed in the presence of xanthate and benzene. This was consistent with the traditional theories (ion-exchange and chemical reaction) of sulfide – collector interaction (Chapter 1). Although Gaudin et al. (1933, 1934) also observed dixanthogen in pyrite system, it was largely ignored as it negated their theories. The presence of ferric xanthate was confirmed by Cases and co-workers (de Danota, 1987; Cases et al., 1989, 1990, 1993). Wang and his coworkers (1989, 1991 and 1995) carried out extensive thermodynamic calculations to establish the presence of ferric xanthate compounds and confirmed it using FTIR studies. Other than ferric xanthate species, presence of ferric-hydroxy xanthate species were also suggested to be responsible for flotation of pyrite. Leppinen (1990) conducted FTIR studies and observed iron xanthate surface compound on the pyrite surface. Fornasiero and Ralston (1992) developed the Gouy-Chapman-Stern model for adsorption of xanthate on pyrite and suggested that the iron hydroxide-xanthate complexes also contribute to the flotation of pyrite. Besides ferric-hydroxy-xanthate species, unoxidized xanthate ions (Fuerstenau and Mishra, 1981) and monothiocarbonate (MTC) (Harris and Finkelstein, 1975) have also been proposed to form on pyrite.

However, the independent studies by Fuerstenau et al. (1968) and Majima and Takeda (1968) showed that dixanthogen was the only species adsorbed on the surface. Until 1968, the significance of dixanthogen as the important species was ignored despite its presence was observed by Gaudin et al. (1933, 1934, 1956) as early as 1930s. Following studies by Fuerstenau et al. (1968) and Majima and Takeda (1968), the presence of dixanthogen on pyrite has been confirmed by various researchers (Fuerstenau et al., 1968; Allison et al., 1972; Finkelstein and

Poling (1977); Pritzker et al., 1985; Leppinen et al., 1989; Cases et al., 1989a, b, 1990, 1993; Prestidge et al., 1993; Sui et al., 1997). Meilczarski (1986) suggested a two-stage adsorption process: formation of iron xanthate monolayer followed by the multilayer coverage of dixanthogen. It is now well established that dixanthogen is the sole species responsible for the hydrophobicity and flotation of pyrite. The oxidation of xanthate to dixanthogen is given by:

$$X_2 + 2e \rightarrow X^- \qquad E_h = -0.060 - 0.059\log[X^-] \qquad [4.2]$$

(b) Pyrrhotite

Similar to pyrite, dixanthogen is believed to be the major xanthate oxidation product on the surface of pyrrhotite. Allison et al. (1972) extracted dixanthogen from pyrrhotite surface for ethyl and higher homologues of xanthate. However, Senior et al. (1994) suggested that pyrrhotite behaves differently than pyrite. They observed that pyrrhotite floated well at pH 7 and was depressed at higher pHs in the presence of potassium ethyl xanthate, which is in contrast with observations made by Fuerstenau et al. (1968) and Hanson and Fuerstenau (1993) for pyrite. They observed, on the other hand, that the flotation of pyrite was depressed at pH 7 in the presence of xanthate. These differences were attributed to ferric-hydroxy-xanthates species (Wang et al., 1989, 1991, 1995). Yoon and his colleagues have also observed small quantities of FeX_3 on the pyrrhotite surface. (Basilio et al., 1993; Yoon et al., 1995).

Montalti et al. (1991) proposed that ethyl xanthate may be oxidized to monothiocarbonate (MTC), ethyl perxanthate (EPX), and dixanthogen on pyrrhotite surface. In a spectroscopic study of xanthate adsorption on pyrite and pyrrhotite at pH 9, Prestidge et al. (1993) observed the formation of EPX and X_2, but could not establish or negate the presence of MTC definitely. However, they concluded that at high potentials, X_2 was the major product. Yoon and his colleagues have also observed that major oxidation product of xanthate on pyrrhotite exists mostly as dixanthogen (Basilio et al., 1993; Yoon et al., 1995).

Hodgson and Agar (1989) also proposed the formation of dixanthogen on pyrrhotite. According to them, the adsorption of xanthate proceeds through columbic interaction on oxidized pyrrhotite surface:

$$FeS + 2H_2O \rightarrow Fe(OH)[S]^+ + 2H^+ + 2e \qquad [4.3]$$

$$Fe(OH)[S]^+ + X^- \rightarrow Fe(OH)[S]X \qquad [4.4]$$

where FeS and $Fe(OH)[S]^+$ represent pyrrhotite and iron (III) hydroxy polysulfides, respectively. Xanthate is further oxidized to dixanthogen. Rao and Finch (1991) suggested a similar

mechanism establishing the need for oxygen to act as electron scavenger. It has been shown that in the absence of oxygen, ferric ions may also act as electron scavenger (Yoon, 1997).

Since pyrrhotite is found in abundance in copper-nickel ores, it is readily activated by the heavy metal ions, such as nickel and copper, present in the flotation pulp (Yoon et al., 1995). The activation mechanism may be represented by:

$$Fe_7S_8 + 4.5Ni^{2+} + 4e \rightarrow (Fe_{4.5},Ni_{4.5})S_8 + 2.5Fe^{2+} \qquad \Delta G^0 = -18.88 \text{ kJ/mol} \qquad [4.5]$$

The thermodynamic data was taken from Thornber (1983), Bard et al. (1985) and Senior et al. (1994). It shows that the nickel-activated pyrrhotite surface may act as if pentlandite. It has already been shown that nickel contamination (which may lead to its activation) increase the uptake of xanthate (Bozkurt et al., 1997).

In order to differentiate between the flotation response of pyrrhotite and pentlandite, Senior et al. (1994) proposed adsorption of xanthate on pentlandite according to:

$$(Fe_{4.5},Ni_{4.5})S_8 + 13.5H_2O + 9X^- \rightarrow 4.5Fe(OH)_3 + 4.5NiX_2 + 8S + 13.5H^+ + 22.5e \qquad [4.6]$$

However, this reaction mechanism was discarded because the thermodynamic (reversible) potential for this reaction (-0.06 V at pH 9 and $[X^-] = 9.3 \times 10^{-5}$ *M*) did not match with the onset of flotation (0.16 V). However, the thermodynamic potential for the formation of dixanthogen is ca. 0.18 V at $[X^-] = 9.3 \times 10^{-5}$ *M*, which is comparatively closer to the onset of flotation of pentlandite.

On the other hand, McNeil et al. (1994) proposed the formation of dixanthogen and nickel xanthate (NiX_2). They studied the adsorption of xanthate on pentlandite by UV (absorbance) spectrophotometry, and observed dixanthogen in the supernatant. Also, it was observed that ~10-25% of xanthate was unaccounted for in the solution. Although they did not exclude the possibility of EPX, MTC, etc., the unaccounted xanthate was attributed to the formation of NiX_2 (McNeil et al., 1994). Poling and Leja (1962) also suggested that both dixanthogen and nickel xanthate will co-adsorb on pentlandite.

Hodgson and Agar (1989) also proposed the formation of NiX_2. They conducted cyclic voltammetry on pentlandite in the presence of xanthate and concluded that unlike pyrrhotite, xanthate adsorbs on pentlandite initially *via* chemisorption and is then oxidized to dixanthogen:

$$Ni_{(s)} + X^- \rightarrow Ni||X + e \qquad [4.7a]$$

$$Ni||X + X^- \rightarrow Ni||X_2 + e \qquad [4.7b]$$

where Ni(s) represents the nickel ions at the surface of pentlandite.

(c) Chalcocite

Chalcocite has been the focus of several electrochemical studies due to controversies surrounding the nature of oxidation product and the exact mechanism behind collector adsorption. Fuerstenau et al. (1971) proposed that at alkaline pH (11.5), xanthate can be oxidized to dixanthogen by copper hydroxide and render it floatable. However, Allison et al. (1972) could only extract metal xanthate from chalcocite which had been reacted with xanthate. The definitive work on chalcocite came from Heyes and Trahar (1979), who showed that the presence of dixanthogen was thermodynamically unfavorable and hence the oxidation product responsible for the flotation was cuprous xanthate (CuX). This was consistent with the results of Gaudin and Schuhmann (1936).

Based on experiments conducted by Harris and Finkelstein (1977), following reactions were suggested for the oxidation of xanthate on chalcocite:

$$Cu_2S + X^- \rightarrow CuS + CuX + e \qquad E_h = -0.234 - 0.059\log[X^-] \qquad [4.8]$$

This reaction proceeded through cupric ions, Cu(II), which could represent any of the copper species in alkaline conditions, i.e, $Cu(OH)_2$, CuO, Cu_2O, or $HcuO_2^-$. On the other hand, Heyes and Trahar (1977) proposed the following mechanism for the formation of CuX:

$$Cu_2S + 2X^- \rightarrow 2CuX + S + 2e \qquad E_h = -0.171 - 0.059\log[X^-] \qquad [4.9]$$

and:

$$Cu_2S + 2X^- + 4H_2O \rightarrow 2CuX + SO_4^{2-} + 8H^+ + 8e$$

$$E_h = 0.195 - 0.015\log[X^-] - 0.059pH \qquad [4.10]$$

For their thermodynamic calculations, data was taken from Kowal and Pomianowski (1973) and Hepel and Pomianowski (1977). However, the electrochemical potential of reactions 4.8 – 4.10 did not match the onset of flotation of chalcocite in presence of xanthate.

Therefore, Koch and McIntyre (1976) and Richardson and his colleagues (Richardson et al., 1984; O' Dell et al., 1984, 1986; Walker et al., 1986) proposed the adsorption of xanthate in conjunction with oxidation of chalcocite and various metastable cooper sulfide structures.

$$Cu_2S \rightarrow Cu_{2-\delta}S + \delta Cu^{2+} + 2\delta e \qquad [4.11]$$

$$Cu_{2-\delta}S + \lambda X^- \rightarrow Cu_{2-\delta-\lambda}S + \lambda CuX + \lambda e \qquad [4.12]$$

$$Cu^{2+} + 2X^- \rightarrow CuX_2 \qquad [4.13]$$

where Cu^{2+} may represent $Cu(OH)_2$ at higher pHs. Table 4.1 shows various reactions between chalcocite (and other copper sulfide structures) and xanthate, i.e, Equations [4.11] – [4.13] with

different δ and λ values (Heyes and Trahar, 1979; Richardson et al., 1984; Young, 1987). The thermodynamic data was taken from Koch and McIntyre (1976), Hepel and Pomianowski (1977), Sparrow et al. (1977), Bard et al. (1985) and Young (1987). The products varied from metastable copper sulfide, cupric sulfide (not covellite), cuprous xanthate, cupric xanthate (unstable) and dixanthogen.

Although cupric xanthate (CuX_2) has been attributed to hydrophobization of chalcocite (Roos et al., 1990), it is unstable and decomposes to CuX and X_2 (Sparrow et al., 1977):

$$2CuX_2 \rightarrow 2CuX + X_2 \qquad [4.14]$$

Paterson and Salman (1968) also stated that the participation of dixanthogen in the xanthate flotation of chalcocite is improbable.

Beside metal xanthate, chemisorption of xanthate has also been cited in literature. Studies conducted by Yoon and his colleagues (Pritzker et al., 1985; Basilio et al., 1985; Leppinen et a., 1989; Woods et al., 1987, 1990, 1994; Young et al., 1988) have shown that xanthate adsorbs on chalcocite *via* chemisorption at low potentials (< –0.28 V at 2×10^{-5} M KEX). The chemisorption of xanthate is pH independent and may be responsible for the onset of flotation as observed by Heyes and Trahar (1979). The presence of chemisorbed xanthate is in agreement with studies done by Szeglowski et al. (1977) and Woods (1971, 1988). However, above –0.28 V, xanthate may adsorb on chalcocite as CuX possibly in multilayers.

(d) Covellite

Gaudin et al. (1933) extracted copper pentylxanthate and dixanthogen from the covellite-potassium pentylxanthate system. According to Rao and Patel (1961), Cu(II) ions react with alkylxanthate ions in aqueous solution to form cuprous xanthate and dixanthogen (Valli and Persson, 1994). Leja et al. (1963) studied adsorption of xanthate on various copper substrates using FTIR. They also concluded that irrespective of preconditioning of substrate, the main constituent was cuprous ethyl xanthate (CuX). However, dixanthogen in aqueous solution may also co-adsorb on initially chemisorbed CuX as also concluded by Wark and Cox (1934).

Similar observations were made by Allison et al. (1972). The reaction products were extracted using carbon disulfide, a good solvent for metal xanthate, dixanthogen and xanthate derivatives. However, cuprous methyl- and ethyl-xanthates are insoluble in carbon disulfide (Allsion et al., 1972). Therefore, metal xanthates could not be detected with lower homologues of xanthate with covellite. With higher homologues (C>2) of xanthate ions both metal xanthate

and dixanthogen were observed. The reaction mechanism suggested was similar to reactions 4.11 and 4.12, where overall reaction would include reduction of cupric ions (Cu^{2+}) of covellite:

$$CuS + 2X^- \rightarrow CuX + \tfrac{1}{2}X_2 + 2e \qquad [4.15]$$

They also concluded that the nature of the surface product did not vary with pH or chain length of the alkylxanthate used.

The reaction mechanism discussed by Rao and Patel (1961) has also been proposed Fuerstenau et al. (1971) and Sparrow et al. (1977). According to Sparrow et al. (1977), Cu^{2+} in acidic and near-neutral pH may oxidize xanthate to dixanthogen *via* CuX_2 (reactions [4.13] and [4.14]). At neutral and alkaline pH, Cu^{2+} exist in cupric-hydroxide forms. Similar mechanism was suggested by Harris and Finkelstein (1977) and Heyes and Trahar (1979) for chalcocite flotation (reaction [4.8]). Fuerstenau et al. (1971) proposed the similar mechanism on the surface of chalcocite by $Cu(OH)_2$ at alkaline pH:

$$Cu(OH)_2 + 2X^- + 2H^+ \rightarrow CuX + \tfrac{1}{2}X_2 + 2H_2O \qquad [4.16]$$

Ackerman et al. (1986a, b) detected substantial release of Cu^{2+} from covellite. Using conventional FTIR, they detected cuprous xanthate (CuX) on covellite surface and dixanthogen in the aqueous phase due to reduction of either Cu^{2+} ions or cupric-hydroxides. It suggests that the xanthate may adsorb on covellite surface according to the reaction:

$$CuS + X^- \rightarrow CuX + S^0 + e \qquad [4.17]$$

whereas, dixanthogen may form in aqueous bulk phase according to reaction [4.2] without adsorbing on the surface.

4.1.3 Butler Volmer Equations for Redox Processes

For a single step redox (usually, one electron) processes:

$$O + ne \rightarrow R \qquad [4.18]$$

the rate of forward (reduction) and backward (oxidation) reactions can be expressed as a function of their respective activation energies (ΔG_f^* & ΔG_b^*) as follows (Jones, 1992):

$$r_f = K_f \exp\left(-\frac{\Delta G_f^*}{RT}\right) \qquad [4.19]$$

$$r_b = K_b \exp\left(-\frac{\Delta G_b^*}{RT}\right) \qquad [4.20]$$

where, K_f and K_b are reaction rate constants for forward and backward reactions, respectively, R is the gas constant and T is absolute temperature. The activation energies (ΔG_f^* & ΔG_b^*) are

related to the change in free energy, ΔG_r, and half-cell electrochemical potential, E_r, for the redox couple according to:

$$\Delta G_f^* - \Delta G_b^* = \Delta G_r \qquad [4.21]$$

$$\Delta G_r = -nFE_r \qquad [4.22]$$

where n is the number of equivalents exchanged and F the Faraday's constant (96500 C/eq.).

At equilibrium, the rate of forward reaction, r_f, is equal to the rate of backward reaction, r_b, i.e.,

$$r_f = r_b = \frac{i_0 a}{nF} \qquad [4.23]$$

where i_0 is the exchange current density, a the atomic weight. Therefore, from Equations [4.19], [4.20] and [4.23], the exchange current density can be written as:

$$i_0 = K_f' \exp\left(-\frac{\Delta G_f^*}{RT}\right) = K_b' \exp\left(-\frac{\Delta G_b^*}{RT}\right) \qquad [4.24]$$

Figure 4.1 shows a schematic representation of activation energy model (Jones 1992). When an overpotential is applied to the electrode, the energy barrier on one side decreases, while it increases on the other side. For cathodic overpotential, η_c, the activation energy barrier for the forward reaction decreases by an amount of $\alpha_c nF\eta_c$, whereas that for the backward reaction increase by the amount of $(1-\alpha_c)nF\eta_c$. Thus, the rate of forward reaction in terms of current density can be written as:

$$i_{\eta c,c} = K_f' \exp\left(-\frac{\Delta G_f^* - \alpha_c nF|\eta_c|}{RT}\right) \qquad [4.25]$$

where α_c is known as the transfer coefficient for the cathodic overpotential and is the fraction of cathodic overpotential taken by forward reaction. Similarly, the rate of backward reaction in terms of current density can be written as:

$$i_{\eta c,a} = K_b' \exp\left(-\frac{\Delta G_b^* + (1-\alpha_c)nF|\eta_c|}{RT}\right) \qquad [4.26]$$

The net cathodic current is given by the difference of cathodic and anodic current at cathodic overpotential:

$$i_C = i_{\eta c,c} - i_{\eta c,a} = K_f' \exp\left(-\frac{\Delta G_f^* - \alpha_c nF|\eta_c|}{RT}\right) - K_b' \exp\left(-\frac{\Delta G_b^* + (1-\alpha_c)nF|\eta_c|}{RT}\right) \qquad [4.27]$$

The Equation [4.27] can be further simplified as following:

$$i_C = K'_f \exp\left(-\frac{\Delta G^*_f}{RT}\right)\exp\left(\frac{\alpha_c nF|\eta_c|}{RT}\right) - K'_b \exp\left(-\frac{\Delta G^*_b}{RT}\right)\exp\left(\frac{\alpha_c nF|\eta_c|}{RT}\right)\exp\left(-\frac{nF|\eta_c|}{RT}\right) \quad [4.28]$$

The first component in the right hand side is given by Equation [4.24] and hence,

$$i_C = i_0 \exp\left(\frac{\alpha_c nF|\eta_c|}{RT}\right) - i_0 \exp\left(\frac{\alpha_c nF|\eta_c|}{RT}\right)\exp\left(-\frac{nF|\eta_c|}{RT}\right) \quad [4.29]$$

or,

$$i_C = i_0 \exp\left(\frac{\alpha_c nF|\eta_c|}{RT}\right)\left(1 - \exp\left(-\frac{nF|\eta_c|}{RT}\right)\right) \quad [4.30]$$

Similarly, for the anodic overpotential, η_a, the net anodic current is given by:

$$i_A = i_0 \exp\left(\frac{\alpha_a nF|\eta_a|}{RT}\right)\left(1 - \exp\left(-\frac{nF|\eta_a|}{RT}\right)\right) \quad [4.31]$$

where, α_a is the transfer coefficient for the anodic overpotential and is the fraction of anodic overpotential taken by the backward reaction. The Equations [4.30] and [4.31] are known as the Butler-Volmer Equations.

At high overpotentials, Equations [4.30] and [4.31] can be rewritten as:

$$i_C = i_0 \exp\left(\frac{\alpha_c nF|\eta_c|}{RT}\right) \quad [4.32]$$

$$i_A = i_0 \exp\left(\frac{\alpha_a nF|\eta_a|}{RT}\right) \quad [4.33]$$

Equations [4.32] and [4.33] can also be rewritten as:

$$|\eta_c| = b_c \log\left(\frac{i_C}{i_0}\right) \quad [4.34]$$

$$|\eta_a| = b_a \log\left(\frac{i_A}{i_0}\right) \quad [4.35]$$

where b_c and b_a are known as the Tafel constants for the half-cell reaction. Equations [4.34] and [4.35] are also known as the Tafel relationship.

For multi-step (multi-electron) redox processes, Bockris (1954) derived Equations similar to the Butler-Volmer Equations, [4.30] and [4.31]:

$$i_C = i_0\left\{\exp\left[-\frac{(\beta+\gamma)n\eta_c F}{\nu RT}\right]-\exp\left[\frac{(1-\beta-\gamma)n\eta_c F}{\nu RT}\right]\right\} \quad [4.36]$$

$$i_A = i_0\left\{\exp\left[\frac{(1-\beta-\gamma)n\eta_a F}{\nu RT}\right]-\exp\left[-\frac{(\beta+\gamma)n\eta_a F}{\nu RT}\right]\right\} \quad [4.37]$$

where, β is the barrier symmetry factor, ($0<\beta<1$), γ the number of charge transfer events prior to the rate determining step (rds), ($|\gamma|<1$) and ν the stoichiometric number (number of occurrence of rds per single occurrence of complete reaction). A comparison of Equations by Bockris [4.36] and [4.37] and Butler-Volmer [4.30] and [4.31] shows that the transfer coefficients, α, can be given by:

$$\alpha_c = \frac{(\beta+\gamma)}{\nu} \quad [4.38]$$

and

$$\alpha_a = \frac{(1-\beta-\gamma)}{\nu} \quad [4.39]$$

In both the cases, the Tafel slopes, b_a and b_c are given by:

$$b_c = \frac{2.3RT}{\alpha_c nF} \quad [4.40]$$

$$b_a = \frac{2.3RT}{\alpha_a nF} \quad [4.41]$$

(a) Dependence of Tafel slopes and charge transfer coefficient on temperature

Although the Tafel slopes are given by Equations ([4.40] and [4.41]), there is no consensus about the exact form of the relationship between Tafel slopes, transfer coefficients (α_a and α_c) and temperature. In the work done by Agar (1947), Parsons, Bockris and his colleagues (1948, 1951, 1986), Conway and his colleagues (1969, 1970, 1986, 1987, 1989) and others (Clouser et al., 1993, Gileadi, 1987) established anomalous Tafel behavior over a wide range of temperatures, pHs and solution conditions. However, it should be noted that, the present investigation is limited to a narrow range of temperature (22 °C to 30 °C) in aqueous solutions. In a comprehensive review of relationship between Tafel slopes, charge transfer coefficients with temperature, Conway (1986) presented four cases for one electron processes:

Case 1. $b = RT/\beta F$ [4.42]

where β is the symmetry factor and is equal to α for one electron single step process. According to Case 1, Tafel slope, b, is directly and linearly proportional to temperature, T.

Case 2. $b = RT/\beta F + K$ [4.43]

where K is a temperature independent constant. Although the Tafel slope, b, is linearly proportional to T, it does not exactly follow the Tafel relationship.

Case 3. $b = RT/\alpha(T)F = R/\lambda F = \text{constant}.$ [4.44]

where λ is a temperature independent constant. According to Case 3, the charge transfer coefficient, α, is linearly proportional to temperature resulting in temperature independent Tafel slopes.

Case 4. $b = K - RT/\alpha(T)F$ [4.45]

where α is not necessarily linear function of T and may given by:

$\alpha = \lambda T^m$, $m>1$ [4.46]

In this case, the Tafel slope may not be a linear function of temperature and may decrease with increase in temperature.

It has been shown by various authors (Conway, 1986; Gileadi, 1987; Clouser et al., 1993 and references therein) that most of the experimental work follows either Case 2 or 3. According to them, the deviation from Case 1 "can be considered as the rule, rather than the exception" (Gileadi, 1987). Therefore, the transfer coefficient, α, may be temperature dependent. However, these relationships have been developed empirically based on the experimental data and results obtained in their studies.

Although the data from the present work has been discussed in the Results sections, it is imperative to mention here that the data obtained in the present study follows the Case 2, i.e., linearly temperature dependent Tafel slopes, b, and temperature independent transfer coefficients, α. Therefore, the charge transfer coefficients ($\alpha = \beta$) were calculated from the plots of b vs. T as following:

$$\frac{\partial b}{\partial T} = \frac{1}{\alpha}\left(\frac{2.3R}{nF}\right) \quad [4.47]$$

4.1.4 Calculation of Activation energy

For $|\eta_c|$ or $|\eta_c| > 2.3\frac{RT}{nF}\left(\sim \frac{0.059}{n}\right)$, the Equations [4.32] and [4.33] can be rewritten as:

$$i_C = K'_f \exp\left(-\frac{\Delta G^*_f}{RT}\right)\exp\left(\frac{\alpha_c nF|\eta_c|}{RT}\right) \quad [4.48]$$

$$i_A = K'_b \exp\left(-\frac{\Delta G^*_b}{RT}\right)\exp\left(\frac{\alpha_a nF|\eta_a|}{RT}\right) \quad [4.49]$$

For simplicity, Equations [4.48] and [4.49] are rearranged as:

$$\log(i_C, T) = \log(K^*_f) - \frac{(\Delta G^*_f - \alpha_c nF|\eta_c|)}{2.3RT} \quad [4.50]$$

$$\log(i_A, T) = \log(K^*_b) - \frac{(\Delta G^*_b - \alpha_a nF|\eta_a|)}{2.3RT} \quad [4.51]$$

Therefore, ΔG^*_f and ΔG^*_b, can be calculated by simple mathematical manipulation of slopes from the plots of log (i_C) and log (i_A) vs. 1/T, respectively.

4.2. OBJECTIVE

The objective to this study is to estimate activation energies for the adsorption of potassium ethyl xanthate (KEX) on various sulfide minerals.

4.3. EXPERIMENTAL

4.3.1 Samples:

Cubic crystals of pyrite (Logrono, Spain) were obtained from Geosciences Resources. The chunks of pyrrhotite (Russia) and chalcocite (Montana, USA) were obtained from the Ward's Natural Science Est, Inc. Pure covellite of unknown source was obtained through the Museum of Natural History, Smithsonian Institution, Washington D.C.

Using a low speed diamond saw, mineral samples were cut into small rectangular pieces of dimensions of 5 × 5 × 10 mm. A copper wire was attached to one of the 5 × 5 faces using conducting silver epoxy and/or indium solder. The electrical contact was covered with non-conducting epoxy, Torr Seal (Varian). The conductivity of the contact was tested using an

ohmmeter before further preparation of the samples. The sample was mounted in a glass (Pyrex) tube (OD = 8mm, ID = 6mm) using epoxy resin (Struers). The surface facing out was in contact with the solution and was renewed by polishing and cleaning in ultrasonic bath as described in Chapter 3.

4.3.2 Reagents

Potassium Ethyl Xanthate (KEX) was obtained from Eastman Kodak Company. It was purified in the usual manner: dissolution in acetone and recrystallization from ether. The purification method was repeated three times to ensure high purity. The xanthate thus obtained was vacuum dried and dissolved in double distilled de-ionized (DI) water to prepare 10^{-2} M solution.

A pH 6.8 buffer solution was prepared by mixing 0.05 M NaH_2PO_4 and 0.025 M NaOH. For Ni-activation of pyrrhotite, 10^{-2} M $NiSO_4$ solution was prepared and an aliquot was added to pH 6.8 buffer to obtain desired (10^{-4} M) concentration. All of the solutions were prepared in DI water.

4.3.3. Apparatus and Procedure

A standard three-electrode electrochemical cell was used. The working electrode and counter electrode consisted of the mineral under study. Standard Calomel Electrode (SCE) was used as the reference electrode and all the potentials were converted to hydrogen scale (SHE) by adding 0.245 V to the SCE values.

The electrochemical cell was connected to a potentiostat (Model 273 by EG&G) and controlled by a computer connected through GPIB interface. The Tafel studies were carried out using 352 SoftCorr Corosiion Measurement software (EG&G). The potentials were scanned ±250 mV from the rest potential value. The mixed potential obtained during Tafel studies differed from the rest potential and the range was adjusted according to the mixed potential obtained. The rest potentials were measured with Keithley 169 multimeter.

4.4. RESULTS AND DISCUSSION

Figures 4.2 – 4.6 show the Tafel plots for the oxidation of xanthate on pyrite, pyrrhotite, Ni-activated pyrrhotite, chalcocite and covellite, respectively. Figure 4.7 and Table 4.2 show the cathodic (solid symbols) and anodic (open symbols) Tafel slopes calculated for pyrite (●,○),

pyrrhotite (▲,△), Ni-activated pyrrhotite (▼,▽), chalcocite (■,□), covellite (◆,◇) from their Tafel plots (Figures 4.2 – 4.6). The Tafel slopes (b_c, b_a) were plotted against temperature and it was observed that the Tafel slopes increased linearly with temperature in accordance with Equation [4.43]. The transfer coefficients (α_c, α_a) were estimated according to the Equation [4.47] and are listed in Table 4.2. It was observed that the intercept K, (Equation [4.43]) could be ignored without introducing significant error (<1%). Therefore, it can be safely accepted that the Tafel slopes are directly proportional to the temperature in accordance with Equations [4.40] – [4.42].

Figures 4.8 – 4.12 show the plots of (a) cathodic and (b) anodic currents vs. temperature at various cathodic ($\eta<0$) and anodic ($\eta>0$) overpotentials for pyrite, pyrrhotite, nickel-activated pyrrhotite, chalcocite and covellite, respectively. These 'current vs. temperature' plots are similar to the Arrhenius plots, where the rate of reaction is represented by the current. The activation energies, ΔG_f^* and ΔG_b^*, were determined from the "Arrhenius-type" current plots (Figures 4.8 – 4.12) using these transfer coefficients and Equations [4.50] and [4.51]. The calculated activation energies are tabulated in Tables 4.3 for all the minerals. Table 4.4 and 4.5 show the free energy of reaction and the reversible potential calculated by various methods for the adsorption of xanthate on the minerals.

4.4.1 Pyrite and Pyrrhotite:

Both pyrite and pyrrhotite are iron sulfides with different crystal structure, magnetic, semi-conducting and electrochemical behavior. However, as discussed earlier, xanthate adsorbs on both of the minerals as dixanthogen and renders them floatable. Therefore, for calculation purpose, dixanthogen was taken as the oxidation product, which means that the value for number of equivalents exchanged, i.e., n in Equation [4.22], is two.

Figure 4.2 and 4.8 show the Tafel plots and the current plots for the oxidation of xanthate on pyrite surface. As shown in Table 4.2, the cathodic Tafel slopes were approximately in the range of 0.225 – 0.231 V/decade, whereas anodic Tafel slope varied between 0.280 through 0.290 V/decade. The cathodic and anodic transfer coefficients were calculated to be 0.131 and 0.105, respectively.

Table 4.3 shows the activation energies calculated at different overpotentials. For forward reaction, i.e., cathodic reduction, the average value of activation energy is 82.03 kJ/mol.

For backward reaction, i.e., the anodic oxidation, the activation energy was estimated to be 121.57 kJ/mol. Thus, the free energy of xanthate adsorption is calculated to be –39.54 kJ/mol, which is in good agreement with the calculated thermodynamic value of –33.96 kJ/mol (Table 4.4) (Bard et al., 1985; Young, 1987).

Table 4.5 shows the reversible potential (E_r) values calculated/estimated for xanthate adsorption on pyrite from various methods. The reversible potential calculated using thermodynamic value of free energy (E_r^{TD}) is 0.176 V. Using free energy value calculated from the Tafel plots, the reversible potential ($E_r^{\Delta G}$) is 0.205 V, which is slightly higher than E_r^{TD}. The reversible potential observed from the Tafel plots (E_r^{Tafel}) was approximately in the range of 0.184 – 0.190 V, which is in good agreement with other two values of reversible potential.

Similar calculations were also carried out for pyrrhotite. Figures 4.3 and 4.9 show the Tafel plots and current plots for the adsorption of xanthate on pyrrhotite. It can be seen from the Table 4.2 that the cathodic and anodic Tafel slopes lie in the range of 0.187 – 0.192 and 0.191 – 0.197, respectively. Using Equation [4.47], the transfer coefficients were calculated to be 0.155 and 0.151 for cathodic and anodic processes, respectively.

The activation energies for the forward and backward reactions are tabulated in Table 4.3. As it can be seen from the table, the average value for forward (cathodic) activation energy is 88.50 kJ/mol, whereas the same for backward (anodic) reaction is 124.85 kJ/mol. Therefore, the free energy of adsorption is equal to –36.35 kJ/mol, which is approximately the same as thermodynamically calculated value of –33.96 kJ/mol for the dixanthogen formation (Table 4.4).

A comparison of the activation energies for pyrite and pyrrhotite would show that these values are very close to each other. This indicates that despite differences in physical and chemical behavior of pyrite and pyrrhotite, the thermodynamics and kinetics of the adsorption of xanthate may be almost the same. The other possibility could be that although the xanthate adsorption mechanisms may be different, it is equally difficult (or easy) for xanthate to adsorb on iron sulfides. This could be further confirmed by studies on other iron sulfides such as marcasite (FeS_2).

Table 4.5 shows the reversible potential calculated from thermodynamic data (E_r^{TD} = 0.176 V), activation energies ($E_r^{\Delta G}$ = 0.188 V), and the Tafel plots (E_r^{Tafel} = 0.193 – 0.201 V).

The values obtained from various methods are approximately close within the range of experimental error.

The Tafel plots and current plots for the nickel-activated pyrrhotite are shown in Figure 4.4 and 4.10. Initially it was assumed that dixanthogen is the oxidation product on the surface of nickel-activated pyrrhotite. Hodgson and Agar (1989) proposed that xanthate adsorbs on both the pyrrhotite and pentlandite as dixanthogen; however, the mechanism is different. The transfer coefficients and activation energies were calculated for the activated pyrrhotite with the assumption of dixanthogen as the oxidation product. However, it was found that the free energy of the adsorption did not match with that of dixanthogen formation. Therefore, the possibility of formation of nickel dixanthate (NiX_2) on activated pyrrhotite surface was also explored (Poling and Leja, 1962). When calculations were carried out based on this assumption, it was observed that the calculated free energy of adsorption (-6.02 kJ/mol) matched closely with the thermodynamic value (-5.67 kJ/mol). This indicates that the xanthate may adsorb on nickel-activated pyrrhotite as NiX_2 rather than as X_2.

There exists another possibility that both the xanthate products (X_2 and NiX_2) are formed on the surface of nickel-activated pyrrhotite, where only NiX_2 is recognized by potentiodynamic technique. This may be due to either of the two reasons: (a) X_2 adsorbs on top of NiX_2 layer (Poling and Leja, 1962) and/or (b) X_2 stays in the aqueous solution and does not adsorb of Ni-activated pyrrhotite surface. However, it clearly shows that besides dixanthogen, metal xanthate may form on the surface of pyrrhotite when it is present in the flotation pulp in the presence of other heavy metal ions.

Tables 4.3 – 4.5 show the calculated activation energies, free energy of reaction and reversible potential values for the adsorption of xanthate on nickel-activated pyrrhotite. As it can be seen that the activation energies for forward and backward reactions on nickel-activated pyrrhotite are much smaller than the same values for pure pyrrhotite. This indicates that it is comparatively easier for xanthate to adsorb on activated pyrrhotite. This may lead to difficulties in efficient separation of pentlandite and pyrrhotite. The values for reversible potential calculated from free energy of activation (E_r^{TD} = 0.031 V), thermodynamics ($E_r^{\Delta G}$ = 0.029 V), and the Tafel plots (E_r^{Tafel} = 0.055 V) are also in excellent agreement.

4.4.2. Chalcocite and Covellite:

The Tafel plots and current plots for the oxidation of xanthate on chalcocite are plotted in Figure 4.5 and 4.11. The reversible potential was observed to be approximately 0.050 V. The range for cathodic and anodic Tafel slopes is approximately 0.273 – 0.285 and 0.160 – 0.165 V/decade, respectively. The transfer coefficients, activation energies and reversible potentials were calculated for all the possible reactions between chalcocite and xanthate leading to the formation of metastable copper sulfide ($Cu_{2-\delta-\lambda}S$), copper xanthates (CuX_2 and CuX) and dixanthogen (Table 4.1). The reactions were eliminated based on the comparison between estimated and thermodynamically calculated values of free energy and reversible potentials. It was observed that xanthate adsorbs on chalcocite according to the Reaction [4.9].

The average activation energies for the cathodic and anodic processes are 34.85 and 48.52 kJ/mol (Table 4.3). The free energy of the reaction can be, therefore, calculated to be –13.68 kJ/mol, which is closer to the thermodynamic free energy value of –12.29 kJ/mole for the Reaction [4.9] (Bard et al., 1985; Young et al., 1987). The reversible potential calculated from the estimated energy values (0.071 V), thermodynamics (0.064 V) and Tafel plots (0.050 V) are listed in Table 4.5.

Figures 4.6 and 4.12 show the Tafel plots and current plots for xanthate oxidation covellite, where the reversible potential is approximately in the range of 0.240 – 0.250 V. The cathodic and anodic Tafel slopes for xanthate oxidation on covellite are estimated to be 0.257 – 0.264 V and 0.275 – 0.281 V/decade, respectively.

As discussed earlier, xanthate may adsorb on covellite *via* either Reaction [4.15] (n = 2) or [16] (n = 1). The thermodynamic reversible potentials for both of the reactions are approximately 0.178 V and cannot be separated on the basis of reversible potential. Based on the calculation for the free energy of reaction, Reaction [4.17] was taken as the adsorption mechanism for xanthate on covellite. The cathodic and anodic activation energies were estimated to be 108.64 and 124.67 kJ/mol (Table 4.7), with free energy of reaction being equal to –16.03 kJ/mol. This value is almost equal to the thermodynamically calculated free energy value of –17.29 kJ/mol for Reaction [4.17]. This shows that xanthate adsorbs on covellite surface as cuprous xanthate (CuX), where X_2 may stay in the aqueous phase without adsorbing on the covellite surface as suggested by Ackerman et al. (1986a and b).

Table 4.7 shows that the activation energies for the xanthate adsorption on covellite and chalcocite. The values of activation energies for covellite are larger than the same for chalcocite indicating that it is easier to float chalcocite compared to covellite. This may be due to the reason that chalcocite has more copper in lattice than covellite. This inference is similar to the flotation studies of copper-iron sulfide minerals conducted by Richardson and Walker (1985). They showed that the lower flotation edge of the minerals shifts to more reducing potential as the copper content of the mineral increases.

4.5. CONCLUSIONS

1. The Tafel Plots can be used to estimate activation energies and free energy of reactions. The values of activation energies and free energy can be made useful in identifying reaction mechanism. Also, the adsorption of xanthate can be optimized using these values.
2. The free energy values calculated from Tafel plots show that xanthate adsorbs on pyrite and pyrrhotite as dixanthogen. Although the mechanisms for dixanthogen formation on pyrite and pyrrhotite differ from each other, their activation energies are almost same indicating a similar flotation responsibility.
3. The calculated values of activation energy and free energy of reaction show that the xanthate adsorbs on nickel-activated pyrrhotite as nickel dixanthate (NiX_2). This is in contrast with the observation that nickel-activated pyrrhotite behaves similar to pentlandite, for which dixanthogen has been cited as the oxidation product. The activation energy values for adsorption of xanthate on nickel-activated pyrrhotite are very small compared to that on pyrrhotite. This indicates that the ease of flotation for pyrrhotite increase in the presence of heavy metal ions, thereby causing a difficulty in the separation from pentlandite.
4. The calculated values of activation energy and free energy suggest that xanthate adsorbs on chalcocite as cuprous xanthate (CuX).
5. Xanthate also adsorbs on covellite as CuX. However, the mechanism for xanthate adsorption on covellite differs from that on chalcocite. Also, the activation energy values for xanthate adsorption on covellite are larger than that for chalcocite indicating that it is easier to float the latter. This may be due to the higher copper content in chalcocite compared to covellite.

4.6. REFERENCES

Ackerman, P.K., Harris, G.H., Klimpel, R.R. and Aplan, F.F., 1986a. *IJMP*, **21**, 141.

Ackerman, P.K., Harris, G.H., Klimpel, R.R. and Aplan, F.F., 1986b. *IJMP*, **21**, 1054.

Agar, J.N., 1947. *Disc. Farad. Soc.*, **1**, 81-86.

Ahlberg, E. and Broo, A.E., 1996b. *IJMP*, **47**, 33-47.

Ahlberg, E. and Broo, A.E., 1996c. *IJMP*, **47**, 49-60.

Allison, S.A., Goold, L.A., Nicol, M.J. and Granville, A., 1972. *Metall Trans.*, **3**, 2613-2618.

Ball, B. and Rickard, R.S., 1976. Flotation – Gaudin Memorial Volume (Ed. M.C. Fuerstenau). AIME: New York. **1**, 458-484.

Bard, A.J., Parson R. and Jordan, J., 1985. Standard Potentials in Aqueous Solution (IUPAC). Marcel Dekker: New York.

Basilio, C.I., Kim, D.S. and Yoon, R.-H., 1993. Final Report submitted to INCO.

Biegler, T., 1976. *J. Electroanal. Chem. Interf. Electrochem*, **70**, 265-275.

Biegler, T., Rand, D.A.J. and Woods, R., 1975. *J. Electroanal. Chem. Interf. Electrochem*, **60**, 151-162.

Bockris, J.O'M. and Gochev, A., 1986. *J. Phys. Chem.*, **90**, 5232-5239.

Bockris, J.O'M. and Roger, P. 1948. *Trans. Farad. Soc.*, **44**, 860-872.

Bockris, J.O'M., 1954. Modern Aspects of Electrochemistry. Butterworths: London. **1**, 180.

Bozkurt, V., Xu, Z., and Finch, J.A., 1997. Processing of Complex Ores (Eds. J.A. Finch, S.R. Rao and I. Holubec). CIM: Montrel (Canada). 101-111.

Cases, J.M., de Donato, P., Kongolo, M. and Michot L.J., 1989a. *Coll. Surf.*, **36**, 323-338.

Cases, J.M., de Donato, P., Kongolo, M. and Michot L.J., 1989a. SME Annual Meeting, Las Vegas (NV). SME: Littleton (CO). Preprint No. 89-62.

Cases, J.M., Kongolo, M., de Donato, P., Michot, L.J. and Erre, R., 1990. *IJMP*, **30**, 35-68.

Cases, J.M., Kongolo, M., de Donato, P., Michot, L.J. and Erre, R., 1993. *IJMP*, **38**, 267-299.

Clouser, S.J., Huang, J.C. and Yeager, E., 1993. *J. App. Electrochem*, **23**, 597-605.

Conway, B.E. and MacKinnon, D.J., 1969. *J. ECS*, **116**, 1665-1674.

Conway, B.E. and Wilkinson, D.P., 1986. *J. Chem. Phys.*, **85(7)**, 14197-4199.

Conway, B.E. and Wilkinson, D.P., 1986. *J. Electroanal. Chem. Interf. Electrochem*, **214**, 633-653.

Conway, B.E. and Wilkinson, D.P., 1986. *J. Electroanal. Chem. Interf. Electrochem*, **210**, 167-171.

Conway, B.E. and Wilkinson, D.P., 1989. *J. Chem. Soc., Farad. Trans. 1*, **85(8)**, 2355-2367.

Conway, B.E., 1986. Modern Aspects of Electrochemistry (Eds. B.E. Conway, J.O'M. Bockris and R. White). Plenum: New York. **16**, Chapter 2, 103-188.

Conway, B.E., MacKinnon, D.J. and Tilak, B.V., 1970. *Trans Farad. Soc.*, **66**, 1203-1226.

Conway, B.E., Tessier, D.F. and Wilkinson, D.P., 1986. *J. ECS*, **136(9)**, 2486-2493.

Conway, B.E., Tessier, D.F. and Wilkinson, D.P., 1986. *J. Electroanal. Chem. Interf. Electrochem*, **199**, 249-269.

Conway, B.E., Wilkinson, D.P. and Tessier, D.F., 1987. *Ber. Bunsen. Phys. Chem*, **91**, 484-488.

Evans, U.R. and Hoar, T.P., 1932. *Proc. Royal. Soc. London*, **137**, 343-365.

Evans, U.R., 1947. Proc. 11th Intl Cong Pure Appl Chem. Lond. **5**, 743.

Evans, U.R., 1963. An Intro. To Metallic Corr., 2nd ed. Edward Arnold: London.

Finkelstein, N.P. and Poling, G.W., 1977. *Minl Sci. Engg.* **9(4)**, 177-197.

Fuerstenau, M.C., Huiatt, J.L. and Kuhn, M.C., 1971. *Trans SME/AIME*, **250**, 227-231.

Fuerstenau, M.C., Kuhn, M.C. and Elgillani, D.A., 1968. *Trans SME/AIME*, **241**, 148-156.

Gaudin, A.M. and Schuhmann, R., 1936. *J. Phys. Chem.*, **40**, 257.

Gaudin, A.M. and Wilkinson, W.D., 1933. *J. Phys. Chem.*, **37**, 833.

Gilealdi, E., 1987. *J. ECS*, **134** 117-120.

Hanson, J.S. and Fuerstenau, D.W., 1993. *IJMP*, **33**, 33-47.

Harris, P.J. and Finkelstein, N.P., 1977. Report No. 1896. NIM, South Africa.

Hepel, T. and Pomianowski, A., 1977. *IJMP*, **4**, 345-361.

Heyes, G.W., and Trahar, W.J., 1977. *IJMP*, **4**, 317-344.

Heyes, G.W., and Trahar, W.J., 1979. *IJMP*, **6**, 229-252.

Hodgson, M. and Agar, G.E., 1989. *Can. Met. Qtr*, **28(3)**, 189-198.

Jones, D.A., 1992. Principles and Prevention of Corrosion, 1st Ed. Macmillan: New York (NY).

Koch, D.F.A. and McIntyre, R., 1976. *J. Electroanal. Chem. Interf. Electrochem*, **71**, 285-296.

Kowal, A. and Pomianowski, A., 1973. *J. Electroanal. Chem. Interf. Electrochem*, **46**, 411-420.

Leja, J., Little, L.H. and Poling, G.W., 1963. *Trans IMM*, **72**, 407-423.

Leppinen, J.O., Basilio, C.I. and Yoon, R.-H., 1989. *IJMP.*, **26**, 259-274.

Majima, H. and Takeda, M., 1968. *Trans. SME*, **241**, 431-436.

McNeil, M., Rao, S.R. and Finch, J.A., 1994. *Can. Metall. Quart.* **23(2)**, 165-167.

O'Dell, C.S., Dooley, R.K., Walker G.W. and Richardson, P.E., 1984. Proc. Intl. Symp. Electrochem. in Mineral and Metal Process. I (Eds. P.E. Richardson, S. Srinivasan and R. Woods). ECS: Pennington (NJ), 81-95.

O'Dell, C.S., Walker, G.W. and Richardson, P.E., 1986. *J. App. Electrochem.*, **16**, 544-554.

Parsons, R., 1951. *Trans. Farad. Soc.*, **47**, 1332-1344.

Peters, E. and Majima, H., 1968. *Can. Metall. Quart.*, **7(3)**, 111-117.

Petrocelli, J.V., 1950. *J. ECS*, **97(1)**, 10-19.

Pillai, K.C. and Bockris, J.O'M., 1984. *J. ECS.*, **131**, 568-572.

Poling and Leja, 1962

Prestidge, C.A., Ralston, J. and Smart, R., 1993. *IJMP*, **38**, 205-233.

Pritzker, M.D., Yoon,R.-H., Basilio, C. and Choi, W.Z., 1985. *Can. Metall. Quart*., **24**, 27-38.

Rand, D.A.J., 1977. *J. Electroanal. Chem*,. **83**, 19-32.

Richardson, P.E., Stout III, J.V., Proctor, C.L. and Walker, G.W., 1984. *IJMP*, **12**, 73-93.

Roger, P. and Bockris, J.O'M., 1951. *Trans. Farad. Soc.*, **47**, 914-928.

Roger, P., 1951. *Trans. Farad. Soc.*, **47**, 1332-1344.

Roos, J.R., Celis, J.P. and Sundarsono, A.S., 1990. *IJMP*, **29**, 17-30.

Salamy, S.G. and Nixon, J.C., 1953. Recent Developments in Mineral Dressing. IMM. 503-516.

Salamy, S.G. and Nixon, J.C., 1954. *Aust J. Chem.* **7**, 146-156.

Senior, G.D., Shannon, L.K. and Trahar, W.J., 1994. *IJMP*, **42**, 169-190.

Sparrow, G. Pomianowski, A. and Leja, J., 1977. *Sepn Sci.*, **12(1)**, 87-102.

Sui, C.C., Brienne, S.H.R. and Xu, Z., 1997. *IJMP*, **49**, 207-221.

Tolun, R. and Kitchener, J.A., 1964. *IMM*, 313-322. 1964

Toperi, D. and Tolun, R., 1969, *IMM*, C191-C197. 1969

Valli, M. and Persson, I., 1994. *Coll. Surf. (A)*, **83**, 199-206.

Walker, G.W., Walters, C.P., and Richardson, P.E., 1986. *IJMP*, **18**, 119-137. 1986 1986

Wang, X. and Forssberg, K.S.E, 1991. *IJMP* **33**, 275-290.

Wang, X., 1995. *J. Coll Interf. Sci.*, **171**, 413-428.

Wang, X., Forssberg, K.S.E. and Bolin, N.J., 1989. *IJMP*, **27**, 1-19.

Wark, I.W. and Cox, A.B., 1934. *Trans AIME*, **112**, 189.

Yoon, R.-H., Basilio, C.I., Marticorena, M.A., Kerr, A.N. and Crawley, R.S. 1995. *Min. Engng*. **8(7)**, 807-816.

Yoon, R.-H., Chen, X. and Nagaraj, D.R. 1997a.. Processing of Complex Ores: Mineral Processing and the Environment (Eds. J.A. Finch, S.R. Rao and I. Holubec). CIM: Montreal (Canada). 91 -100.

Young, 1987. Dissertation, Virginia Polytech. Insti. And State Univ. Virginia (USA).

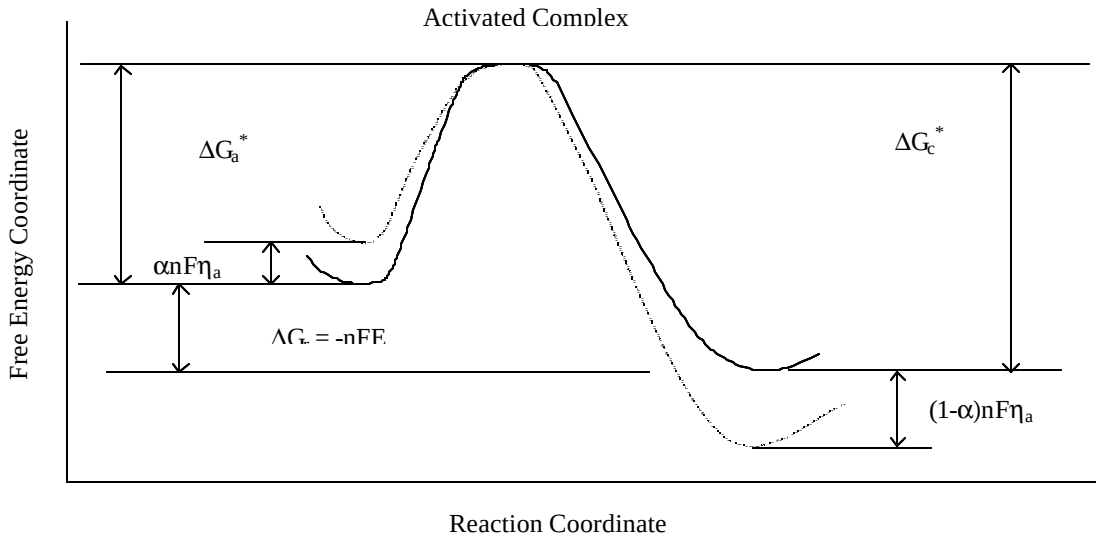

Figure 4.1 The Activation Energy Model (Jones, 1992)

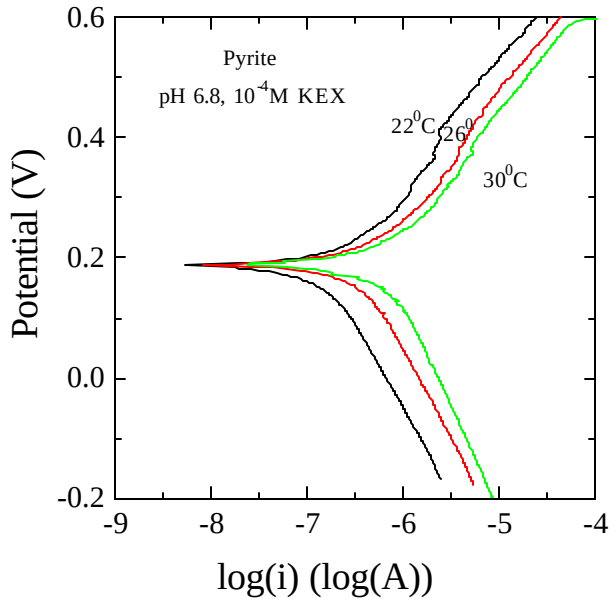

Figure 4.2. The Tafel plots for pyrite at 22°, 26° and 30°C in 10^{-4} M KEX solution at pH 6.8.

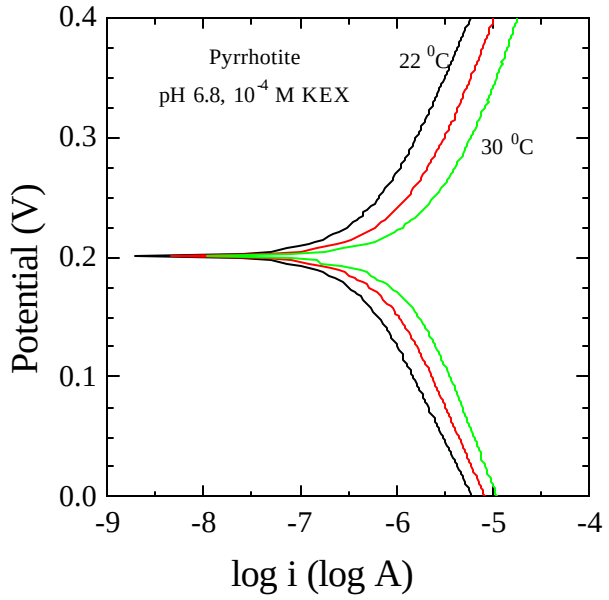

Figure 4.3. The Tafel plots for pyrrhotite at 22°, 26° and 30°C in 10^{-4} M KEX solution at pH 6.8.

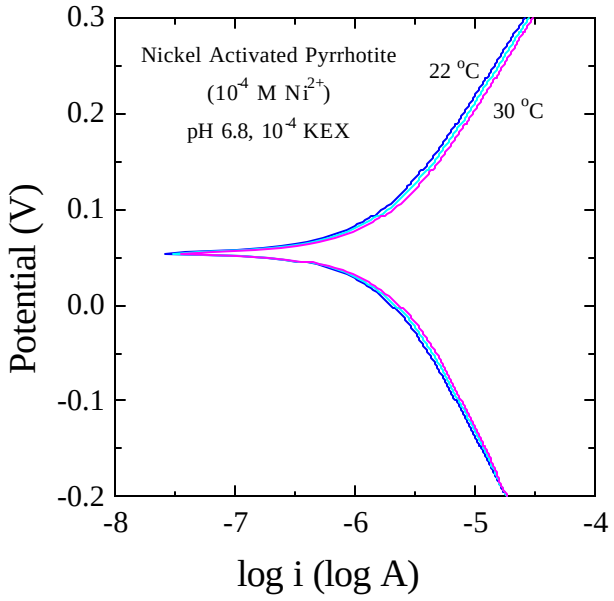

Figure 4.4. The Tafel plots for nickel-activated pyrrhotite at 22°, 26° and 30°C in 10^{-4} M KEX solution at pH 6.8.

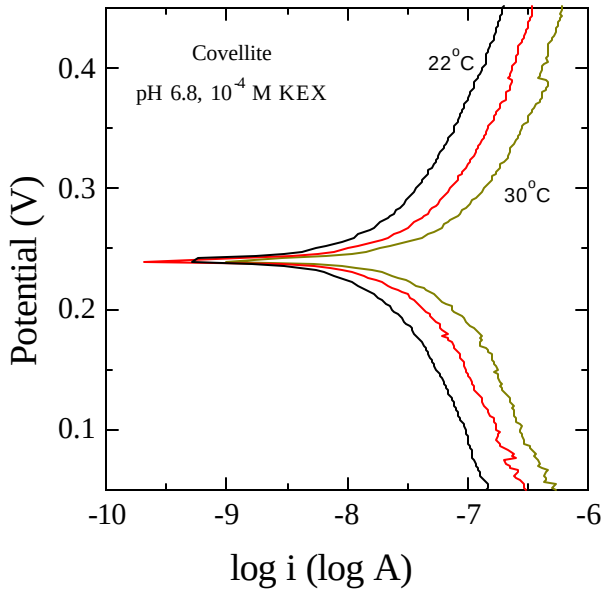

Figure 4.5. The Tafel plots for chalcocite at 22°, 26° and 30°C in 10^{-4} M KEX solution at pH 6.8.

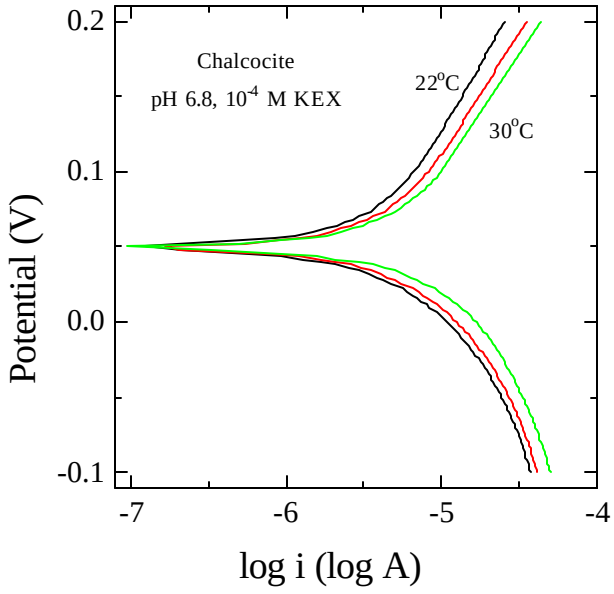

Figure 4.6. The Tafel plots for covellite at 22°, 26° and 30°C in 10^{-4} M KEX solution at pH 6.8.

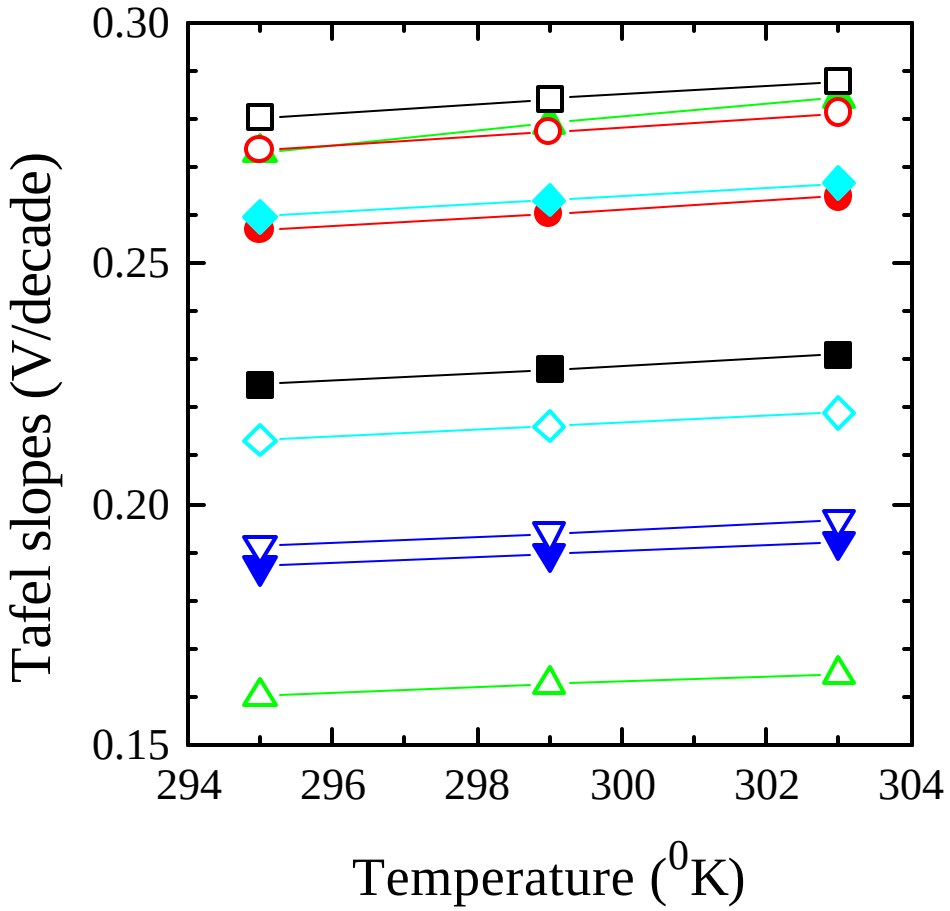

Figure 4.7. The cathodic (solid) and anodic (open) Tafel slopes as a function of temperature for pyrite (●,○), pyrrhotite (▲,△), nickel-activated pyrrhotite (▼,▽), chalcocite (■,□), covellite (◆,◇).

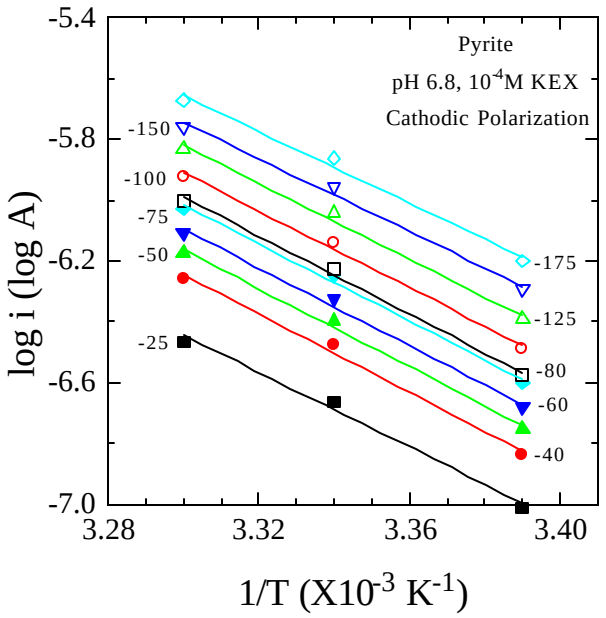

(a)

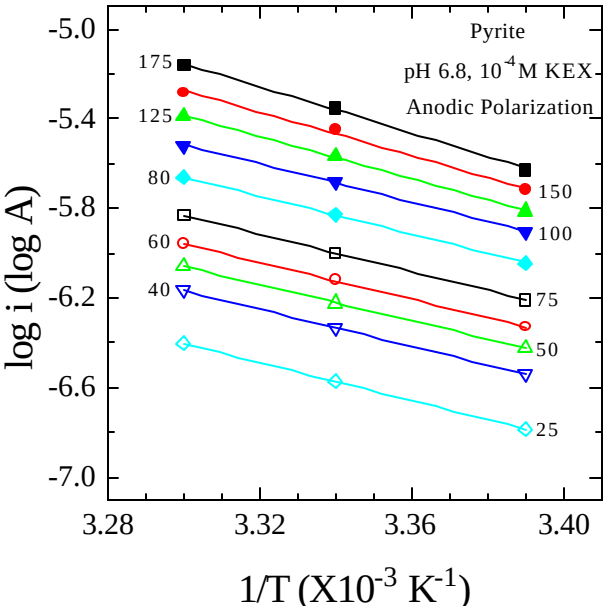

(b)

Figure 4.8. The Arrhenius-type current plots for (a) cathodic and (b) anodic polarization of pyrite in 10^{-4} M KEX solution at pH 6.8. The numbers shown beside each line represents the corresponding overpotential in millivolts.

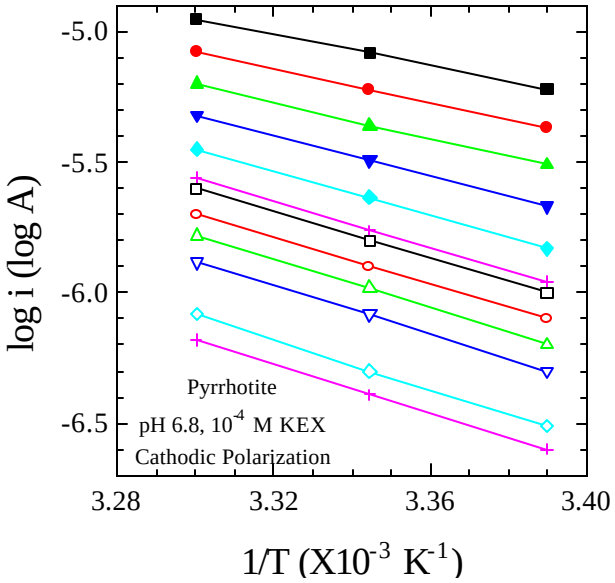

(a)

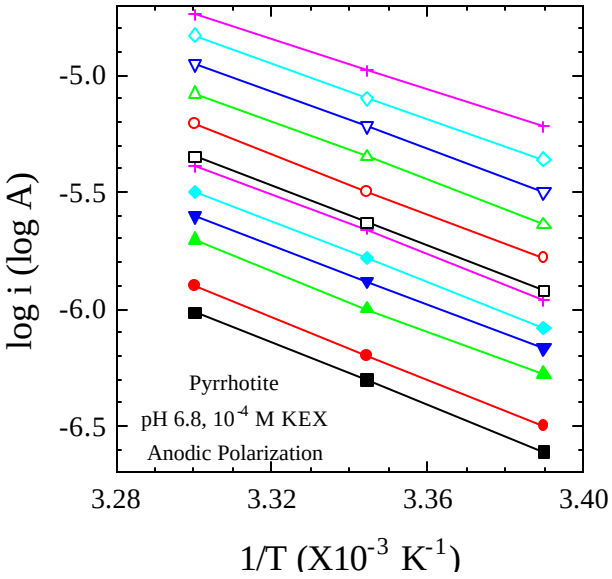

(b)

Figure 4.9. The Arrhenius-type current plots for (a) cathodic and (b) anodic polarization of pyrrhotite in 10^{-4} M KEX solution at pH 6.8.

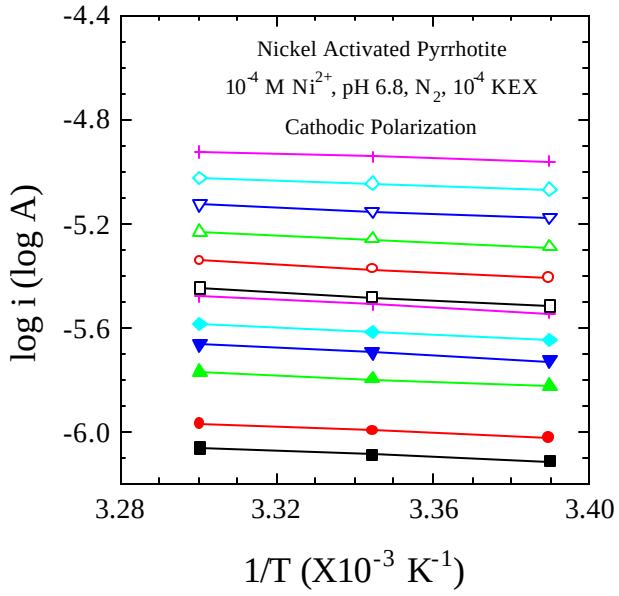

(a)

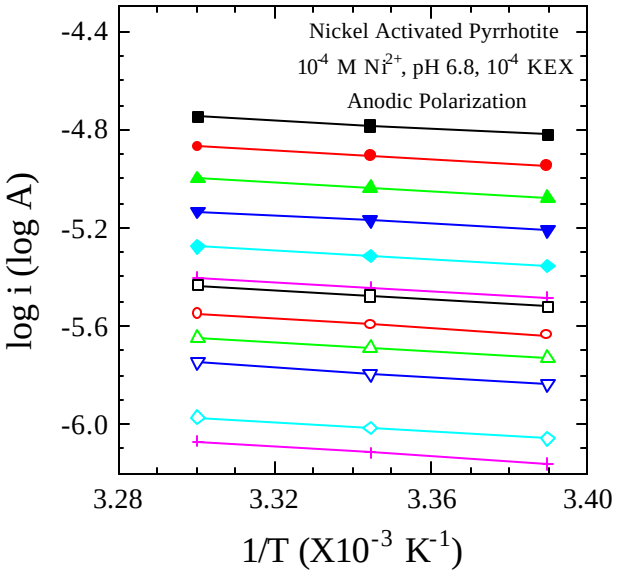

(b)

Figure 4.10. The Arrhenius-type current plots for (a) cathodic and (b) anodic polarization of nickel-activated pyrrhotite in 10^{-4} M KEX solution at pH 6.8.

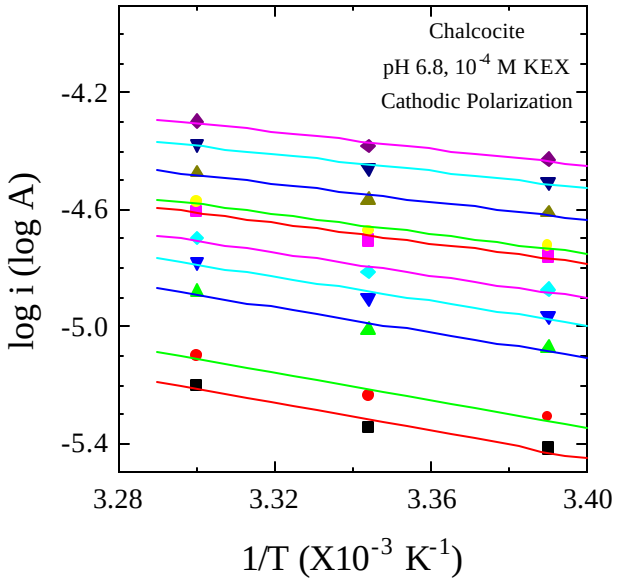

(a)

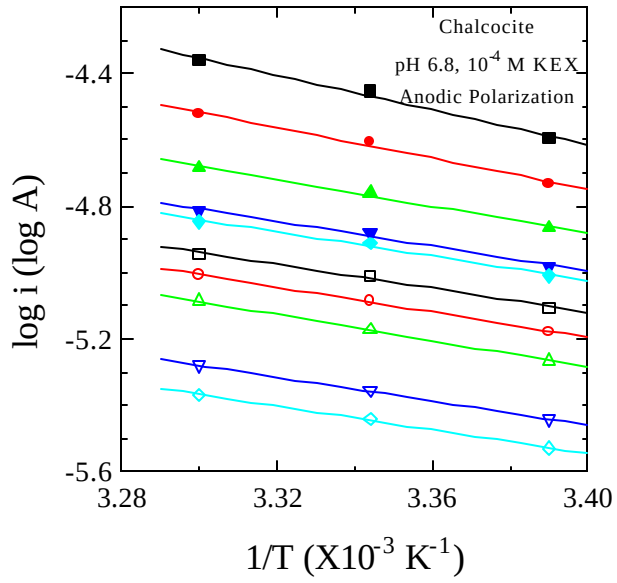

(b)

Figure 4.11. The Arrhenius-type current plots for (a) cathodic and (b) anodic polarization of chalcocite in 10^{-4} M KEX solution at pH 6.8.

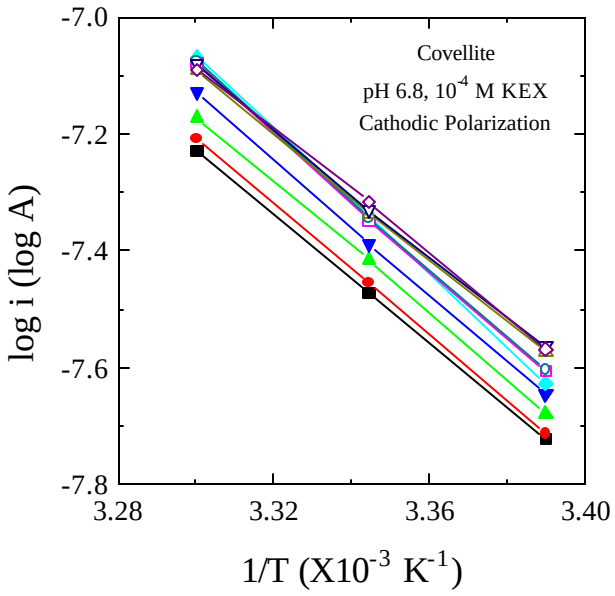

(a)

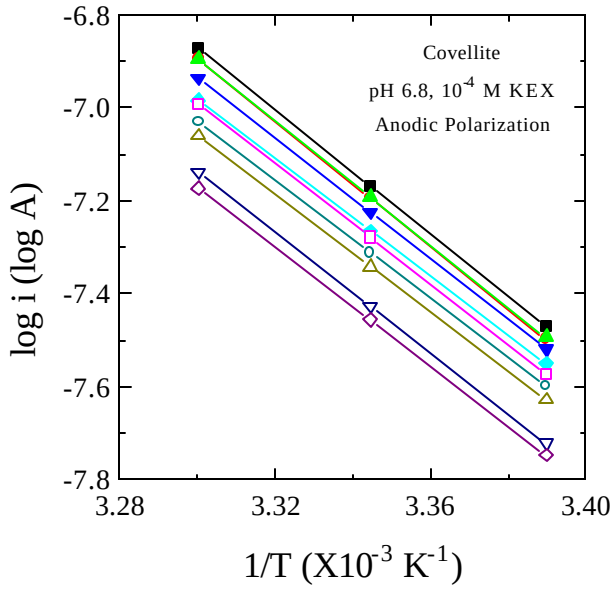

(b)

Figure 4.12. The Arrhenius-type current plots for (a) cathodic and (b) anodic polarization of covellite in 10^{-4} M KEX solution at pH 6.8.

Table 4.1. Possible reactions between chalcocite and xanthate.

Reaction			DG_r (kJ/mol)	E_r (mV)
$Cu_2S + 0.04X^-$	→	$Cu_{1.96}S + 0.04CuX + 0.04e$	0.54	-0.141
$Cu_2S + 0.07X^-$	→	$Cu_{1.93}S + 0.07CuX + 0.07e$	0.64	-0.095
$Cu_2S + 0.17X^-$	→	$Cu_{1.83}S + 0.17CuX + 0.17e$	0.96	-0.058
$Cu_2S + 0.25X^-$	→	$Cu_{1.75}S + 0.25CuX + 0.25e$	2.13	-0.088
$Cu_2S + 0.335X^-$	→	$Cu_{1.665}S + 0.335CuX + 0.335e$	1.14	-0.035
$Cu_2S + 0.62X^-$	→	$Cu_{1.38}S + 0.62CuX + 0.62e$	0.29	-0.005
$Cu_2S + X^-$	→	$CuS + CuX + e$	-1.90	0.020
$Cu_2S + X^-$	→	$2CuX + S + 2e$	-12.29	0.064
$Cu_2S + 2X^-$	→	$CuS + CuX + 0.5X_2 + 2e$	-18.88	0.098

Table 4.2. Cathodic and Anodic Tafel Slopes and Transfer Coefficients for Pyrite, Pyrrhotite, Nickel-Activated Pyrrhotite, Chalcocite and Covellite.

Mineral	Tafel slopes, b (V/decade)						N_e	Transfer Coefficients	
	Cathodic			Anodic				Cathodic (α_c)	Anodic (α_a)
	22^0C	26^0C	30^0C	22^0C	26^0C	30^0C			
Pyrite	0.225	0.228	0.231	0.280	0.284	0.288	2	0.131	0.105
Pyrrhotite	0.187	0.190	0.192	0.191	0.194	0.197	2	0.155	0.151
Ni-Act. Pyrrhotite	0.260	0.263	0.267	0.213	0.216	0.219	2	0.113	0.137
Chalcocite	0.273	0.279	0.284	0.160	0.163	0.165	2	0.106	0.183
Covellite	0.257	0.260	0.264	0.274	0.277	0.281	1	0.225	0.211

Table 4.3. Cathodic and Anodic Activation Energies at Different Overpotential values for Pyrite, Pyrrhotite, Nickel-Activated Pyrrhotite, Chalcocite and Covellite.

Overpotential (mV)	Activation Energy (kJ/mol)				
	Pyrite	Pyrrhotite	Ni-Act. Pyrrhotite	Chalcocite	Covellite
125	121.68	122.85	19.86	48.93	128.95
100	122.94	123.89	19.59	49.08	128.95
80	124.21	124.09	19.82	48.61	124.29
75	123.37	125.27	19.82	47.37	121.27
60	123.37	126.07	19.89	46.62	124.49
50	123.80	124.95	19.25	47.95	121.30
40	124.24	124.90	20.80	49.28	121.70
25	117.90	125.28	19.98	50.37	125.12
-25	82.81	93.42	12.58	34.08	108.08
-40	80.68	92.11	13.35	34.20	108.38
-50	78.97	90.80	14.94	34.78	110.81
-60	80.47	90.06	15.07	35.08	119.42
-75	82.17	88.03	16.07	34.44	112.57
-80	82.17	87.13	16.43	35.12	112.79
-100	83.89	83.66	16.34	35.13	103.22
-125	85.18	79.13	15.10	35.94	103.05

Table 4.4. The Cathodic (ΔG^*_f) and Anodic (ΔG^*_b) Activation Energies, Free Energy of Reaction from Activation Energies (ΔG_r) and Thermodynamic Data (ΔG_r^{TD}) for Pyrite, Pyrrhotite, Nickel-Activated Pyrrhotite, Chalcocite and Covellite

Mineral	Activation Energy		Free Energy of Reaction	
	Cathodic (ΔG^*_b)	Anodic (ΔG^*_f)	From ΔG^*s (ΔG_r)	Thermodynamic Data (ΔG_r^{TD})
Pyrite	121.57	82.03	-39.54	-33.96
Pyrrhotite	124.85	88.50	-36.36	-33.96
Ni-Activated Pyrrhotite	20.26	14.24	-6.02	-5.67
Chalcocite	48.52	34.85	-13.68	-12.29
Covellite	124.67	108.64	-16.03	-17.27

Table 4.5. The Reversible Potential Values Calculated from Activation Energies ($E_r^{\Delta G}$), Thermodynamic Data (E_r^{TD}) and Tafel Plots (E_r^{Tafel}) for Pyrite, Pyrrhotite, Nickel-Activated Pyrrhotite, Chalcocite and Covellite.

Mineral	Reversible Potential		
	Activation Energies ($E_r^{\Delta G}$)	Thermodynamic Data (E_r^{TD})	Tafel Plots (E_r^{Tafel})
Pyrite	0.205	0.176	0.184-0.190
Pyrrhotite	0.188	0.176	0.193-0.201
Ni-Activated Pyrrhotite	0.031	0.010	0.055
Chalcocite	0.071	0.064	0.050
Covellite	0.166	0.179	0.240-0.250

CHAPTER 5

STUDIES OF THE PYRRHOTITE DEPRESSION MECHANISMS BY DETA AND SO_2

5.1 INTRODUCTION

The Sudbury basin nickel-copper ore contains chalcopyrite, pentlandite and pyrrhotite as the major sulfide minerals. Although pyrrhotite is the most abundant of the three sulfide minerals, it is of little commercial value. Also, it is the major source of SO_2 emitted during the processes of smelting and converting. Therefore, it is desirable to reject as much pyrrhotite as possible before the copper-nickel concentrate enters the smelter. However, the removal of pyrrhotite during copper-nickel flotation is difficult because of its considerable floatability.

5.1.1. Pyrrhotite Floatability

Pyrrhotite has considerable natural hydrophobicity (collectorless floatability). Hodgson and Agar (1984) suggested that when pyrrhotite ($FeS_{1.13}$) is oxidized superficially, polysulfides are formed at the surface and induce collectorless floatability:

$$FeS_{1.13} + H_2O = [Fe(OH)_a](S_2) + S_2^{2-}(aq) + H^+ + e, \quad [5.1]$$

in which S_2 represents polysulfide. Similarly, Luttrell and Yoon (1984) suggested that polysulfides are responsible for the flotation of chalcopyrite. In a study of pyrrhotite in the presence of xanthate, same authors (Hodgson and Agar, 1989) proposed another mechanism, in which pyrrhotite (FeS) oxidizes to form an iron (III) hydroxy-polysulfide, as follows:

$$FeS + H_2O = Fe(OH)S^+ + H^+ + 2e\ . \quad [5.2]$$

These authors suggested that xanthate (X^-) adsorbs on the positively-charged iron hydroxy-polysulfide *via* a columbic interaction:

$$Fe(OH)[S]^+ + X^- = Fe(OH)[S]X \quad [5.3]$$

This mechanism suggests that the hydrophobicity of superficially oxidized pyrrhotite increases further in the presence of xanthate.

However, Yoon and his colleagues showed that xanthate adsorbs on pyrrhotite mostly as dixanthogen (X_2), while small amounts of iron xanthate (FeX_3) were also observed (Basilio et al., 1993; Yoon et al., 1995). Figure 5.1 shows a schematic Tafel plot for xanthate adsorption on pyrrhotite, where the oxidation product is X_2.

5.1.2 Inadvertent Activation

More studies conducted at the Center for Coal and Minerals Processing (CCMP) showed that pyrrhotite is readily activated by the heavy metal ions present in flotation pulp, for e.g., nickel ions (Ni^{2+}), (Yoon et al., 1995). The activation mechanism may be represented by the following reaction:

$$Fe_7S_8 + 4.5Ni^{2+} + 4e \rightarrow (Fe_{4.5},Ni_{4.5})S_8 + 2.5Fe^{2+} \qquad \Delta G^0 = -18.88 \text{ kJ/mol} \qquad [5.4]$$

where Fe_7S_8 and $(Fe_{4.5},Ni_{4.5})S_8$ represents pyrrhotite and pentlandite, respectively. The thermodynamic data are from Thornber (1983), Bard et al. (1985) and Senior et al. (1994). The negative standard free energy of this reaction indicates that the activation mechanism is spontaneous. The presence of the nickel ions on the surface of the activated pyrrhotite should decrease the reversible potential ($E_r^{Ni\text{-}Po}$) for xanthate adsorption, as shown in Figure 5.1. Nickel-activated pyrrhotite may act as pentlandite vis-à-vis pyrrhotite.

5.1.3. Pentlandite-Pyrrhotite Separation

Xanthate adsorbs on pyrrhotite as X_2, whereas it adsorbs as NiX_2 on pentlandite. The reversible potential (E_r) for the dixanthogen formation is about 80 mV at 10^{-4} M potassium amyl xanthate (KAX) (Finkelstein and Poling, 1977). The cyclic voltammetry studies conducted by Hodgson and Agar (1989) show that KAX (10^{-4} M) begins to adsorb on pentlandite at about -100 mV. Similarly, for 10^{-4} M potassium ethyl xanthate (KEX), the reversible potential for the dixanthogen formation is about 180 mV, whereas that for NiX_2 is –90 mV (Finkelstein and Poling, 1977; ??). This potential difference of 180 mV for the adsorption of KAX (or 270 mV for the adsorption of KEX) may serve as the window of selectivity for the separation of pyrrhotite and pentlandite by flotation. However, the nickel-activated pyrrhotite behaves similarly to pentlandite, thereby narrowing the window of selectivity narrower, as shown in Figure 5.1.

5.1.4. Pyrrhotite Depression

(a) Depression by DETA

The use of DETA as pyrrhotite depressant has been patented by International Nickel Company (INCO) (Kerr et al., 1991; Marticorena et al., 1994). The depressing action of DETA was studied at CCMP (Basilio et al., 1993; Yoon et al., 1995) using spectroscopy techniques. The Fourier transform infra red (FTIR) spectra of the pyrrhotite specimens contacted with xanthate solutions show the presence of dixanthogen and small amounts of iron xanthate. In the

presence of DETA, however, the amount of xanthate adsorbed on pyrrhotite surface decreased substantially. The UV-Vis spectroscopy studies also showed that DETA hinders xanthate adsorption (Basilio et al., 1993). The XPS analysis of the pyrrhotite specimens contacted with solutions containing heavy metal ions in the presence and absence of DETA shows that the role of DETA is to prevent metal ions from activating pyrrhotite. The LIMS studies conducted by Kelebek et al. (1996) and the atomic absorption spectroscopy studies conducted by Xu et al. (1997) showed the same results. It is likely that DETA forms soluble complexes with the heavy metal ions in solution (for e.g., Ni^{2+}) to prevent the activation of pentlandite (Equation [5.4]). The studies conducted at INCO and CCMP showed that the depressing action of DETA was enhanced under the oxidizing conditions. It was proposed that under oxidizing conditions, the activation products (NiS and CuS) are oxidized to nickel (or copper) oxides/hydroxides, which would more readily interact with DETA and be solubilized.

(b) DETA as a Potential Control Agent

Although studies have shown that DETA itself is not a potential controlling agent, it may control the pulp potential by complexing with Fe^{2+} ions. The titration experiments conducted by Kelebek et al. (1995b) also support the view that DETA can stabilize the potential by complexing Fe^{2+} ions. This is similar to the change in pulp potential in the presence of cyanide ions (CN^-) and EDTA:

$$Fe(H_2O)_6^{3+} + e \rightarrow Fe(H_2O)_6^{2+} \qquad E^0 = 0.77\ V \qquad [5.5]$$

$$Fe(CN)_6^{3+} + e \rightarrow Fe(CN)_6^{2+}, \qquad E^0 = 0.36\ V \qquad [5.6]$$

$$Fe(EDTA)^- + e \rightarrow Fe(EDTA)^{2-} \qquad E^0 = -0.12\ V \qquad [5.7]$$

As it can be seen that the complexing with CN^- ions decreases the pulp potential and thus, the depressing action of cyanide may be attributed to the mild reducing conditions created by Reaction [5.6]. Although EDTA is not known as a reducing agent, Trahar et al. (1994) showed that EDTA addition to a flotation pulp decreased pulp potential substantially. This is due to the complexation with the Fe^{2+}/Fe^{3+} ions, which changes the equilibrium and decreases E^0. Unfortunately, the appropriate thermodynamic data are not available to determine the changes in the redox potentials of the Fe^{2+}/Fe^{3+} couple in the presence of DETA.

(c) Depression by DETA/SO2 Combination

Kelebek et al. (1995a) patented the use of DETA and SO_2 combination for Falconbridge Copper Company. They showed that the pyrrhotite is depressed more consistently in the

presence of SO_2 and the selectivity of the process increases with increasing SO_2 dosage as long as the SO_2-to-DETA ratio is kept constant. Since the SO_2 is a well-known reducing agent, the Falconbridge process appears to be in conflict with the previous studies at INCO and CCMP, where it was found that DETA works well under oxidizing conditions.

Kelebek and his co-workers offered several different mechanisms concerning the beneficial effect of using SO_2

- SO_2 destroys the hydrophobic collector coatings, such as dixanthogen (X_2) and ferric hydroxy xanthates ($Fe(OH)_2X$), formed on pyrrhotite (Kelebek et al., 1995b).
- SO_2 may remove the hydrophobic surface oxidation products, such as elemental sulfur (S^0) and/or polysulfides (S_{n+1}^{2-}), from pyrrhotite. The following reactions have been suggested for the proposed mechanism (Kelebek et al., 1996):

  $$S^0 + SO_3^{2-} = S_2O_3^{2-} \quad [5.8]$$

  $$2(S_{n+1})^{2-} + (n+3)SO_3^{2-} + 2e + 3H_2O = (n+2)S_2O_3^{2-} + 6OH^- \quad [5.9]$$

- SO_2 oxidizes to dithionate ($S_2O_6^{2-}$), which in turn forms an insoluble precipitate with the Ni^{2+}-DETA complex, as follows (Kelebek et al., 1996):

  $$S_2O_6^{2-} + Ni(DETA)_2^{2+} = [Ni(DETA)_2]S_2O_6 \quad [5.10]$$

- SO_2 helps in maintaining the low potentials. Kelebek (1995b; 1996) proposed that at low potentials, hydrophilic species, such as $Fe(DETA)^{2+}$ and $Fe(OH)DETA^+$ complexes, are stable, whereas hydrophobic species, such as ferric hydroxy xanthate ($Fe(OH)_2X$), are not favored. Therefore, the ratio between the hydrophilic and hydrophobic species increases with decreasing potential, thereby improving the effect of DETA under reducing environment. A problem with this argument is, however, that the iron-DETA complexes are soluble species and may not adsorb on pyrrhotite to render the mineral hydrophilic.

However, the mechanisms proposed by Kelebek and his co-workers are not based on substantial evidence. For example, no evidence was given for the removal of hydrophobic species, e.g., X_2 and S_{n+1}^{2-}, from pyrrhotite.

Based on the previous studies, it may be inferred that the combined use of SO_2 and DETA may represent an effective means of keeping the pulp potentials in a region, where the adsorption of xanthate on pyrrhotite can be prevented while the same on pentlandite is allowed. This may be achieved by a combined action, in which SO_2 keeps the dissolved iron in a reduced

state and DETA stabilizes the Fe^{2+} ions by forming complexes. Since DETA reacts only with Fe^{2+} ions, but not with Fe^{3+} ions (a well-known oxidizing agent, Yoon et al., 1997), preventing the formation of Fe^{3+} ions in solution would help maintain low pulp potentials.

5.2. OBJECTIVE

The objective of this study is to investigate the effect of DETA and SO_2 on the electrochemical behavior of pyrrhotite and elucidate their role in pyrrhotite depression.

5.3. EXPERIMENTAL

5.3.1 Samples:

The chunks of pyrrhotite (Russia) were obtained from the Ward's Natural Science Est., Inc. Using a low speed diamond saw, mineral samples were cut into small rectangular pieces of dimensions of 5 × 5 × 10 mm. A copper wire was attached to one of the 5 × 5 faces using conducting silver epoxy and/or indium solder. The electrical contact was covered with non-conducting epoxy, Torr Seal (Varian). The conductivity of the contact was tested using an ohmmeter before further preparation of the samples. The samples were mounted in a glass (Pyrex) tube (OD = 8mm, ID = 6mm) using epoxy resin (Struers). The surface facing out was in contact with the solution and was renewed by successive polishing at 600 grit and 0.05 μ alumina polishing, cleaning in ultrasonic bath and rinsing with deionized water.

5.3.2 Reagents:

Potassium Ethyl Xanthate (KEX) was obtained from Eastman Kodak Company. Xanthate was purified in the usual manner: dissolution in acetone and recrystallization from ether. The purification method was repeated three times to ensure high purity. The xanthate thus obtained was vacuum dried and dissolved in double distilled de-ionized (DI) water to prepare 10^{-2} M solution. DETA (Assay > 97%) was obtained from Alfa Aesar. A 10^{-2} M solution was prepared and an appropriate amount was added to the cell to achieve the desired concentration (10^{-5} M for most of the experiments).

A pH 6.8 buffer solution was prepared by mixing 0.05 M NaH_2PO_4 and 0.025 M NaOH. Similarly, a pH 2 buffer solution was prepared by mixing 0.05 M KCl and 0.013 M HCl. Ferrous and ferric solutions were prepared by mixing their respective chloride salts in pH 2

buffer solution to obtain concentration of 10^{-2} M. Sodium sulfite (SO_3^{2-}) solution was used to emulate the effect of SO_2.

For nickel-activation of pyrrhotite, 10^{-2} M $NiSO_4$ solution was prepared and an aliquot was added to pH 6.8 buffer to obtain desired (10^{-4} M) concentration. For present study, an electrode was activated for 15 minutes as it was observed that activation current reached a steady state value at about 15 minutes. All of the solutions were prepared in DI water.

5.3.3 Apparatus and Procedure:

A standard three-electrode electrochemical cell was used. The working electrode consisted of the mineral under study. A platinum wire/mesh was used as the counter electrode, except for Tafel studies where counter electrode consisted of the mineral. Standard Calomel Electrode (SCE) was used as the reference electrode and all the potentials were converted to hydrogen scale (SHE) by adding 0.245 V to the SCE values.

For cyclic voltammetric studies, the electrochemical cell was connected to a potentiostat (RDE4 by PINE). The electrochemical system was connected to a computer through Keithley A/D interface and data was acquired digitally. In order to conduct Tafel studies, the electrochemical cell was connected to a potentiostat (Model 273 by EG&G) and controlled by a computer connected through GPIB interface. The Tafel studies were carried out using 352 SoftCorr Corrosion Measurement software (EG&G). The rest potentials were measured with Keithley 169 multimeter.

For contact angle measurements, the captive bubble technique was employed as the surface of the mineral electrode faced vertically downwards in the solution. The bubbles were generated on the electrode surface using a micro (or 1 ml) syringe with the needle bent upwards and the angle was measured through the aqueous phase. The contact angles were measured using Rame-Hart Goniometer.

5.4 RESULTS AND DISCUSSION

5.4.1 Contact Angle Measurements

Figures 5.2 and 5.3 show the contact angles measured as a function of potential on the surface of pyrrhotite and nickel-activated pyrrhotite in the absence and presence of xanthate, DETA and SO_3^{2-}. As it can be seen from Figure 5.2, the contact angle for pyrrhotite increase slightly at about 0.250 V, indicating hydrophobicity in the absence of collector. As discussed

earlier, this may be due to the formation of polysulfides according to either reaction [5.1] (Hodgson and Agar, 1984) or reaction [5.2] (Hodgson and Agar, 1989), where $[Fe(OH)_a](S_2)$ and $Fe(OH)S^+$ represent iron (III) hydroxy-polysulfides.

In the presence of xanthate, contact angle begins to increase at about 0.150 V for pyrrhotite and 0 V for nickel-activated pyrrhotite. The potentials at which xanthate adsorption begins correspond to the reversible potential for the formation of dixanthogen on pyrrhotite and nickel dixanthate on nickel-activated pyrrhotite:

$$2X^- \rightarrow X_2 + 2e \qquad E_r = -0.060 - 0.059\log[X^-] = 0.176 \text{ V at } [X^-] = 10^{-4} \text{ M} \qquad [5.11]$$

$$(Fe_{4.5},Ni_{4.5})S_8 + 13.5H_2O + 9X^- \rightarrow 4.5Fe(OH)_3 + 4.5NiX_2 + 8S + 13.5H^+ + 22.5e$$

$$E_r = -0.057 - 0.024\log[X^-] - 0.035pH = 0.007 \text{ V at pH} = 6.8, [X^-] = 10^{-4} \text{ M} \qquad [5.12]$$

Although the formation of dixanthogen vs. nickel dixanthate on pentlandite is debatable, the recent Tafel studies, as described in Chapter 4, concur with the formation of latter (Poling and Leja, 1962, Hodgson and Agar, 1989, McNeil et al., 1994 and Senior et al., 1994).

In order to study the effect of DETA and SO_3^{2-}, contact angles were also measured in their presence in 10^{-4} M KEX solutions at pH 6.8. Figures 5.2 and 5.3 show that in the presence of 10^{-5} M DETA, the contact angle on both pyrrhotite and nickel-activated pyrrhotite decreased and remained about $5 - 8^0$ for the whole range of potential under study. This can be explained in terms of chelation of ferrous ions with DETA to form soluble complexes. This may have two-fold effect; first, by chelating with ferrous ions, it maintains the potentials low enough to inhibit oxidation of xanthate to dixanthogen. Second, it hinders the formation of iron (III) hydroxy polysulfides, which according to Hodgson and Agar (1989), are the sites for xanthate adsorption. It is also possible that chelation of ferrous ions on the surface may passivate the surface and hence inhibit xanthate adsorption. However, previous spectroscopic studies showed that DETA does not adsorb on the surface (Basilio et al., 1993; Yoon et al., 1995). For nickel-activated pyrrhotite, beside the above stated possibilities, DETA has an additional role of deactivating pyrrhotite by forming soluble complexes with nickel ions on the surface (Basilio et al., 1993; Yoon et al., 1995; Kelebek et al., 1996; Xu et al., 1997). This, in turn, would result in a decreased xanthate adsorption and hence, a decrease in contact angle.

Figures 5.2 and 5.3 also show the contact angle in the presence of 10^{-4} M SO_3^{2-}. In the presence of SO_3^{2-}, the contact angle begins to increase on pyrrhotite at ~0.300 V and on activated pyrrhotite at ~0.150 V. Kelebek et al. (1995b) proposed that SO_3^{2-} may destroy the xanthate

products on the pyrrhotite surface; however, the increase in contact angle at higher potential indicates otherwise. The potentials at which contact angle begins to increase are higher in the presence of SO_3^{2-} than in its absence. The anodic shift in reversible potentials can be explained in terms of the reducing nature of SO_3^{2-}, which suggests that additional overpotential is required in the presence of SO_3^{2-} to oxidize xanthate on the mineral surface. This mechanism is similar to that proposed by Miller (1970) and Pattison (1981) for pyrite, who suggested that SO_3^{2-} can reduce the pulp potential below that of dixanthogen formation. When both DETA and SO_3^{2-} were added into the system, contact angle dropped to almost 0^o indicating improved effect of the combination. This shows that the SO_2 reduces the hydrophobicity further when added in the presence of DETA. Therefore, a total effect of DETA/SO_3^{2-} combination leads to a complete prevention of the xanthate adsorption.

5.4.2. Cyclic Voltammetry

Figure 5.4 shows the cyclic voltammograms of pyrrhotite i) without any reagent, ii) at 10^{-5} M DETA, and iii) at 10^{-4} M SO_3^{2-} in the absence of xanthate at pH 6.8. The voltammograms exhibit three anodic (A1, A2 and A3) and two cathodic peaks (C1 and C2). In the absence of xanthate, DETA and SO_3^{2-}, the anodic peaks can be characterized as follows:

A1: $Fe^0 + 2H_2O \rightarrow Fe(OH)_2 + 2H^+ + 2e$ $E_r = -0.465$ V (pH = 6.8) [5.13]

A2: $nFe_7S_8 + 14nH_2O \rightarrow 7nFe(OH)_2 + 8S_n^{2-} + 14nH^+ + (14n-16)e$ [5.14]

where S_n^{2-} (n > 2) represents polysulfides. At pH 6.8, the reversible potentials for the formation of S_3^{2-}, S_4^{2-} and S_5^{2-} polysulfides are 0.379 V, 0.268 V and 0.217 V, respectively.

A3: the products from A2 are further oxidized to $Fe(OH)_3$, SO_4^{2-}, $S_2O_y^{2-}$ etc.

The cathodic peaks can be characterized as follows:

C1: Reverse of A2

C2: $Fe_7S_8 + 8H^+ + 16e \rightarrow Fe + 8HS^-$ $E_r = -0.748$ V (pH = 6.8) [5.15]

In the presence of DETA, peak A2 becomes larger. This may be due to extraction of ferrous ions by DETA from ferrous hydroxides to form soluble complexes:

$$Fe(OH)_2 + 2H^+ + 2DETA \rightarrow Fe(DETA)_2^{2+} + 2H_2O \quad [5.16]$$

Thus, the overall reaction may be given as:

$$nFe_7S_8 + 14nDETA \rightarrow 7nFe(DETA)_2^{2+} + 8S_n^{2-} + (14n-16)e \quad [5.17]$$

The reversible potential for reaction [5.17] for polysulfides S_3^{2-}, S_4^{2-} and S_5^{2-} are 0.478 V, 0.363 V and 0.307 V, respectively. Similarly peak C2 is increased due to extraction of Fe^{2+} ions from the reduction products.

In the presence of SO_3^{2-}, peak A2 becomes smaller. This may be due to the removal (or decomposition) of polysulfides in the presence of SO_3^{2-} (Kelebek et al., 1996). The proposed reaction is:

$$S_n^{2-} + (n+2)SO_3^{2-} + 6H^+ + 2e \rightarrow (n+1)S_2O_3^{2-} + 3H_2O \qquad [5.18]$$

where, the reversible potentials for S_3^{2-}, S_4^{2-} and S_5^{2-} polysulfides are 0.421 V, 0.446 V and 0.477 V, respectively.

In order to verify if SO_3^{2-} removes polysulfides, contact angles were measured on gold electrode held at 0.150 V in 10^{-4} M Na_2S solution at pH 6.8 (Figure 5.5). Using cyclic voltammetry, and contact angle measurements (not shown) it was determined that polysulfides form at 0.150 V on the gold surface placed in a 10^{-4} M Na_2S solution. This is consistent with previous studies by Chander and Briceno (1989). The contact angle in the absence of SO_3^{2-} and DETA was measured to be 32°. The contact angle dropped immediately in the presence of SO_3^{2-} with or without 10^{-5} M DETA. However, in the presence of 10^{-5} M DETA alone, contact angle decreased relatively little. This suggests that SO_3^{2-} attacks polysulfides, whereas DETA does not.

Figure 5.6 shows the cyclic voltammograms of pyrrhotite in the presence of DETA and SO_3^{2-} in a 10^{-4} M KEX solution at pH 6.8. The effect of DETA and SO_3^{2-} is visible on peak A2, which demonstrates their depressing action. In the absence of DETA and SO_3^{2-}, peak A2 represents formation of dixanthogen as given by Reaction [5.11]. However, according to Hodgson and Agar (1989) xanthate adsorption takes place through formation of iron (III) hydroxy polysulfides. Therefore, peak A2 may encompass formation of iron (III) hydroxy polysulfide. The depressing action of DETA is perceptible from the decrease in peak height. As discussed in previous section, DETA, due to its chelation with ferrous ions, may inhibit formation of iron (III) hydroxy polysulfides. Also, it may hinder xanthate adsorption by passivating the surface by attaching to ferrous ions on the surface; however, previous studies showed that DETA does not adsorb on pyrrhotite surface (Basilio et al., 1993; Yoon et al., 1995). On the other hand, in the presence of SO_3^{2-}, the peak shifted anodically indicating reducing behavior of SO_3^{2-} and the need of overpotential for xanthate adsorption.

5.4.3. Tafel studies

Figure 5.7 shows the Tafel plots of pyrrhotite in the presence of 10^{-4} M KEX, 10^{-5} M DETA and 10^{-4} M SO_3^{2-}. It is essential to mention here that Tafel plots here do not necessarily represent xanthate adsorption on pyrrhotite. In the absence of DETA and SO_3^{2-}, the Tafel plot for xanthate alone represents adsorption of xanthate as dixanthogen. The mixed potential is about 0.200 V, which is approximately closer to thermodynamic value of dixanthogen formation (Reaction [5.11]).

Figure 5.7 shows that in the presence of DETA and SO_3^{2-}, the mixed potential drops below that of xanthate alone. As discussed earlier, the decrease in mixed potential in the presence of DETA may be due to the stabilization of ferrous ions and, hence, lower potentials. For SO_3^{2-}, it is comprehensible, as it is a reducing agent. Surprisingly, the mixed potential in the presence of both DETA and SO_3^{2-} is higher than that in SO_3^{2-} alone. As stated earlier, the Tafel plots do not represent xanthate adsorption. The Tafel plots in the presence of both DETA and SO_3^{2-} may represent some other reactions. Kelebek et al. (1996) proposed the formation of nickel-DETA-dithionate complex as follows:

$$2SO_3^{2-} \rightarrow S_2O_6^{2-} \qquad [5.19a]$$

$$Ni(DETA)_2^{2+} + S_2O_6^{2-} \rightarrow [Ni(DETA)_2]S_2O_6 \qquad [5.19b]$$

Therefore, it is possible that DETA and SO_3^{2-} may form similar complexes with ferrous ions and thus, control the potential. Also, it was suggested that dithionate formation involves ferric hydroxide originating from pyrrhotite. The Tafel plot in the presence of DETA and SO_3^{2-} may represent dithionate formation.

In order to better understand the role of DETA and SO_3^{2-} as potential controlling agents, the rest potentials of a platinum electrode were measured in their solutions at pH 6.8 with incremental addition of ferrous and ferric ions. Table I shows the direction of change of potential when either DETA or SO_3^{2-} or iron ions were added in the solution. Here the relative changes in the potential values are of importance as the measured values could not analyzed due to the lack of appropriate thermodynamic data for DETA complexes. When DETA was added to the pH 6.8 solution, the rest potential of the platinum electrode changed only slightly. However, with addition of ferrous ions, the potential decreased further. The addition of ferric ions in the presence of DETA had no effect on the rest potential. Similarly, the rest potential decreased when DETA was added to a ferrous/ferric solution at pH 6.8. This indicates that DETA has the

ability to extract ferrous ions from its hydroxides and form soluble complexes, thereby controlling the redox potential of the system. As it is well known that the DETA does not form complexes with ferric ions, the addition of ferric ions (and conversion into ferric hydroxide) did not change the redox potential. Similar measurements were conducted with the addition of the SO_3^{2-}. It was noticed that addition of SO_3^{2-} and ferrous ions decreased the rest potential, whereas the addition of ferric ions increased it. This is due to the fact that SO_3^{2-} and ferrous ions are reducing agents, whereas ferric ions are oxidant (Miller, 1970; Pattison, 1981; Yoon et al., 1997).

5.5 CONCLUSIONS

Electrochemical studies were carried out to understand the depressing action of DETA, SO_3^{2-} and their combination. The depressing action of DETA alone can be explained in terms of a chelating agent. The chelating properties of DETA provides a multi-facet role for its depressing action:

- Potential controlling agent:

  The chelation of heavy metal ions is not an electrochemical process; however, it can help DETA control the potential indirectly. The chelation of DETA with Fe^{2+} ions leads to their stabilization, thereby reducing the pulp potential. The pulp potentials may decrease below the reversible potential for xanthate adsorption. This in turn, prevents the adsorption of xanthate on pyrrhotite.

- Inhibitor:

  By forming soluble complexes with Fe^{2+} ions, DETA inhibits the formation of iron (III) hydroxy polysulfides (Reaction [5.2]). Since these polysulfides are believed to be the site for xanthate adsorption, their absence leads to the inhibition of xanthate adsorption (Reaction [5.3]).

- Deactivator:

  DETA chelates with nickel or copper ions and deactivates the inadvertently activated pyrrhotite in the flotation pulp. This in turn leads to a decrease in the adsorption of xanthate on pyrrhotite.

  The depressing action of SO_2 (or SO_3^{2-}) can be summarized as:

- Reducing agent:

SO_2 helps to maintain lower pulp potentials thereby preventing the oxidation of xanthate.

- Decomposes polysulfides

  The experiments showed that SO_2 reacts readily to decompose polysulfides, thereby reducing the hydrophobicity of the mineral. Also, SO_2 may decompose iron (III) hydroxy polysulfides formed on pyrrhotite, thereby eliminating the xanthate adsorption sites.

Therefore, it may be concluded that DETA and SO_2 complement each other to depress pyrrhotite. SO_2 prevents the oxidation of pyrrhotite, maintains the ferrous form of iron (Fe^{2+}), and reduces the polysulfides. At the same time, DETA chelates with the Fe^{2+} ions, which not only maintains the lower pulp potentials, but also inhibits the formation of iron (III) hydroxy polysulfides on pyrrhotite. The reduced pulp potentials and the absence of polysulfides prevent the adsorption of xanthate on pyrrhotite thereby leading to its depression.

5.6 REFERENCES

Bard, A.J., Parson R. and Jordan, J., 1985. Standard Potentials in Aqueous Solution (IUPAC). Marcel Dekker: New York.

Basilio, C.I., Kim, D.S. and Yoon, R.-H., 1993. Final Report submitted to INCO.

Chander, S. and Briceno, A., 1989. Precious and Rare Metal Tech. (Eds. A.E. Torma and I.H. Gundiler). Elsevier: New York. 137-148.

Hodgson, M. and Agar, G.E., 1984. Proc. Intl. Symp. Electrochem. in Mineral and Metal Process. I (Eds. P.E. Richardson, S. Srinivasan and R. Woods). ECS: Pennington (NJ). 185-201.

Hodgson, M. and Agar, G.E., 1989. *Can. Met. Qtr*, **28(3)**, 189-198. Kelebek, S, Fekete, S.O. and Wells, P.F., 1995b. Proc. XIX Intl. Min. Process. Congress, San Francisco. SME: Littleton (CO). **Vol. 3**, Ch. 30, 181-187.

Kelebek, S. 1996. *Trans. IMM. (Sect. C: Min. Process. Extr. Metall.)*. **105**, C75-88.

Kelebek, S., Wells, P.F. and Fekete, S.O. 1995a. US Patent No. 5,411,148.

Kelebek, S., Wells, P.F. and Fekete, S.O. 1996. *Can. Met. Qtr.*, **35(4)**, 329-336.

Kerr, A.N., Liechti, D., Marticorena, M.A. and Pelland, D.A., 1991. US Patent No. 5,074,993.

Luttrell, G.H. and Yoon, R.-H., 1984a. *IJMP*, **13**, 271-283.

Luttrell, G.H. and Yoon, R.-H., 1984b. *Coll. Surf.* **12**, 239-254.

Marticorena, M.A., Hill, G., Kerr, A.N., Liechti, D. and Pelland, D.A., 1994. Innovations in Minerals Processing (Ed. T. Yalchin). ACME: Sudbury (Ontario). 5-21.

Miller, J.D., 1970. Report to E.P.A. Water Quality Office. Univ. of Utah, Dept. of Mineral Engng, Salt Lake City (Utah).

Pattison, I.G., 1981. Dissertation submitted to University of Melbourne (Australia).

Poling, G.W. and Leja, J., 1962. *Can. Metall. Quart.*, **1(2)**, 109-128.

Trahar, W.J., Senior, G.D. and Shannon, L.K., 1994. *IJMP*, **40**, 287-321.

Xu, Z., Rao, S.R., Finch, J.A., Kelebek, S. and Wells, P. 1997. *Trans. IMM. (Sect. C: Min. Process. Extr. Metall.)*, **106**, C15-20.

Yoon, R.-H., Basilio, C.I., Marticorena, M.A., Kerr, A.N. and Crawley, R.S. 1995. *Min. Engng*. **8(7)**, 807-816.

Yoon, R.-H., Chen, X. and Nagaraj, D.R. 1997a.. Processing of Complex Ores: Mineral Processing and the Environment (Eds. J.A. Finch, S.R. Rao and I. Holubec). CIM: Montreal (Canada). 91 -100.

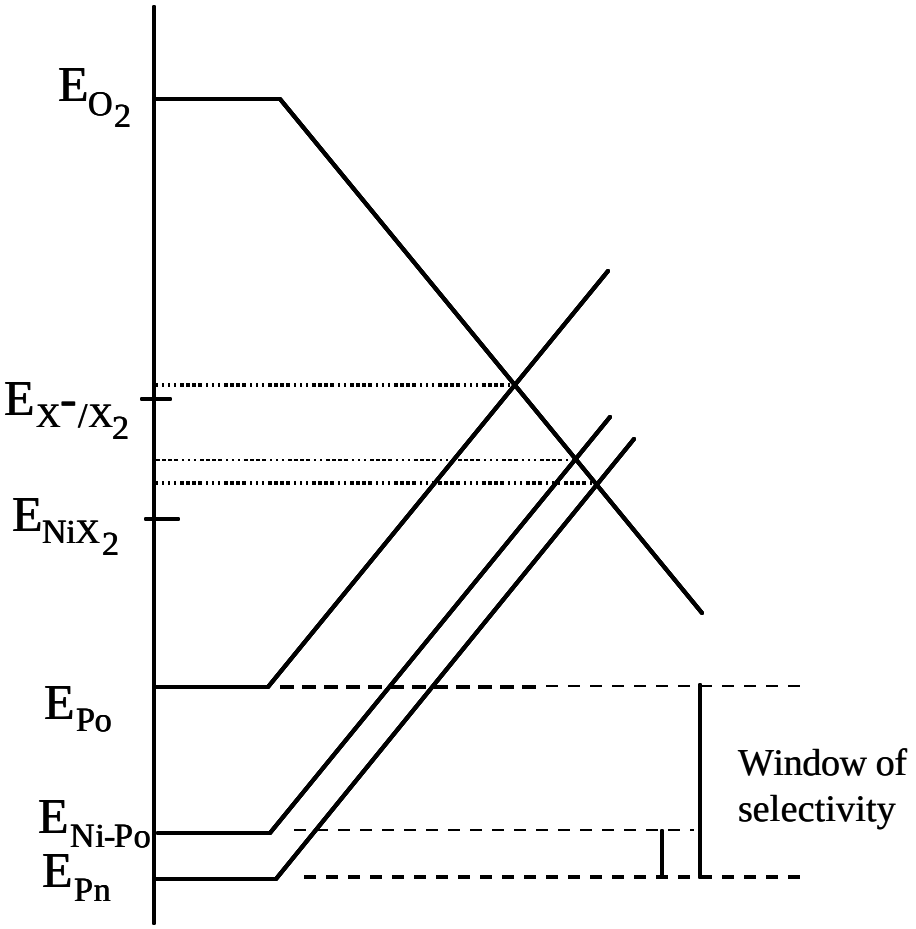

Figure 5.1 Evans diagram showing the mixed potential reactions between oxygen reduction and xanthate adorption on pyrrhotite (E_{Po}), pentalndite (E_{Pn}) and nickel-activated pyrrhotite ($E_{Ni\text{-}Po}$).

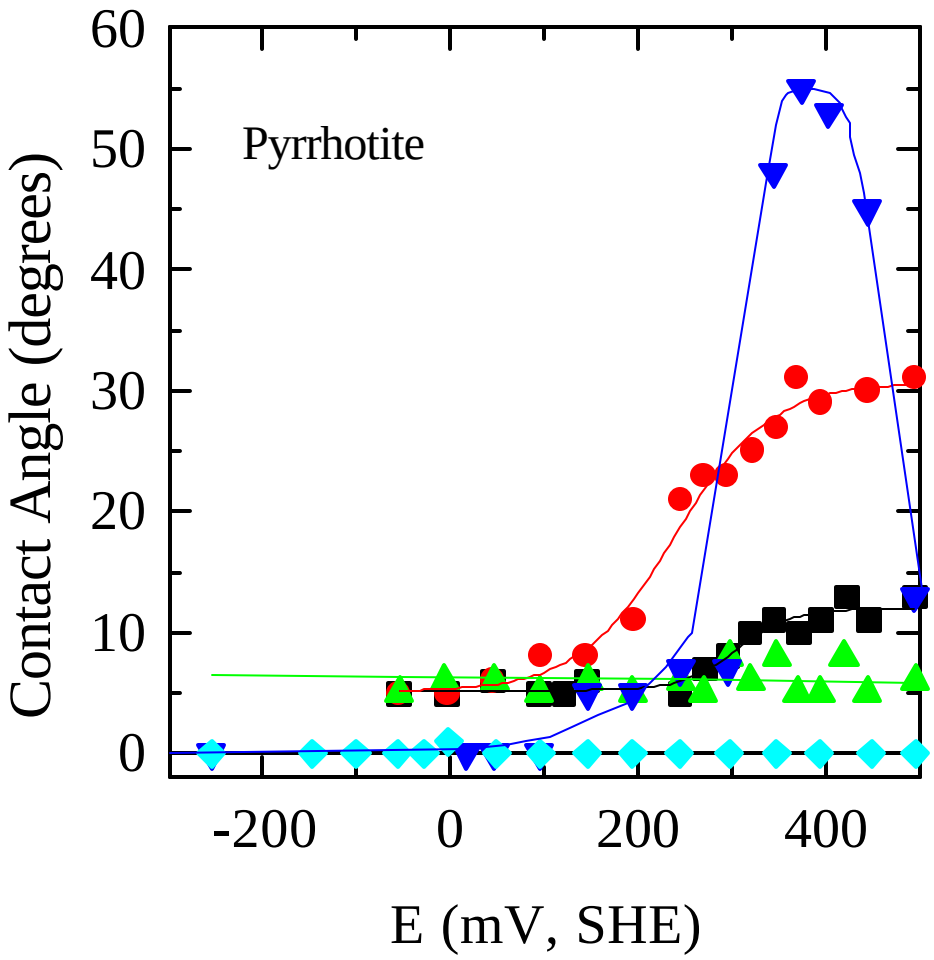

Figure 5.2. Contact angle measurements on pyrrhotite in the absence reagents (■), in a 10^{-4} M KEX solution (●), in a 10^{-4} M KEX and 10^{-5} M DETA solution (▲), in a 10^{-4} M KEX and 10^{-4} M SO_2 solution (▼) and in a 10^{-4} M KEX, 10^{-5} M DETA and 10^{-4} M SO_2 solution (◆) at pH 6.8.

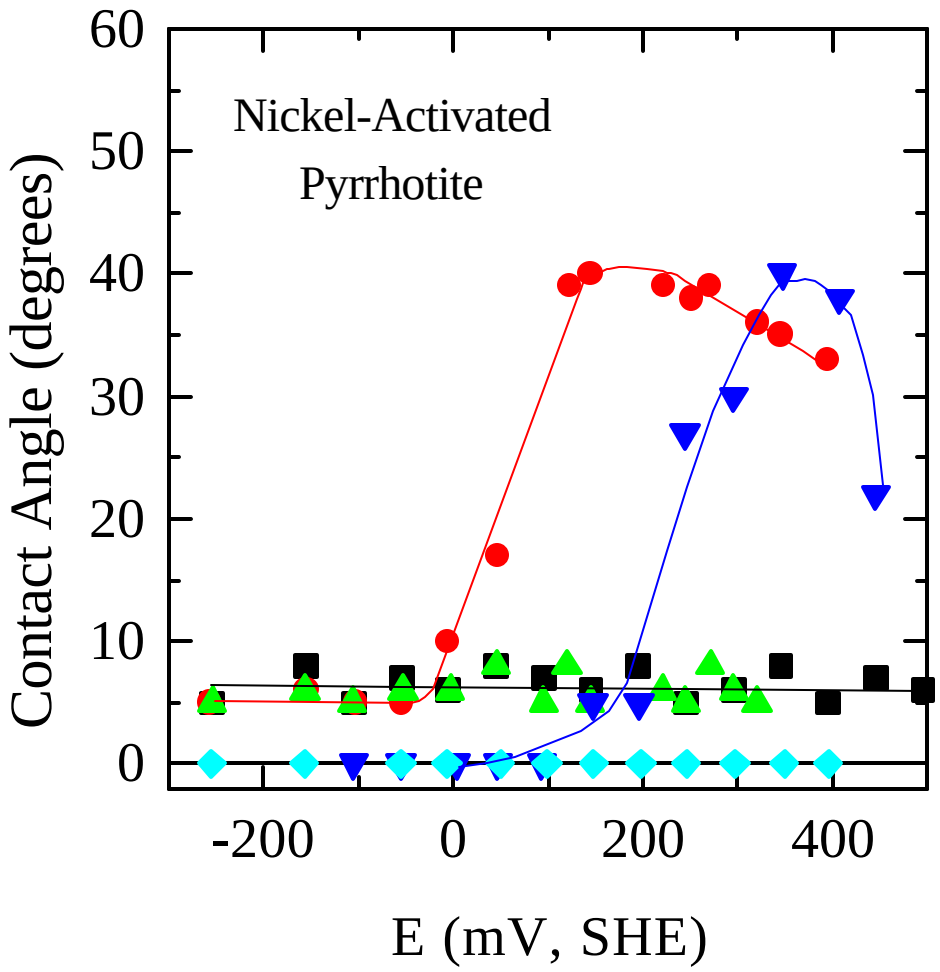

Figure 5.3. Contact angle measurements on nickel-activated pyrrhotite in the absence reagents (■), in a 10^{-4} M KEX solution (●), in a 10^{-4} M KEX and 10^{-5} M DETA solution (▲), in a 10^{-4} M KEX and 10^{-4} M SO_2 solution (▼) and in a 10^{-4} M KEX, 10^{-5} M DETA and 10^{-4} M SO_2 solution (◆) at pH 6.8.

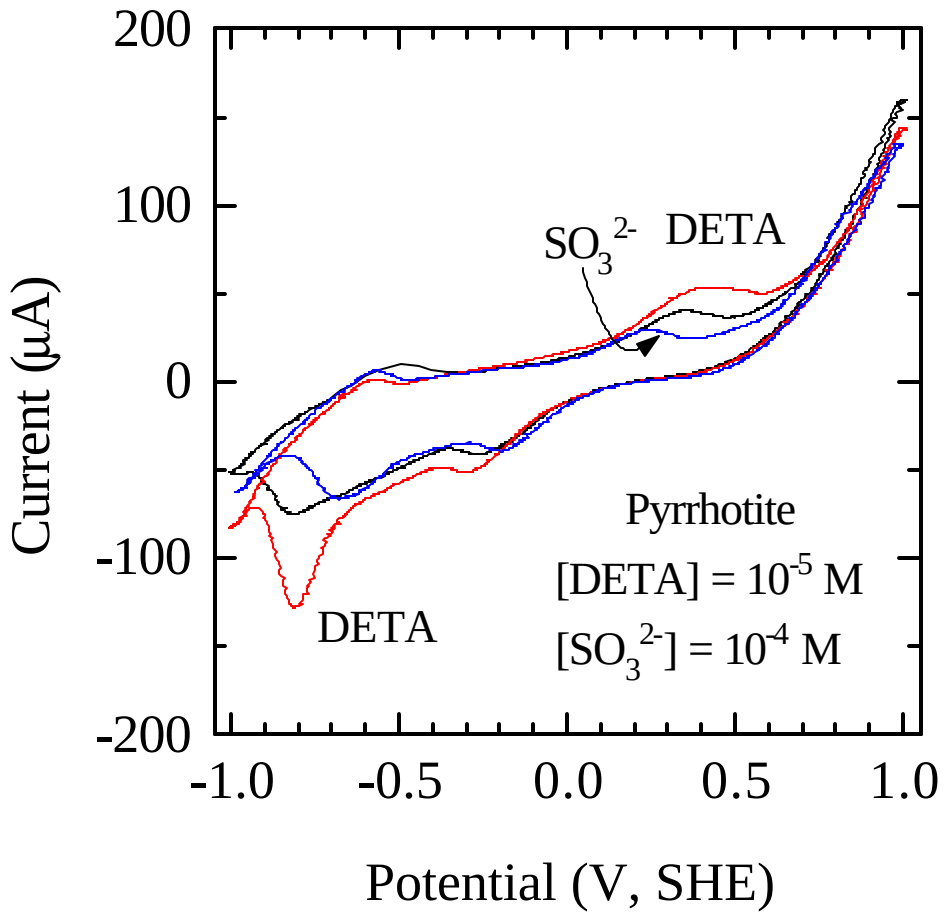

Figure 5.4. Cyclic voltammogram of pyrrhotite in the absence and presence of DETA and SO_2.

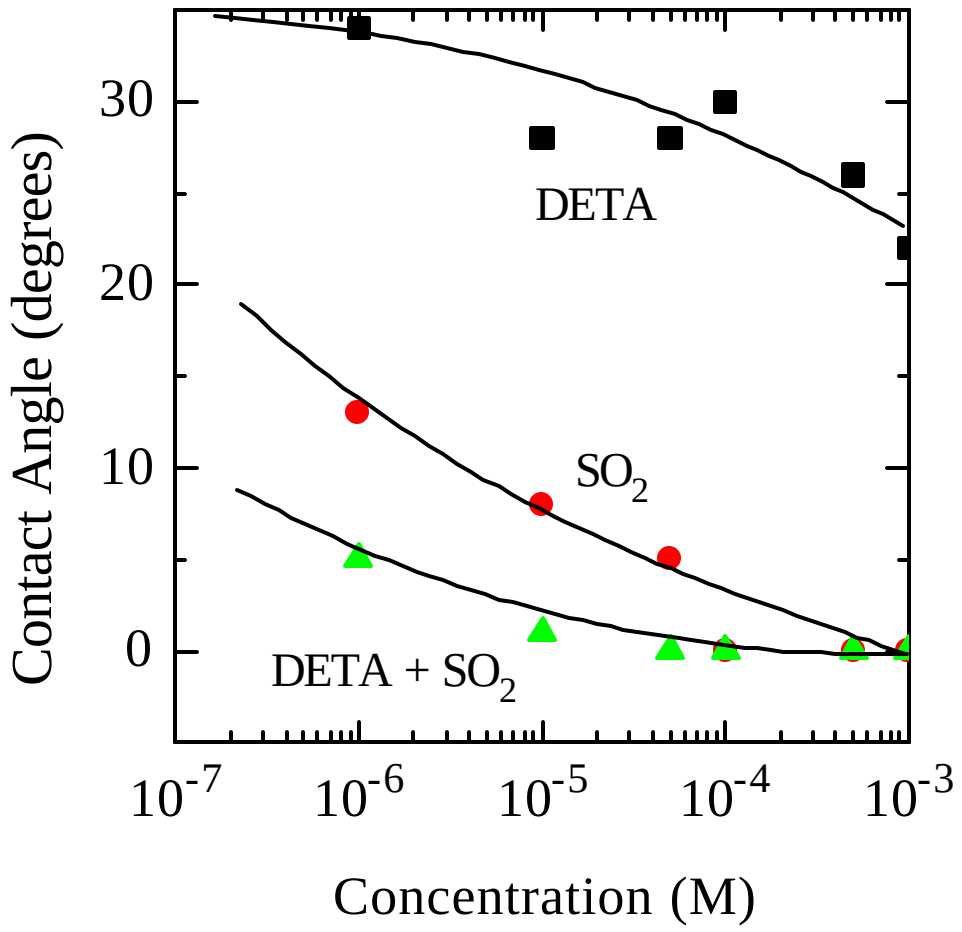

Figure 5.5 Contact angle measuremets for a gold elctrode in the presnece of (i) DETA (■), (ii) SO_2 (●) and (iii) both DETA and SO_2 (▲) in a 10^{-4} M Na_2S solution. The electrode was potentiostated at 0.150 V in 10^{-4} M Na_2S solution to form polysulfides.

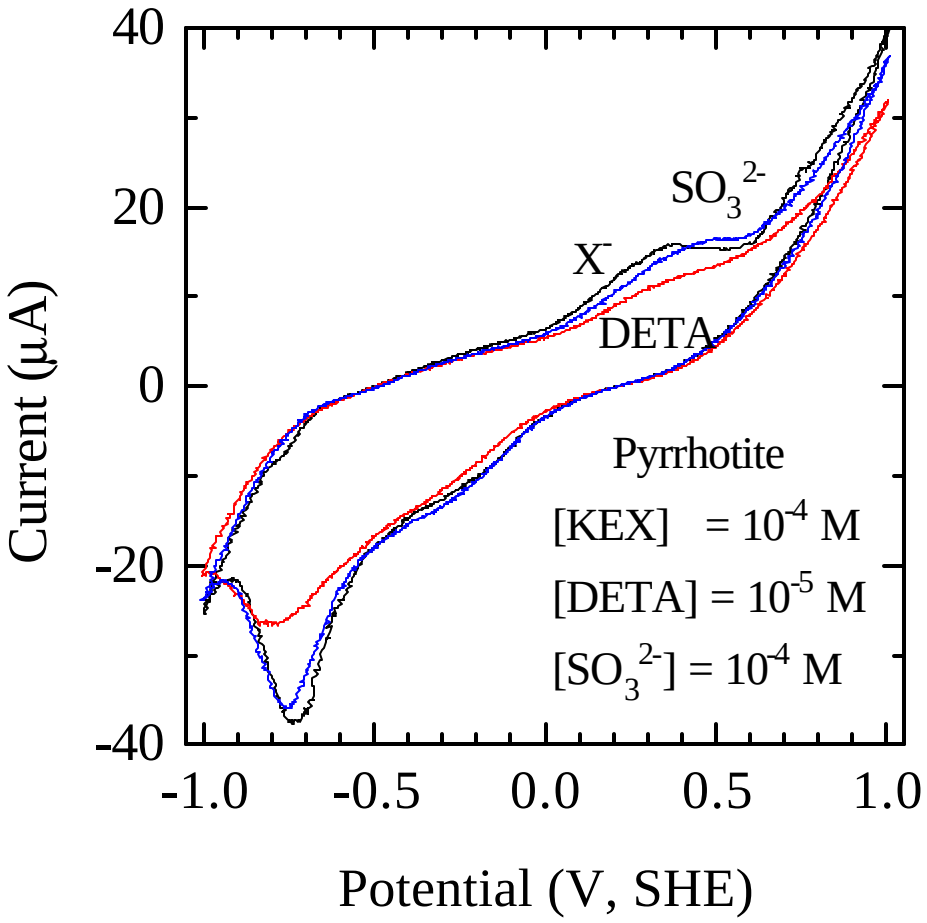

Figure 5.6. Cyclic voltammogram of pyrrhotite in the absence and presence of xanthate, DETA and SO_2.

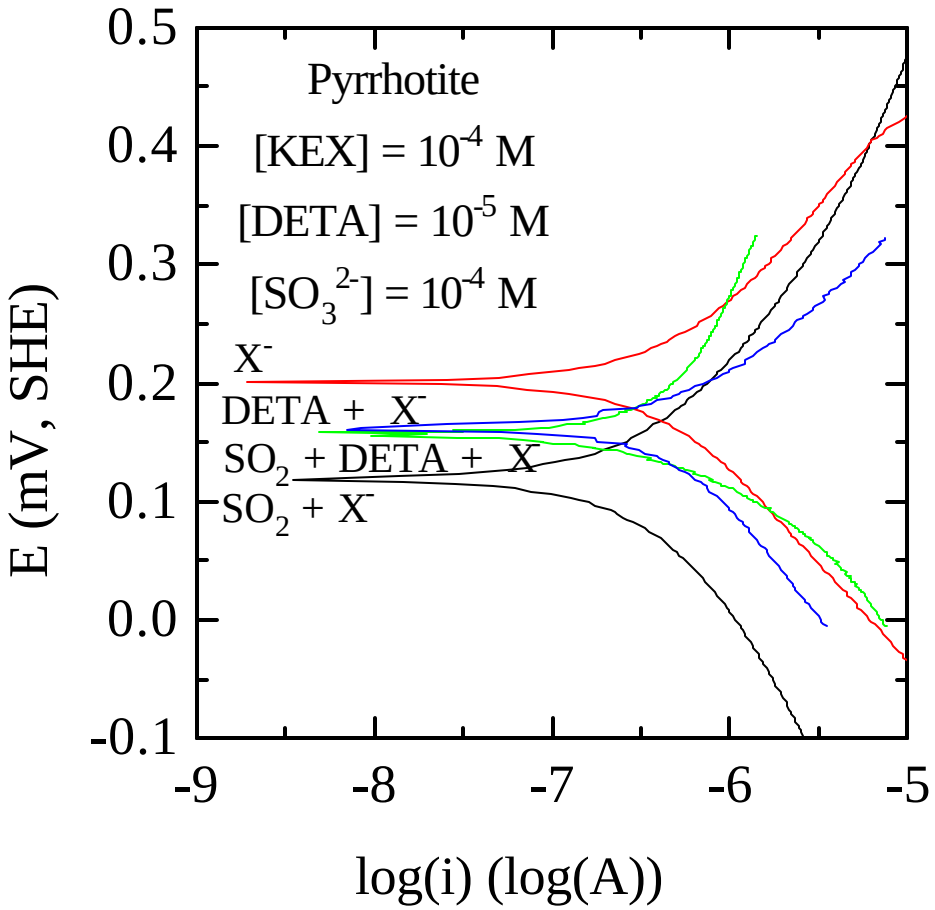

Figure 5.7 Tafel plots of pyrrhotite in the absence and presence of 10^{-5} M DETA and 10^{-4} M SO_2 in 10^{-4} KEX solution at pH 6.8.

Table 5.1. The relative changes in the rest potential of a platinum electrode when reagents are added to a pH 6.8 buffer solution.

Reagent	**Reagent addition**		**In reagent solution**	
	Alone	10^{-4} M Fe^{2+}/Fe^{3+}	Fe^{2+} addition	Fe^{3+} addition
10^{-5} M DETA	×	↓	↓	×
10^{-4} M SO_3^{2-}	↓	↓	↓	↑

CHAPTER 6

CONCLUSIONS

In the present study, various electrochemical techniques were applied to study the kinetics of xanthate adsorption and sulfide oxidation. The major conclusions of this study are summarized as follows:

1. The redox processes of pyrite were studied using Electrochemical Impedance Spectroscopy (EIS), and it was observed that the rate of reaction increases with progressive oxidation and reduction. Therefore, at higher oxidation potentials, hydrophilic oxidized iron species are formed rapidly at the surface suppressing pyrite flotation. However, at moderate oxidizing potentials, the iron species are not replenished fast enough leaving hydrophobic sulfur species on the surface and rendering pyrite floatable. This observation is consistent with the flotation results obtained by Tao et al., (1994) and Yoon et al., (1996).
2. EIS studies revealed that pyrite behaves like an inert electrode over a range of approximately 1.1 V. This is because of the irreversibility of the reaction products to small overpotentials of the AC signal (~5 mV). The shift in this range of the potential was about 65 mV/pH, which is consistent with the expected shift in the thermodynamic potential for oxidation and reduction reactions with pH (~59 mV/pH).
3. It was observed that polishing of the mineral surface brings changes in the nature of the surface. EIS revealed that polishing introduces a pair of resistance-capacitance in addition to the charge transfer resistance (R_{CT}) and double layer capacitance (C_{DL}). This could be due to either the formation of oxidation products on the surface or the creation of defects in the space-charge region. Also, polishing may change the area of the surface thereby changing R_{CT} and C_{DL}.
4. The galvanic experiments conducted to study the adsorption of xanthate on chalcopyrite and copper-activated sphalerite showed that ferric ions (Fe^{3+}) can serve as the electron scavenger and complete the redox process of xanthate adsorption. The results showed that the kinetics of the xanthate adsorption is faster in the presence of Fe^{3+} ions than in air.
5. It was observed that xanthate adsorption increases with the availability of Fe^{3+} ions. The single electrochemical cell, which simulates the conditioners more closely that the galvanic

electrochemical cell, also showed that xanthate can adsorb on sulfide minerals in the absence of oxygen as long as Fe^{3+} ions are present in the solution.

6. Xanthate adsorption was also observed at pH 6.8 in 10^{-4} Fe^{3+} solution where most of the iron is present as $Fe(OH)_3$. This indicates that $Fe(OH)_3$ precipitates may have served as a reservoir for Fe^{3+} ions during the process of xanthate adsorption on the mineral surface.
7. Tafel studies were successfully carried out to estimate the activation energies and the free energy of reaction for the adsorption of xanthate on pyrite, pyrrhotite, nickel-activated pyrrhotite, chalcocite and covellite. The calculated free energy of reaction was also instrumental in identifying the adsorption products.
8. Tafel studies showed that that xanthate adsorbs on pyrite and pyrrhotite as dixanthogen (X_2). Despite differences in their surface chemistry and adsorption mechanisms, the activation energies were almost the same. On the other hand, it was identified that xanthate adsorbs as cuprous xanthate (CuX) on both chalcocite and covellite. However, the activation energies were different because of the different mechanisms involved. The activation energy values showed that chalcocite was easier to float compared to covellite. This may be due to the reason that chalcocite has more copper in the lattice. This is consistent with the flotation studies of copper-iron sulfide minerals by Richardson and Walker (1985).
9. For nickel-activated pyrrhotite, which behaves similar to pentlandite, nickel dixanthate (NiX_2) was found to be the oxidation product. The cathodic and anodic activation energies for xanthate adsorption on nickel-activated pyrrhotite were determined to be 20.26 and 14.24 kJ/mol. These values are smaller than the activation energies for xanthate adsorption on pyrrhotite (ΔG_f^* = 124.85 kJ/mol and ΔG_b^* = 88.50 kJ/mol). This indicates that the activation of pyrrhotite may accelerate its flotation leading to difficulty in separation from pentlandite.
10. Electrochemical studies of the depressing action of DETA and SO_2 on pyrrhotite show that they complement each other. DETA alone acts as a good depressant mainly due to chelation with metal ions (Ni^{2+}, Fe^{2+}). Chelation with the Ni^{2+} ions leads to the deactivation of pyrrhotite. Chelation with the Fe^{2+} ions in the solution helps in maintaining lower pulp potentials and inhibiting formation of iron hydroxy polysulfide species. On the other hand, SO_2 is shown to lower the pulp potentials and decompose polysulfides. Thus,

the combination of DETA and SO_2 leads to (i) a decrease in the pulp potential below the reversible potential for xanthate adsorption and (ii) depletion of polysulfides. Therefore, the overall effect of DETA and SO_2 combination is the inhibition of xanthate adsorption on pyrrhotite leading to its depression.

CHAPTER 7

FUTURE WORK

The present study was divided into four parts, each of which is still an on-going research. Based on the results obtained, following recommendations can be made:

1. The results obtained with chronoamperometry of pyrite suggest that pyrite may be stable along a narrow belt in its stability region in an Eh-pH diagram. Therefore, Eh-pH diagrams can be further improved by measuring stable potentials of pyrite at different concentration of soluble species and at more pHs. Also, the effect of source of pyrite can be studied.
2. Based on galvanic coupling experiments, one may try to accomplish xanthate adsorption using other oxidants, such as permanganate or perchlorate.
3. It has been shown in Chapter 3 that ferric ions are effective electron scavengers for the adsorption of thiol collectors. The results indicate that the kinetics of xanthate adsorption is substantially faster in the presence of ferric ions than in the presence of oxygen as electron scavengers. This mechanism may be related to the industrial practice that thiol collectors are added to grinding mills. The possibility of ferric ions acting as an electron scavenger in grinding mills should be investigated.
4. Tafel studies could be extended to measure kinetics of the adsorption and desorption of other flotation reagents. Also, it could be used to study the oxidation and reduction of sulfide minerals in other environments. One specific example is pyrite. It will be useful to study pyrite oxidation in light of its infamous relationship to acid mine drainage.
5. It has been found that the role of SO_2 used in conjunction with DETA is to reduce polysulfides on the surface of pyrrhotite. It would be useful to find other reducing agents such as sodium sulfide to accomplish the same objective.

VITA

Neeraj K. Mendiratta was born and raised in Alwar, a small city in the culturally rich India. After finishing his primary education, he joined the Mining Engineering program at Indian Institute of Technology, Kharagpur. He graduated with a Bachelor's in the Spring of 1993. Immediately after his graduation, he joined Virginia Tech for masters. Two years laters he was promoted to the Ph.D. program in the Materials Engineering and Science Program. He is a member of the Electrochemical Society, the National Association of Corrosion Engineers, the Society of Mining Engineers and the Canadian Institute of Mining Engineers. Currently he is working as a Research Associate with Dr. Roe-Hoan Yoon at the Center for Coal and Minerals Processing in Virginia Tech.